Degenotoxification of pharmaceuticals by molecular imprinting and organic solvent nanofiltration

A thesis presented to

the Faculty of Chemistry

at the Technical University of Dortmund

for the degree of

Doctor of Philosophy in Chemistry

(*Ph.D. – Dr. rer. nat.*)

by

György Székely

born on the 23rd of May, 1986 in Budapest, Hungary

Supervisors:

PD Dr. Börje Sellergren, Prof. Dr. Ralf Weberskirch (Technical University of Dortmund)

Dr. William Heggie (Hovione FarmaCiencia SA)

August 2012

Copyright

Declaration

The work presented in this thesis was carried out mainly in the Chemistry Discipline, Research and Development, Hovione FarmaCiencia SA (Lisbon, Portugal) and in the Faculty of Chemistry, the Technical University of Dortmund (Dortmund, Germany), whilst the ExploraSep® screening was performed in MIP Technologies, a subsidiary of Biotage AB (Lund, Sweden), and is a result of the original work of the author, except where acknowledged in the text. The thesis was composed by the author and was not submitted to any other degree or professional qualification.

György Székely 27. Jul. 2012.

György Székely

technische universität dortmund

HOVIONE

MARIE CURIE ACTIONS

European Commission

Acknowledgements

My sincere thanks first and foremost go to my supervisors PD Dr. Börje Sellergren, Prof. Dr. Ralf Weberskirch and Dr. William Heggie, who gave me this great opportunity to do my PhD studies at the Faculty of Chemistry, Technical University of Dortmund and Chemistry Discipline, R&D, Hovione FarmaCiencia SA. They have not only been a great scientific advisors and mentors but also gave me intellectual freedom to follow my own ideas throughout my PhD research work.

I would like to offer my gratitude to Dr. Marco Gil and João Bandarra who have closely followed my work along these past years and provided knowledge, feedback and insight from a pharmaceutical manufacturing perspective throughout my PhD studies. They have truly contributed to narrowing the gap between academic research and industrial needs related to my research project. I acknowledge with thanks and appreciation my consultant Dr. Frederico Ferreira from the Technical University of Lisbon for his continuous support and availability, and of course the abundant late-night meetings throughout my PhD project.

Very special thanks go to my ex-colleagues and friends from the Budapest University of Technology and Economics, Péter Pogány and József Kupai for their great advice and fruitful discussions, but most of all for enriching my life so much in their own way for many years. I would like to express my satisfaction about the successful collaboration on molecular modeling with Peter. I would like to thank Dr. Sérgio Marques from the Technical University of Lisbon for enabling use of the NMR facilities at the IST-UTL center and technical assistance with the measurements. Furthermore, I would like to thank to all my colleagues both in Dortmund and Hovione for the many interesting and engaging discussions, among which special thanks go to Dr. Javier Urraca, Mahadeo Halhalli, Emelie Fritz from Dortmund and to Bruno Henriques, Dr. Rui Loureiro and Katalin Kováts from Hovione. I am grateful to Carlos Alvarez for sharing his knowledge and experience about design of experiments and for the useful discussions.

Many thanks to Dr. Ecevit Yilmaz and Rüstem Keçili from MIP Technologies Biotage AB for their help and support during my technical placement and also making my stay in Sweden quite enjoyable! I am grateful to Dr. Andrew Livingston for enabling my secondment in Imperial College and to his group for their never-ending advice and the excursions … without which I would not have enjoyed as much my time in London! The vibrant and welcoming multinational environment of the group was a great help both academically and socially.

I wish to acknowledge the financial support of the European Commission under FP7 – Marie Curie Actions, contract PITN-GA-2008-214226 [NEMOPUR] for my PhD scholarship. Furthermore, I am pleased to thank Hovione as well for giving me the opportunity of carrying out most of my research work in its R&D center. The stimulating environment of this company has helped immensely in improving my organizational skills and gave me great opportunities for networking and broadening my knowledge in various fields, not to mention the possibility of being able to express my scientific ideas.

At last but not least, I would like to thank my family for their patience and continuous support throughout my studies.

Table of contents

Glossary of the recurrent abbreviations used in this thesis

$\Delta\delta$	chemical shift change
Φ	solvent flux
λ	arbitrary time tolerance constant
Θ	surface coverage
AA	acetamide
ABDV	2,2'-azobis(2,4-dimethylvaleronitrile)
ACR	acrolein
AI	accelerating index
A_m	membrane area
A_{peak}	peak area
API	active pharmaceutical ingredients
AR	apparent recovery
BE	2-bromo-ethanol
BET	Brunauer-Emmett-Teller adsorption theory
Beta	Betamethasone
BSSE	basis set superposition error analysis
CCF	central composite face
$C_{F,x}$	concentration of solute x in feed
CHU	1,3-dicyclohexylurea
CMI	capacity modification index
COST	changing one single factor at a time
$C_{P,x}$	concentration of solute x in permeate
$C_{R,x}$	concentration of solute x in retentate
CVM	continuous variation method
D	diavolume, dilution ratio
DCM	dichloromethane
DFT	fensity functional theory
DMAP	4-dimethylaminopyridine
DMCC	N,N-dimethylcarbamoyl-chloride
DMS	dimethylsulfate
DoE	design of experiment
E_{col}	collision energy
E_{con}	cone voltage
EDMA	ethylene glycol dimethacrylate
EMA	European Medicine Agency
EtMS	ethyl methanesulfonate
EtTS	ethyl p-toluenesulfonate
F	flow
FC	flash chromatography

FDA	Food and Drug Administration
FF	fractional factorial design
FIA	flow injection analysis
FTE	full time equivalent
FTIR	Fourier transform infrared spectroscopy
G	gradient
GTI	genotoxic impurity
Halo	Halobetasole proprionate
IF	imprinting factor
IPU	1,3-diisopropylurea
Irb	Irbesartan
K	association constant
KP	Keppra
LA	Lacosamide
LOD	limit of detection
LOQ	limit of quantification
MAA	either protonated or deprotonated methacrylate
MAA^-	methacrylate anion
MAAH	methacrylic acid
MEK	methyl ethyl ketone
MeMS	methyl methanesulfonate
Meta	Mometasone furoate
MeTS	methyl p-toluenesulfonate
MIBK	methyl iso-butyl ketone
MIP	molecularly imprinted polymer
MRM	multiple reaction monitoring
MS	mass spectrometry
MsCl	methanesulfonyl chloride
MTBE	methyl tert-butyl ether
Mw	molecular weight
NBO	natoral bond orbital analysis
NIP	non-imprinted polymer
OSN	organic solvent nanofiltration
p	pressure
PDMS	polydimethylsiloxane
PI	performance index
PMP	1,2,2,6,6-pentamethylpiperidine
Pred	Prednisolone
Q^2	predictability
R	reproducibility
R^2	model fit

RC	recrystallization
Rf	retention factor
Roxi	Roxithromycin
RSD	relative standard deviation
R_x	membrane rejection of solute x
S/N	signal to noise ratio
SEM	scanning electron microscopy
Sep	separation of peaks
SIM	single ion monitoring
SPE	solid phase extraction
Suma	Sumatriptan
t	time
T	temperature
TA	thioacetamide
TGA	thermogravimetric analysis
THF	tetrahydrofuran
TLC	thin layer chromatography
TTC	threshold of toxicological concern
V	validity of the model
V_{add}	volume of fresh solvent added during diafiltration
V_F	feed volume
V_{inj}	injection volume
V_P	volume of permeate
V_{po}	pore volume
V_R	volume of retentate
V_{SE}	spherical equivalent volume
$V_{swelling}$	specific swelling volume
x	mole fraction

Summary

The thesis discusses molecular imprinting (MI) and organic solvent nanofiltration (OSN) as tools for degenotoxification of pharmaceuticals. The manufacturing of active pharmaceutical ingredients (APIs) often involves the use of highly reactive reagents, which could remain as undesired residues in the final product. Genotoxic impurities (GTIs) represent an accentuated class of compounds that can participate in an electrophilic attack on the nucleophilic center(s) of the DNA. Pharmaceutical regulatory authorities have recently issued guidelines on the control of GTIs. In general, GTIs have severe impact on the product risk assessment and hence, degenotoxification of APIs is of great interest to the Pharmaceutical Industry. A comparative study of flash chromatography and recrystallization, both conventional API purification technologies, versus OSN was performed in order to evaluate the feasibility and sustainability of OSN as a potential API purification technology. Solvent recycling, mass and carbon intensity and energy consumption were considered. A cost analysis was also carried out in order to take into account both environmental and economical aspects during the process comparison. OSN was proven to be competitive and hence various solvent resistant nanofiltration membranes were screened in THF, MEK and DCM. Eleven GTIs and nine APIs of industrial interest were used as model compounds and various diafiltration studies – featuring increasing technical difficulties – were carried out. GTIs with higher rejections can present significant challenges to OSN. For this reason, the effect of pressure change on solute rejection was explored to improve degenotoxification without provoking an increase in API loss. Subsequently, 1,3-diisopropylurea (IPU) – representing an OSN case with higher GTI rejection – was chosen for further investigation involving MI. Commercially available ExploraSep® Plate A with scavengers featuring different hydrophobic and carboxylic acid moieties that can possibly bind IPU were screened. Due to the limited performance of the hit scavenger, novel scavengers were designed to selectively bind IPU in the presence of APIs. The design constituted methacrylic acid (MAA) as functional monomer and ethylene glycol dimethacrylate as cross-linker whilst involving the exploitation of 1,2,2,6,6-pentamethylpiperidine (PMP) as deprotonating agent. The novel imprinted along with the corresponding non-imprinted scavengers were successfully tested for degenotoxification in the presence of various APIs of different chemical classes. On comparing the effectiveness of imprinting and nanofiltration, it was concluded that the scavengers function better at low GTI concentrations, whilst OSN at high GTI concentrations. Hence, a synergistic OSN-MI hybrid approach was proposed for IPU removal and the recovery of non-specifically bound API by

means of selective elution from the scavenger was developed. The effect of the deprotonating agent, PMP, both on the self-assembly prior to polymerization and on the molecular recognition of imprinted scavengers, was investigated by both experimental (NMR, FTIR) and *in silico* (DFT) tools. The continuous variation method revealed the presence of higher-order complexes and the appearance of self-association, which were both taken into account during the determination of the association constants. The assessment of the impact of the deprotonating agent on the molecular recognition behavior of scavengers called for introduction of performance-modification indicators such as capacity modification index, accelerating index and overall performance index.

Zusammenfassung

In dieser Arbeit wurden das molekulare Prägen (MI) und die Nanofiltration organischer Lösungsmittel (OSN) als Werkzeuge für die Entfernung genotoxischer Substanzen aus pharmazeutischen Stoffen untersucht. Die Herstellung von aktiven pharmazeutischen Wirkstoffen (APIs) beinhaltet oft die Verwendung von hochreaktiven Reagenzien welche als bedenkliche, genotoxische Reststoffe im Endprodukt verbleiben können. Genotoxische Verunreiningen (GTIs) stellen hierbei eine Gruppe von Stoffen dar, die elektrophile Reaktionen mit nucleophilen Gruppen der DNS eingehen können. In der pharmazeutischen Industrie ist das Interesse bezüglich der Entfernung von GTIs von höchster Bedeutung, da GTIs gegebnermassen ein erhöhtes Risiko für das pharmazeutische Produkt darstellen. Zwei herkömmliche API Aufreinigungstechniken, die Flash Chromatographie und die Umkristallisierung wurden in einer Machbarkeitsstudie mit OSN verglichen um deren Tragfähigkeit als Aufreiniungsschritt zu ermitteln. Hierbei wurden das Recycling des Lösungsmittels, Massenverluste, Kohlenstoffbelastung und Energieverbrauch berücksichtigt. Es wurde auch eine Kostenanalyse vorgnommen, um die wirtschaftlichen und umweltrelevanten Aspekte der verschiedenen Prozesse zu vergleichen. Dabei hat sich ergeben, dass OSN eine gleichwertige Leistung aufzeigt, weswegen die Untersuchung auf lösungsmittelresistente Membranen erweitert wurde. Eine Reihe von APIs und dazugehörigen GTIs wurden als Modelsubstanzen in verschiedenen Diafiltrationsversuchen untersucht. Dies erwies sich als technische Herausforderung, da GTIs ebenfalls von den Membranen ausgeschlossen wurden. Um die Entfernung von GTIs zu optimieren und die Verluste von API zu verringern, wurde der Einfluss von Druck auf den Ausschluss von gelösten Stoffen untersucht. In einer weiteren Studie wurden molekular geprägte Materialien auf ihre

Selektivität bezüglich 1,3-Diisoproylurea (IPU) untersucht, da diese einen höheren Ausschluss aufweisen. Handelsübliche ExploraSep® Platten A basierend auf selektiv bindenden Harzen mit hydrophoben und Carbonsäure-Gruppen wurden auf Bindung zu IPU untersucht. Da diese jedoch eine unzureichende Funktionalität aufwiesen, wurden neue Harze mit Methacrylsäure und mit Hilfe eines Deprotonierungsreagenzes synthetisiert. Diese neuartigen geprägten Polymere und die entsprechenden nicht-geprägten Kontrollpolymere zeigten eine erfolgreiche Entfernung von GTIs von verschieden APIs. Der Vergleich von geprägten Polymeren und OSN ergab, dass die geprägten Harze besser bei geringen GTI Konzentrationen funktionieren und die OSN Membranen besser bei hohen. Diese Erkenntis führte dann zu einer synergistischen Kombination von OSN und MI um IPU zu entfernen und unspezifisch gebundenes API in einem selektiven Waschschritt vom Harz zu lösen. Mittels NMR wurde der Einfluss des Deprotonierungsreagenzes sowohl auf die Vorpolymerisation als auch auf die Wiedererkennungseigenschaften des Harzes untersucht. Es wurde beobachtet, dass sich Komplexe höherer Ordnung und auch Selbst-Assoziationen ausbilden, welche dann in der Bestimmung der Assoziationskonstanten berücksichtigt wurden. Die Einführung von Leistungs-Änderungs-Indikatoren, wie zum Beispiel Kapazitäts-Änderungs-Index, Beschleunigungs-Index und Gesamtleistungs-Indikatoren wurden vorgeschlagen.

1. Introduction

My PhD research project falls into two areas that, at first glance, appear to be rather different, but that are in reality closely related through the common thread of separation science on a molecular scale. The major thrust of the work is at the interface of process chemistry and material science. In short, the aim was to develop and implement new methodologies for pharmaceutical downstream processing, particularly for the removal of genotoxic impurities (degenotoxification). Having a synthetic organic chemistry background, I think of systems on the molecular level which provided me with a perspective that is different from that of pure engineers, with whom I collaborated extensively during the past years. Because efficient degenotoxification requires operations on the molecular level, I was able to propose solutions to scientific problems that are not on the "radar screen" of these colleagues. Improved properties have been gained from the profound molecular scale design. To understand the basic principles that govern the recognition of the novel scavengers a thorough investigation has been carried out. It is worth mentioning that besides separation science – which is the core of the present thesis – both membranes and molecular imprinting are of paramount importance on account of many potential applications in diverse fields such as bio- and chemisensors[1,2], targeted delivery of drugs[3], tools in drug discovery[4] and catalysis of chemical reactions[5,6].

1.1. Identification of the problem – genotoxic impurities in pharmaceuticals

Cancer is the second cause of death in Western countries, after the circulatory diseases. Therefore, nowadays cancer and its prevention are among the most critical health issues. According to the World Health Organization (WHO), the worldwide cancer burden is set to increase by 50% in 10 years unless further preventive measures are put into practice. Therefore, there is an increasing awareness dedicated to potential causes of cancer. Most pharmaceutical products are manufactured either by applying a total synthesis approach or modification of a naturally occurring product. In both cases a wide range of reactive molecules are introduced into the synthetic sequence many of which are genotoxic themselves or may form genotoxic compounds that can contaminate the final product reaching patients. Thus, pharmaceutical regulatory agencies such as the Food and Drug Administration (FDA) and European Medicinal Agency (EMA) have raised concerns on the presence of genotoxic impurities (GTIs) in active pharmaceutical ingredient (APIs) that could impact negatively on

human health and have issued guidelines controlling their limits in APIs. To address their concerns, R&D scientists have to identify GTIs early on during process development, develop analytical methods and demonstrate the control of synthetic processes leading to GTIs. The objective of the present chapter is to highlight the importance of GTIs in API manufacturing and present examples and reagents related to them. As shown in Figure 1, obtained from the ISI Web of Science, July 2012, there is an increase in the literature on this topic demonstrated by the increasing number of hits on "*genotoxicity*" and hits on "*genotoxic impurity*" in literature searches[7]. The graph based on the former search shows the overall importance of the field of genotoxicity including chemistry, analytical methods, manufacturing, purification, diseases, medical aspects, genotoxicity tests, mechanism of action, assessment and environment, whilst the latter search shows the increasing attention of GTIs by the industry, mainly related to drugs and food.

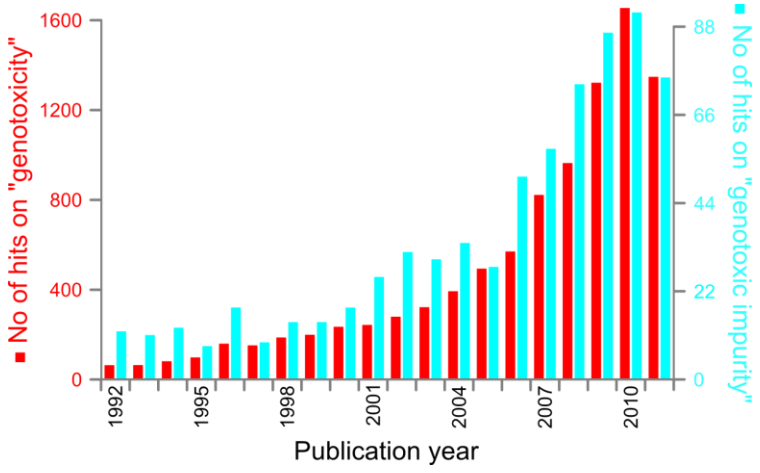

Figure 1 – Importance of genotoxicity demonstrated by the increasing number of publications on "genotoxicity" and "genotoxic impurity"

Detailed reviews on the risk assessment[8], toxicology[9] and mechanism of action[10] of such compounds can be found in the literature. The book *Genotoxic Impurities* edited by Teasdale provides an exhaustive discussion on the identification and control of such impurities in API manufacturing[11]. It should be noted, that compounds categorized as GTIs actually include a broad range of unrelated chemicals with very different structures and from very different chemical families. These compounds have in common their ability to react with DNA resulting in an associated carcinogenic risk. However, from a chemical point of view they do not have common chemical-physical properties or chemical structural elements that can contribute to easy identification. On the other hand, their presence in the manufacture of APIs is not stochastic, since these chemicals often have specific inherent roles in the chemical

routes used in API synthesis. In-silico systems such as DEREK can be used for determination of structural alerts, however for numerous chemical classes, structural alerts can over-predict genotoxicity due to factors such as high molecular weight, hydrophilicity, high reactivity, steric hindrance, molecular symmetry, and facile metabolism[12,13]. The mechanism of action of genotoxins involves an electrophilic attack on the nucleophilic center(s) of the DNA, these being: nitrogen and oxygen atoms of pyrimidine and purine bases and the phosphodiester backbone which could, in some circumstances, lead to strand breaks (Figure 2). Bidentate genotoxic agents can react with two nucleophilic sites resulting in: (i) one single molecule giving a bicyclic or tricyclic system; (ii) involving two different molecules in the same or the opposite DNA strand affording inter- or intrastrand cross-linkages respectively or; (iii) linking a protein and a DNA strand giving a DNA-protein adduct[4]. Besides the chemical nature of the genotoxic agent, the stereospecificity of the reactions also depends on steric factors and nucleophilicity, for instance the most nucleophilic sites of the DNA bases are endocyclic nitrogens such as N3 and N7 of guanine and adenine, on the contrary, exocyclic oxygens are less nucleophilic[14].

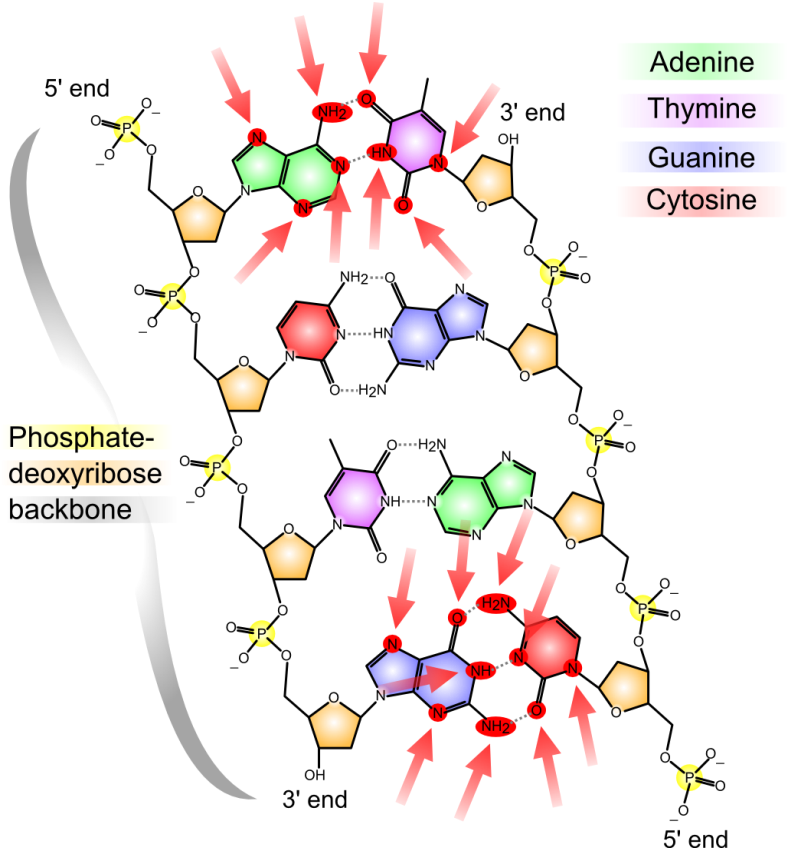

Figure 2 – Attack of the DNA by genotoxins where the arrows indicate the target nucleophilic sites of the DNA bases

Impurities, especially genotoxic impurities have been at the centre of increasing regulatory and industry attention in the last decade. EMA was the first authority to implement detailed guidelines on how such impurities should be controlled shortly followed by the FDA. Both authorities agreed on the implementation of the *Threshold of Toxicological Concern* (TTC) which sets a limit of 1.5 $\mu g.day^{-1}$ for known and potential carcinogens unless experimental evidence justifies higher limits. Higher levels can be applied in shorter-term studies during the clinical testing of the APIs. The rational behind such low values is to ensure that even if a substance was later found to be carcinogenic negligible risk would be maintained[15]. An exhaustive effort has to be made by the industry to meet such requirements and since many of the potentially genotoxic agents turned out to pose far less risk than originally supposed, the TTC approach is considered to be conservative. Nonetheless, GTI thresholds at such low levels are here to stay and the industry has been addressing this challenge with a variety of control and purification strategies. Regardless of the strategy selected for GTI mitigation, before its implementation it is crucial to identify and map the occurrence of the GTI in the API manufacture steps. Table 1 provides a list of genotoxic-alerting functional groups associated with the various reactions commonly employed today in pharmaceutical development and manufacturing[16]. Using this table as starting point, an overview on genotoxic impurities, focusing only on individual chemical classes which were experimentally investigated in the thesis will follow. The knowledge systematically gathered on GTI formation helped in the assessment of both new and alternative synthetic routes and allowed us to make a more confident decision to embark on purification strategies. Early realization of possible genotoxic contamination of the API improves time lines and safety by avoiding wasted effort on processes with no long-term future and in addition directs the focus on the relevant purification technology.

Table 1 – Common synthetic transformations related to potential genotoxic alerts

Bond formation				Alerting group	Associated reactions
C-O	C-C	C-N	AHC*		
X	X	X		Halides & sulfonates	Williamson ether synthesis
X	X	X	X	Michael acceptors	Michael reaction
X	X	X		Epoxides	Sharpless asymmetric epoxidation
X		X	X	Aldehydes	Aldol & Claisen condensation
X				Haloalkanes	Heck, Sonogashira, Kumada, Suzuki
		X	X	(Alkyl)aminoaryls	common intermediate

*aromatic heterocycle

1.1.1. Sulfonic esters and their precursors

Sulfonic esters are alkylating agents, which are a class of potentially genotoxic compounds[17]. They are called alkylating agents due to their ability *per se*, or after metabolic activation, of adding alkyl residues to the reactive nucleophile sites of the DNA bases. They cover a wide range of chemical structures from the simple methyl group to more complex structures featuring aromatic systems with various functional groups. Hence, there is a growing concern expressed by regulatory authorities in relation to contamination of APIs by these GTIs. Usually sulfonic esters are not introduced into the API synthetic route directly, but by contamination by side-reactions. Precursors of genotoxic impurities during API synthesis are called forgenotoxins. Forgenotoxins of sulfonic esters are alkyl and aryl sulfonic acids and the corresponding halides and anhydrides which can all form sulfonic esters. Examples of such compounds are mesylates (methanesulfonates), triflates (trifluoromethanesulfonates), tosylates (p-toluenesulfonates), besylates (benzenesulfonates) and nosylates (p-nitrosulfonates). Sulfonic ester impurities are often contaminants of APIs: (i) due to their formation in side-reactions between sulfonic acids or halides and alcohols or; (ii) as reactants carried over from incomplete reactions. When any of the forgenotoxin is used in an API synthesis there is always a possibility of the formation of genotoxic sulfonic esters. In particular, reactions containing sulfonic acids, sulfonic halides or sulfonic anhydrides in the presence of an alcohol, even if only in residual amounts, have the potential to yield sulfonic esters. Therefore, the European Pharmacopoeia production requirement for APIs marketed as sulfonic acid salts specifies that is compulsory to demonstrate that in such cases any formed ester is removed during the API purification process[8]. Hence, it is crucial for scientists working in the field of API manufacturing to be aware of the forgenotoxins and their use in drug synthesis. Due to their synthetic versatility sulfonate derivatives are common and useful reagents in the pharmaceutical industry especially in reactions where carbonium ion initiation is needed. They are widely used as salt forming agents, good leaving groups in nucleophilic substitutions reactions, protecting groups and for the resolution of enantiomers. Sulfonic acids are common salt forming agents used in the last step of the API synthesis. The conversion of an API to a salt enhances its stability and water solubility and helps its isolation as final product (Figure 3). Elder *et al.*[18] overviewed the utility, safety and regulation of APIs formulated as sulfonic acid salts. The potential for the tosylate salt forming agent to react with the alcoholic solvent to give a potentially genotoxic alkylating ester is a concern.

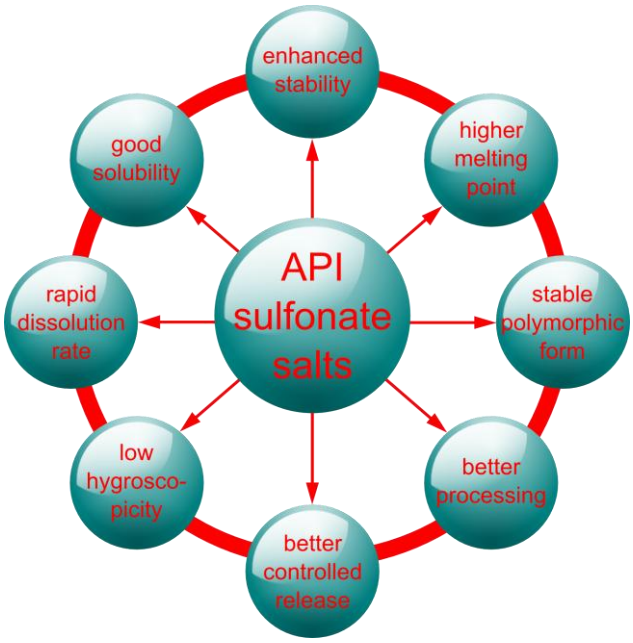

Figure 3 – Utility of sulfonate salts in API manufacturing

A particular but representative example, in which the formation of GTI has severe impact in API supply, is the Viracept case study. In 2007, contamination with genotoxic sulfonate ester, ethyl mesylate (EtMS) led to the global recall of this drug[19]. The case was investigated and it was established that the main GTI accumulation took place in the final manufacturing step. In this step the API salt, nelfinavir mesylate is formed as a soluble product by addition of methanesulfonic acid (MsOH) to a suspension of nelfinavir in ethanol. In the final step spray drying is used to isolate the dissolved nelfinavir mesylate salt from the ethanolic solution. The problem was that during this salt formation acidic conditions, combined with long reaction times and elevated temperatures, were used which favors MsOH reaction with ethanol to give the corresponding genotoxic ester, the primary source of GTI contamination in the process. Additional sources for accumulation of EtMS were also identified, such as supply of MsOH already containing some EtMS as impurity, reaction of MsOH with ethanol used to clean MSA holding tank and not properly removed before refilling, and cleaning of the spray dryer with ethanol, whose vapors could reach the MsOH hold tank through the ventilation system contributing again to additional EtMS formation[20]. Therefore, the conclusion of the Viracept case study points out that GTI contamination of API can result from a wide range of difficult to anticipate sources: pH adjustment problems; charging speed of a chemical to the reaction mixture; raw material supplier; pipelines and reagent holder tanks; cleaning procedures; drying procedures; prolonged reaction time; elevated temperature; introducing genotoxic reagent during the API production (more significant in the final steps).

1.1.2. Dialkylsulfates

The most common dialkylsulfates used in the pharmaceutical industry are the methyl and ethyl derivatives, the latter having been used as a war gas[21]. Being a strong methylating agent dimethyl sulfate (DMS) is used to introduce a methyl group in atoms featuring unshared electron pairs, such as oxygen, nitrogen, carbon, sulfur, phosphorus and some metals. Comparing with the alkyl halide type methylating agents, DMS is more favorable due the higher reaction rate and lower possibility of by-product formation[22]. Usually methylation with dimethyl sulfate requires the presence of a base, either: (i) to intensify the reactivity of the reaction site (e.g. converting the phenolic hydroxyl group of vanillin to sodium phenolate during the first step of Papaverine synthesis) or; (ii) to neutralize the by-products of the reaction, monomethyl sulfate (MMS) and sulfuric acid, for example in the case of the methylation of aliphatic alcohols. Usually only one of the methyl groups of DMS reacts in the methylation reaction because the MMS formed is a much weaker alkylating agent than the original DMS. Although, for research purposes – in small scale preparations – there is little necessity to use both methyl groups, in manufacturing – large scale production – in cases where the substrate is reactive enough to be methylated by MMS (e.g.: the sodium salt of mercaptans) it is desirable to utilize both groups if possible. In order to do so the reaction conditions are adjusted as follows: (i) increase the reaction temperature and; (ii) apply anhydrous conditions and avoid excess base to suppress the competing reactions with water and the hydroxide ion. To obtain the best results the base can be introduced to the reaction mixture continuously in small portions as the reaction proceeds but limiting this to the extent of the acid formed to minimize the competing reaction with the hydroxide ion. Non-aqueous solvent-base systems such as DMF/K_2CO_3 can be used in certain cases.

1.1.3. Alkyl halides

Methyl, ethyl and propyl halides are used widely as industrial alkylating agents. Although the mechanism of their toxicity is still not fully understood, they have been shown to directly alkylate critical biologically active macromolecules such as proteins and DNA[23]. Geminal, vicinal and ω-bifunctional alkyl halides are also directly used in API synthesis of which ω-alkyl dihalides are common linking agents due to their ability to connect API intermediates via consecutive alkylation. It was hypothesized that bifunctional alkanes cause genotoxic damage by the glutathione-dependent pathway and consequent formation of toxic

methanethiol[24]. Nitrogen and sulfur mustards (e.g. 2,2-dichlorodiethylsulphide) represent a special class of alkyl halides and have been used as chemical weapons. They are potential alkylating agents and their toxicity is attributed to cross-ling between DNA strands[25]. The source of alkyl halide contamination in APIs can be derived not only from direct use of alkyl halides, but from side-reactions between alcoholic solvents and hydrogen halides or de-quaternization of ammonium salts. APIs may be contaminated with genotoxic alkyl halides when a reaction takes place in alcoholic solvent at reflux temperature in the presence of hydrogen halides. These reaction conditions may be applied in cyclization, decarboxylation, sulfonyl cleavage, N-arylation and API salt formation. Alcoholic hydrogen chloride can also be used for ring openings.

1.1.4. Acetamide and thioacetamide

Acetamide (AA) is a known carcinogen, thus the awareness of its formation in API manufacturing is crucial[26]. Acetamide is not used directly, but its derivatives such as 2- and N-bromoacetamide or trifluoroacetamide are often used as building blocks in drug synthesis. These derivatives initially contain acetamide as impurity but also the 2- and N- derivatives have potential to form acetamide depending on the reaction conditions. Another source of carcinogenic acetamide contamination is the hydrolysis of the widely used solvent acetonitrile under acidic or basic conditions at elevated temperature. Acetonitrile is not only used as a solvent in the pharmaceutical industry, but also as a reagent in API synthesis. For instance it is directly used as a reagent in the synthesis[27] of Corontin. Thioacetamide (TA) is anticipated to be a human carcinogen based on evidence of carcinogenicity in experimental animals[28]. TA is an organosulfur compound soluble in water and serves as a source of sulfide ions in the synthesis of organic and inorganic compounds, thus often non reacted portions contaminate later phases of API synthesis.

1.1.5. N,N-dimethylcarbamoyl-chloride

N,N-dimethylcarbamoyl-chloride (DMCC) is listed under amides in the thesis for the sake of simplifying the classification of genotoxic impurities, but note that it is a half acyl chloride, half amide of carbonic acid and its reactions are driven by the acyl chloride moiety. DMCC is also considered carcinogenic[29] and it is used as an alkylating agent, similar to the sulfonate esters describe above, providing good leaving groups, thus it is used as a chemical

intermediate in the production of dyes, pesticides and pharmaceuticals[30]. An example of its application in API synthesis is in N-heterocyclic compounds, for example Carbamayepine[31].

1.1.6. Aminopyridines

Derivatives of aminopyridines are often used as starting material or catalyst during API synthesis. During the preparation of glucocorticoids in order to replace the 21-hydroxyl group with a chlorine, sulfonyl chlorides are used in a 4-dimethylaminopyiridne (DMAP) catalyzed sulfonylation reaction[32]. DMAP has alerting structures for genotoxicity and thus can be considered a potentially genotoxic impurity[33,34]. Besides the sulfonylation reactions DMAP is also used in acylations[35], esterifications[36,37], amino group protections with Boc[38,39] and sylilations[40].

1.1.7. Ureas

1,3-diisopropylurea (IPU) and 1,3-dicyclohexylurea (CHU) are the most common impurities of the urea chemical class, which are potentially genotoxic impurities[41]. Ureas are the direct and unavoidable hydrolyzation product of carbodiimides. Carbodiimides are stabilizing, coupling and condensing agents in the preparation of peptides and nucleotides; versatile dehydration reagents in organic synthesis[42,43] and often used to activate carboxylic acids towards amide or ester formation[44].

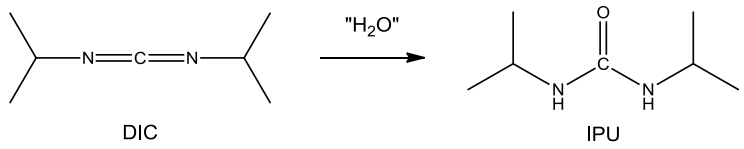

Scheme 1 – Formation of 1,3-diisopropylurea from dehydrating agent 1,3-diisopropylcarbodiimide

Reagents such as 1,3-diisopropylcarbodiimide (DIC) and 1,3-dicyclohexylcarbodiimide (DCC) are the most important discoveries that helped to drive the field of peptide synthesis[45] and probably the most popular of the carbodiimides-type coupling reagents in use today[46]. IPU and DCC are considered to be dehydrating agents inasmuch as the results are a loss of water from the amino and carboxyl groups involved in the coupling. Carbodiimide mediated crosslinking is usually used in the polymerization of polypeptides, and thus widely used in

immobilization procedures (e.g., attaching proteins to a carboxylated surface) and in immunogen preparation (e.g., attaching a small peptide to a large carrier protein). In this reaction, carbodiimides react first with carboxylic acid groups to form an active *O*-acylisourea intermediate, this intermediate is easily displaced by nucleophilic attach from primary amino group in the reaction mixture. The primary amine forms an amide bond with the original carboxyl group, and the by-product is released as a soluble urea derivative. The *O*-acylisourea intermediate is unstable in aqueous solutions, and its hydrolysis result on regeneration of the carboxyl group and release of an N-unsubstituted urea[47] (Scheme 2).

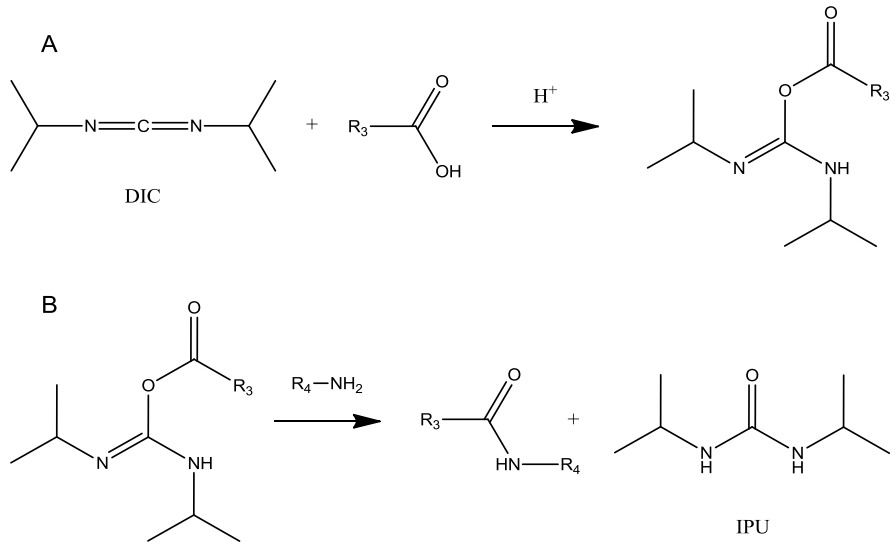

Scheme 2 – Use of carbodiimides in API synthesis with urea formation: (A) DIC reacts with carboxylic acid group and activates the carboxyl group, allowing it to be coupled to the amino group in the reaction mixture; (B) DIC is released as a urea derivative after displacement by the nucleophile, R_4NH_2

1.1.8. Aldehydes

Aldehydes are important molecules used as building block in the production of pharmaceuticals, however many of them are inherently genotoxic, and thus when reactions are incomplete, their removal is required. Acrolein (ACR) is an unsaturated aldehyde, and was selected as a GTI representative of this class. Acrolein is a severe pulmonary irritant and lachrymatory agent, causes serious damage to skin, and exposure to it in concentrations of 2 ppm is immediately harmful. Acrolein was used as a chemical weapon during World War I. Studies on rats have shown an increase in cancerous tumors from ingestion (but not from inhalation). Also in vitro studies show that acrolein can react directly with DNA and proteins

to form stable adducts and that it induces gene mutations in mammalian cells, nevertheless ACR is used as reactant during the synthesis of various APIs, e.g. Methionine[48].

1.2. Design of experiments for the analysis of genotoxic impurities

The pharmaceutical regulatory authorities, such as FDA and EMA periodically issue guidelines on the limits of GTIs in APIs. These guidelines make it critical to be able to determine ultra low levels of traces impurities and also imply the continuous assessment of additional purification steps for the removal of GTIs from the API[49,50]. Prior to the investigation of potential degenotoxification methodologies, reliable analytical methods had to be developed for the trace analysis of the model impurities, which is illustrated through the example of DMAP. Impurity trace determination at ppm levels calls for highly sensitive analytical methodologies, which pose tremendous challenges on analytical chemists in the pharmaceutical quality control sector. Sun *et al*. have recently published an article with case studies on a systematic method development strategy for the analysis of genotoxic impurities considering various factors such as method selection, risk assessment and validation[51]. The analysis of potentially genotoxic aminopyridines is required in fields such as environmental studies, toxicology and pharmaceutical quality control. Vanhoenacker *et al*. reported on arylamine and aminopyridine analysis both with and without the application of derivatization agents in matrices such as vitamin C, bromhexine, ephedrine and penicillin[52]. It is of interest to note, that although DMAP is potentially genotoxic, it has been recently suggested as a pre-column derivatization agent for the analysis of genotoxic alkylation compounds such as alkyl halides, sulfonates, azides and aldehydes[53]. The matrices chosen for this study are glucocorticoids since the analyte of interest is a widely used catalyst during their synthesis and possesses a risk of contamination of the drug products. Recent review by Liu *et al*. provides an industrial perspective with regard to the analysis of various structural classes of GTIs that are commonly encountered during pharmaceutical development and manufacturing[49]. For further reading the book entitled *Genotoxic Impurities* edited by A. Teasdale, providing an exhaustive discussion on the identification and control of such impurities in API manufacturing, is suggested[11].

Besides obtaining a reliable method for GTI analysis, the objective of the present analytical work was to explore the application of (i) design of experiment (DoE) optimization in LC-MS/MS method development comprising both LC and MS instrumentation in one single DoE

stage and (ii) DoE robustness testing. Such an approach addresses the industrial call for a quick method development methodology and considers the effect of LC parameters on the MS detection. Thorough understanding of a given analytical task is crucial to obtain optimal analytical methods. Furthermore, to work efficiently in terms of time and resources, the method development has to be performed in a highly organized and conscious manner. Hence, in order to fulfill these requirements, design of experiments[54], quality by design[55] and design space computer modeling[56] have gained increased attention in pharmaceutical analysis during recent years. A review on the quality by design approaches for the control of genotoxic impurities can be found in the literature[57]. The development of analytical methods is conventionally made by trial and error, changing one single factor at a time (i.e. each factor has to be optimized separately, in a consecutive manner) which is often abbreviated as COST. While a trained analyst can obtain an acceptable result following this approach it takes excessive time and does not allow the analyst to reach really optimum conditions and may produce different results from different starting points. DoE is a statistical tool being used in a number of fields that can also be useful in analytical method development. It is a systematic approach that reduces time, accounts for experimental error and considers interactions between variables of the analytical method. Carefully selected sets of experiments using the DoE approach – in which all relevant factors are varied simultaneously – ensures that the analyst obtains the maximum amount of relevant information. The methodology starts by a risk assessment to define the variables to be studied. In the present work variables of both LC and MS were considered and the objective was to determine the best ranges to maximize peak area (A_{peak}) and S/N ratio and minimize running time, while still achieving an acceptable separation of the analytes.

1.3. Purification of pharmaceuticals

As described in Chapter 1.1 the pharmaceutical regulatory authorities periodically issue guidelines on the limits of GTIs in pharmaceutical manufacturing, making the addition of a GTI removal step in API purification crucial. GTIs can be successfully reduced below the limits set by regulatory authorities following three different strategies. In the first strategy, the use and generation of GTIs in the synthetic route is avoided by searching for different chemical sequences to reach the same API or intermediate[58]. In very particular cases, this strategy can be achieved without significant losses of yield. Examples of redesigning the synthetic process specifically to avoid GTIs can be found in the literature, e.g. the synthesis of

Zauategrast Sulfate originally involved the use of methanesulfonic acid, but due to the potential risk of generating genotoxic ethyl mesylate it was replaced by an alternative acid[59]. In many cases, the use of reagents and intermediates that are reactive and synthetically useful, which likely makes them interact with DNA, are often unavoidable. Furthermore, it may not be practical to change the synthetic steps during development, particularly when the processes are scaled up, to control or reduce GTIs. Therefore, a second strategy to achieve GTI-free drug products is based on prevention, focusing on elimination or reduction of GTI concentration either before the critical API synthetic step or during the reaction. This can be achieved by altering appropriate reaction conditions such as: (i) proportions of reaction components; (ii) interchanging of the reaction addition modes; (iii) changing the key starting materials; (iv) starting with different intermediates or; (iv) changing functional groups with structural alerts. Furthermore, a deeper Quality by Design (QbD) investigation can contribute to a better control of GTIs (Figure 4)[60].

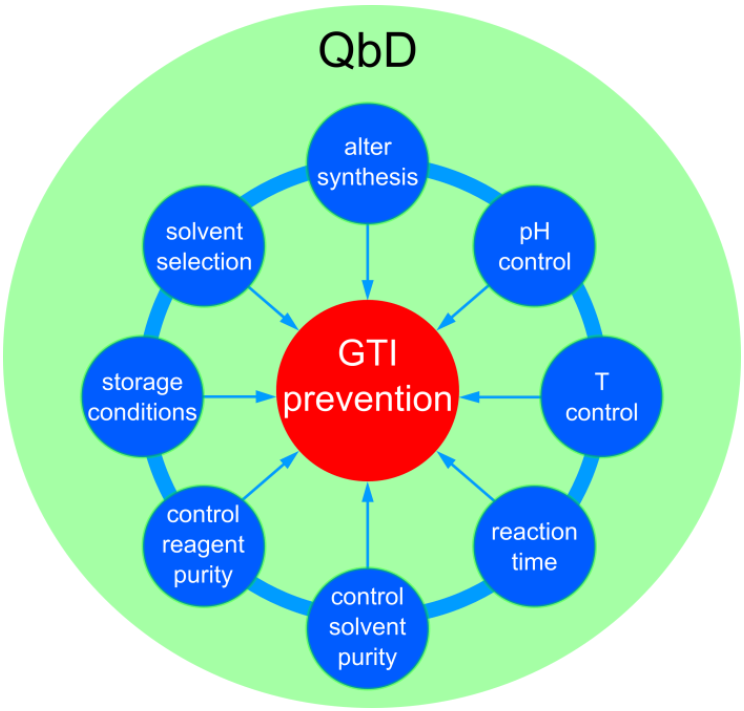

Figure 4 – Quality by design strategy for GTI prevention

Nevertheless, in many cases, the API contamination with GTIs is unavoidable, which results in extensive analytical and purification process development. For instance, depending on API daily dosage, a specification of 70 ppb was set for an especially potent genotoxin in a drug candidate[61]. Such ultra low levels in the specifications of APIs pose additional analytical and processing difficulties. Therefore, the third strategy involves direct API purification from

GTIs. Several workup processes have been proposed to address such issues, including crystallization, drying to remove volatiles, washings, resolution, preparative column chromatography, fractional distillation, membrane processes, use of resins and scavengers. It should be noted, that most of the API purification processes are not GTI-specific, but remove other impurities from the crude API as well. However, application of scavengers is a selective way for the removal of a GTI. Usually the higher the selectivity of a purification process regarding a specific impurity, the lower the API loss and the higher the removal efficiency of the impurity in question. However, as other impurities remain in the crude API, the overall purity of the API remains low with respect to all the other impurities present. Therefore GTI removal from API post reaction streams is of utmost concern for the industry and it is still without a consensual effective solution. The difference between *point-of-source* and *end-of-pipe* GTI removal is schematically illustrated in Figure 5.

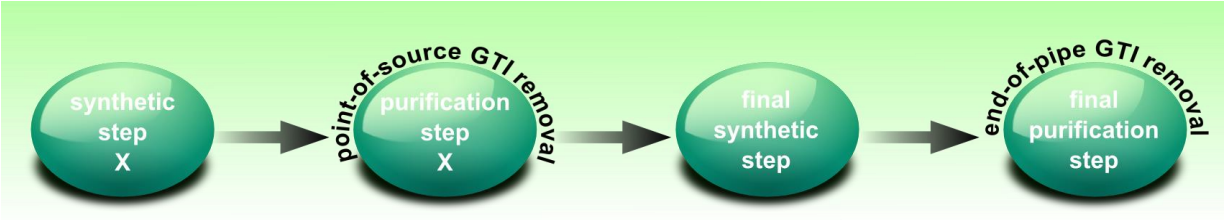

Figure 5 – Point-of-source and end-of-pipe GTI removal

Higher removal of impurities can be usually obtained by increasing the number of cycles within a given purification technology, e.g. number of extractions, number of recrystallizations. However, increasing the number of cycles also leads to undesirable higher API loss. Consider an example of an API stream with a contamination of 1 g of GTI for each 100 g of API, and a purification process in which, for each stage, 80% of the GTI is constantly removed with the sacrifice of 3% of the API. To reduce the GTI from a concentration of 1 $g.L^{-1}$ in solution (corresponding to an API concentration of 100 $g.L^{-1}$) to 64 $\mu g.L^{-1}$ would require 6 cycles, and a cumulative API loss of 17% of the API in the purification alone. Therefore, to drive conventional API purifications to reach ultra low GTI content, through an increase in the number of cycles, would lead to unacceptable API loss. The use of an additional *end-of-pipe* GTI purification could complement the already existing intercalated purification steps[50,62,63]. Nevertheless, the removal efficiencies are usually concentration dependent, decreasing at lower GTI concentrations. When reactive GTIs are carried forward in the API synthetic sequence they can suffer further reactions, potentially

producing different GTIs, and make the respective identification more difficult. In such cases, it may be advantageous to follow a *point-of-source* degenotoxification strategy. For implementation of this strategy, identification and mapping of the reactions where GTIs are present is crucial.

Conventional purification steps used in API post reaction synthesis include recrystallization, extraction, resins, distillations, adsorbents and chromatography. On the contrary, organic solvent nanofiltration (OSN) and molecularly imprinted polymers (MIPs) can be perceived as advanced techniques proposed recently (Figure 6). As in any separation, the efficiency of the separation depends of the differences in chemical and physical properties of the two entities to be separate and/or their relative affinities for a selective agent. A brief review of the techniques that are discussed in the thesis follows. Note, that these emerging technologies being the main topic of the thesis – organic solvent nanofiltration and molecular imprinting – are intended to expand the chemists' and engineers' toolbox to address API degenotoxification and will be discussed in details in chapters 1.4 and 1.5.

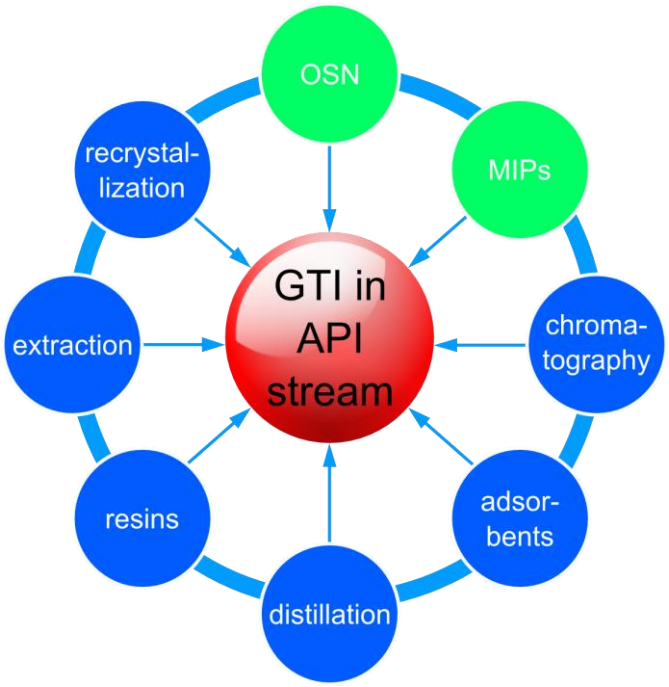

Figure 6 – Conventional (blue) and advanced (green) API purification technologies

Recrystallization is one of the most important isolation and purification process in the fine chemical industry, e.g. API manufacturing, due to its ability to give high purity products. However, selection of optimal conditions for recrystallization – solvent system, temperatures,

time and cooling rate – is challenging and time-consuming[64]. The API is isolated as a crystalline solid phase whilst the impurities remain dissolved in the liquid phase (the mother liquors). Crystallization is also broadly used in chiral separations, namely through diastereomeric resolutions[65,66]. Solvent(s), temperature and pH of the recrystallization system all play an important role in the effectiveness of the purification process[67]. Recrystallization is not only a purification process that determines the purity and residual solvent content of the API, but also determines the crystalline properties in terms of polymorphic form, crystal habit, bulk density and size distribution – all of which affect downstream drying and formulation[68,69]. More importantly, the crystalline properties and respective polymorphic forms are responsible for drug bioavailability. Therefore, once a route is approved for API production, the crystallization step of the final API is usually maintained. Depending on process optimization, a significant fraction, up to 30% of the API can remain in the mother liquors or be lost through washes of the crystals[70]. API crystals are usually isolated by filtration and the impurities can be carried forward with the API stream, sometimes as part of the crystal lattice, due to insufficient washing.

Fractional distillation can be used to purify volatile APIs[71]**.** However, distillation is also broadly used for removal of solvents and solvent exchanges, in particular when switching from a high boiling point solvent to a lower boiling point solvent. Solvent exchanges from high boiling point solvent to lower boiling point solvents or when thermo-sensitive compounds are involved can be achieved using OSN[8]. Volatile organic impurities, mainly resulting from residual solvents[72,73] can also be removed through distillation. Most of the GTIs considered in the present work – with the exception of acrolein – have low volatility.

Adsorbents such as activated carbon and resins are broadly used to remove impurities from APIs[74,75]. Adsorption based separations are based on different affinities of the different compounds for the adsorbent. Therefore, high affinity of the GTI combined with lower API binding is desirable in this case. Screening of the different commercially available absorbents for metallic API impurities has been evaluated using microtubes and microplates[76,77]**.** Specific studies include removing genotoxic formaldehyde using activated carbon containing amine groups[78] and removal of an aldehyde impurity using polystyrene-based sulfonylhydrazine resin[79]. Removal of GTIs such as alkyl mesylates and tosylates has also been evaluated using different commercially available resins[74]. These adsorbents and resins can be used as stationary phases in chromatography.

Column chromatography is a typical post reaction work up in organic chemical synthesis to remove impurities from APIs. On one hand, sophisticated stationary phases are applied in the pharmaceutical industry for chiral purification[80,81] but on the other hand for API degenotoxification standard silica gel has been used of pharmaceutical grade as stationary phase[82]. In this technique a solvent, such as ethyl acetate, ether, acetone, dichloromethane and mixtures thereof are used as eluents. Polystyrene or methacrylate based commercially available adsorbent matrices using aqueous solutions at different pHs and ionic strengths are also reported[83]. Particle size, column dimensions and eluent flow and pressure are critical parameters.

1.4. Green process engineering

In order to assess the viability of OSN as an API purification technology, a process comparison has been carried out in respect to environmental and economic aspects. Recrystallization and flash chromatography as conventional techniques were selected for drug degenotoxification as conventional purification technologies for the process comparison. Process development is considered to be the most important design stage due to its crucial effect both on the whole lifecycle of a process and on its performance[84]. Furthermore, the major part of the production costs of pharmaceuticals is caused by downstream processing[85]. The pharmaceutical industry has been pioneering process optimization concerning the optimization of the purification of final product[86] as well as on introducing green metrics[87,88,89,90] to stimulate process effectiveness that minimize environmental impacts[91]. The model compounds selected for the process comparison study were Meta, as a representative API, and MeMS and DMAP as impurities. Several related synthetic routes and purification processes for Meta can be found in the literature[92,93,94]. As shown in Scheme 3, the reagent system to convert the 21-hydroxyl functionality to chloride during manufacturing usually comprises of the use of methanesulfonyl chloride (MsCl) and DMAP in dichloromethane (DCM)[32,95,96]. As a drawback of this methanesulfonylation reaction step, MsCl may form genotoxic MeMS in the presence of methanol and DMAP may also contaminate the final product, making this system particularly relevant to be used as model system in the current study. The former impurity is a known genotoxin while the latter is a potentially genotoxic impurity with two structural alerting functional groups: aromatic and alkyl amines[33].

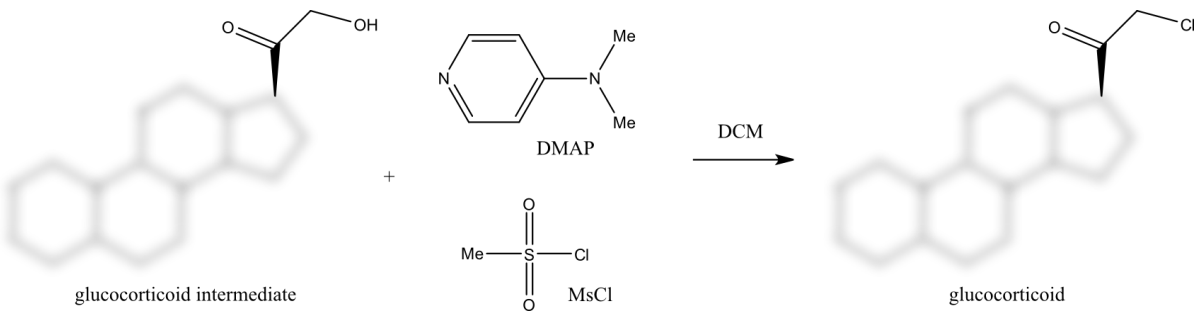

Scheme 3 – Application of MsCl and DMAP during the synthesis of glucocorticoids (MsCl can form genotoxic MeMS in the presence of MeOH)

It is worth mentioning that the solvent of the Meta post-reaction stream is DCM, which is categorized as an undesirable solvent in the pharmaceutical industry both by GSK[97,98] and Pfizer[99]. Therefore, the use of DCM in API manufacturing is decreasing, e.g. it has fallen from position 3 to 8 in the ranking of process solvents used between 1990 and 2000 in GSK. However, due to the excellent solubility properties of DCM, in 2005 DCM still represented about 75 mass percentages in contribution to GSK's process solvents[100] emphasizing the industrial importance and presence of DCM. Several green metrics are proposed in the literature to evaluate green economy of synthetic routes[89,101] including mass, energy and carbon intensity, however literature data on downstream process comparison is scarce[86,102,,103]. Recently published papers give an insight to how companies such as GSK pharmaceuticals[87], L´Oréal cosmetics and Repsol refinery[104] approach green aspects related to processes. The present assessment focuses on solvent use, energy consumption and selective agent disposal as well as purification performance and costs. Pharmaceutical downstream processes usually consume large amount of solvents, hence the effect of a solvent recovery distillation unit both on environmental and financial costs is assessed.

1.5. Organic solvent nanofiltration

Degenotoxification by OSN mainly relies on the molecular size difference between the API and the GTI, although other properties such as shape and polarity also contribute to their rejection. The aim is to achieve high genotoxin removal through the permeate and low API loss in the retentate. The main challenge of genotoxin removal by membranes lies in the fact that most of them are highly reactive species and thus can attack the polymeric membrane framework at molecular level. Additionally, polymeric membranes are usually prepared by phase inversion in dipolar aprotic solvents such as dimethylformamide and dimethylsulfoxide,

hence similar harsh solvents can easily attack and dissolve the active layer of the membrane. The performance of this technique is highly dependent on the membrane selected and on the respective rejection curve. There are several commercially available polymeric and ceramic membranes that are stable in organic solvents. Examples include Koch SelRO membranes, StarMem series developed by W. R. Grace & Co, DuraMem series from Evonik MET, SolSep membranes, GMT-oNF-2 from Borsig Membrane Technology GmbH and Inopor or Pervap ceramic membranes. The molecular weight cut off (MWCO) is commonly used to characterize nanofiltration membranes. The MWCO of a given membrane corresponds to the molecular weight of a compound, obtained by interpolation, rejected at 90%. Different suppliers use different reference solutes and solvents as standards. Koch typically uses dyes, e.g. Sudan IV or glucose in solvents such as acetone and ethyl acetate or water. MET usually uses a sequence of linear alkanes dissolved in toluene.

In the last 10 years, the number of commercially available polymeric membranes for OSN that are compatible with a broad range of solvents has dramatically increased. At the end of the 90s, the available membranes to process solvents were mainly limited to the Koch SelRO membranes, StarMem and SolSep Membranes. The Koch SelRO membranes were the first commercially available OSN membranes and offered thin film composite (TFC) membranes with MWCO of 250, 400 and 700 Da. These membranes are claimed to be stable in alcohols, alkanes, alkenes, ketones, ethers, formaldehyde, chlorinated solvents (dichloromethane, carbon tetrachloride, trichloroethane, dichloroethane, methylene chloride) and solvents such as propylene oxide, nitrobenzene, tetrahydrofuran, acetonitrile, ethyl acetate or dioxane. StarMem membranes, patented by W. R. Grace & Co, have been distributed by Membrane Extraction Technology (MET), now Evonik MET. These integral skinned polyimide membranes were available with MWCO of 200, 220 and 400 Da and are claimed to be stable in alcohols, alkanes, aromatics, alkyl ethers, alkyl ketones, and alkyl acetates. New generations of membranes with enhanced solvent stability have been developed for polar solvents[105]. Recently, Evonik MET, launched a new generation of integral skinned cross linked polyimide membranes, the DuraMem series. Compared with StarMem, these membranes are claimed to be stable in further solvents such as dimethylformamide and tetrahydrofurane and expand the temperature maximum limit form 60 to 100 ºC. They are available with MWCO of 150, 200, 300, 500 and 900 Da, thus covering also the gap between 400 and 1,000 Da[106]. SolSep offers five membranes with MWCO between 300 and 750 Da[107,108] and these membranes are claimed to be compatible with alcohols, esters, ketones,

aromatics, chlorinated solvents, but more information on these membranes is scarce. Polymeric membranes are available as flat sheets and also as spiral-wound elements, thus facilitating scale-up. There are also OSN ceramic membranes commercially available from Inopor with MWCO between 450 and 750 Da[109].

The OSN membrane screening study in the thesis focuses on the development of membrane purification of APIs from common classes of GTIs. A total of nine APIs from four different chemical families namely N-heterocycles, steroids, macrolides and amides were selected as model compounds. The API families and their pharmacological importance, as well as their molecular structures are summarized in Table A1 in the Appendix. The model GTIs cover four chemical classes: sulfonate esters, ureas, aldehydes, and amides. Their structures and molecular weights are resumed in Table A2 in the Appendix. The comparison of the molecular weights of these compounds are represented in Figure 7, with the majority of the GTIs on the Mw lower range (55–225 Da) and API on the upper Mw range 170–840. Thus the OSN strategy consists in pushing the GTIs through the membrane, as the APIs are retained. The OSN can be operated in diafiltration mode, i.e. adding additional fresh solvent to compensate for the solution leaving the system through the permeate. Two OSN membranes (Table 2) with MWCO in the range of 250–350 Da were selected, namely SolSep NF010206 with a reported rejection of 95% for a 300 Da compound[107] and GMT-oNF-2 were purchased as a flat sheet from SolSep BV and from Borsig Membrane Technology GmbH, respectively. Membranes with different MWCO could be selected for specific Mw ranges of API and GTI.

Table 2 – Description of GMT-oNF-2 and SolSep NF010206 membranes

	GMT-oNF-2	SolSep NF010206
T_{max} (ºC)	80	120
p_{max} (bar)	35	20
separation characteristics	R(93%) ~327 Da	R(95%) ~300 Da
solvents	alkanes, aromatics, alcohols, ethers, ketones	alcohols, esters
type	silicone polymer-based composite type	not available

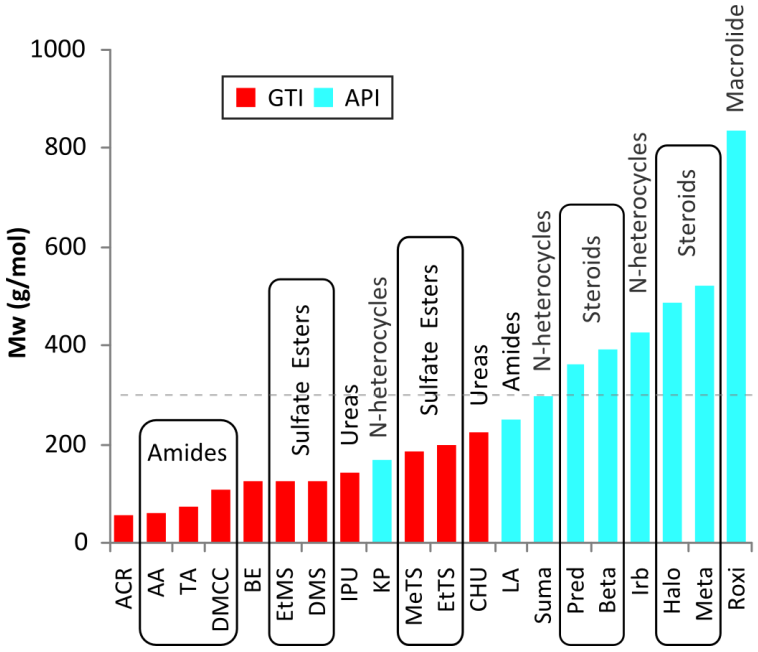

Figure 7 – Molecular weight of the selected model compounds. The dotted line indicates a Mw of 300 Da.

Hybrid processes featuring OSN and adsorbents has been developed for the removal of palladium catalysts from post-reaction solutions[110]. The Suzuki post-reaction solution was subjected to OSN, the palladium being retained by the membrane whilst the API was collected in the permeate. In a consecutive step the genotoxic palladium level was reduced further by using commercially available adsorbents. In a similar fashion a hybrid OSN-MIP process has been evaluated in the thesis for API degenotoxification. It should be mentioned, that besides pharmaceutical purification, control of genotoxins is also an environmental concern. Nanofiltration featuring DESAL 51 HL, DESAL 5 DL, UTC-20, UTC-60 membranes was applied for the removal of genotoxic atrazine – banned as a total herbicide in Europe since 1991 – from different water matrices including distilled water, tap water and river water[111].

Since StarMem membranes were first used in large-scale solvent recovery in the MAX-DEWAXTM lube dewaxing process in 1998[112], several other applications have been reported in both academic studies and industrial applications. These studies used the membranes listed above to develop different applications, including solvent recovery[113,114], purifying products[115], assisting chiral separations[116], recycling catalyst[110,117,118,119] and ionic liquids[120,121,122,123] performing solvent exchange operations[124,125] and developing membrane bioreactors[126]. The fundamentals of solute and solvent transport across these membranes have

been exhaustively studied and mathematical models have been developed[127,128,129,130,131,132,133]. Therefore, it is believed that OSN is becoming a mature technology, soon to be ready to be implemented by the pharmaceutical industry to solve challenges such the one targeted in the present thesis. A general scheme of OSN based API purification is demonstrated in Figure 8.

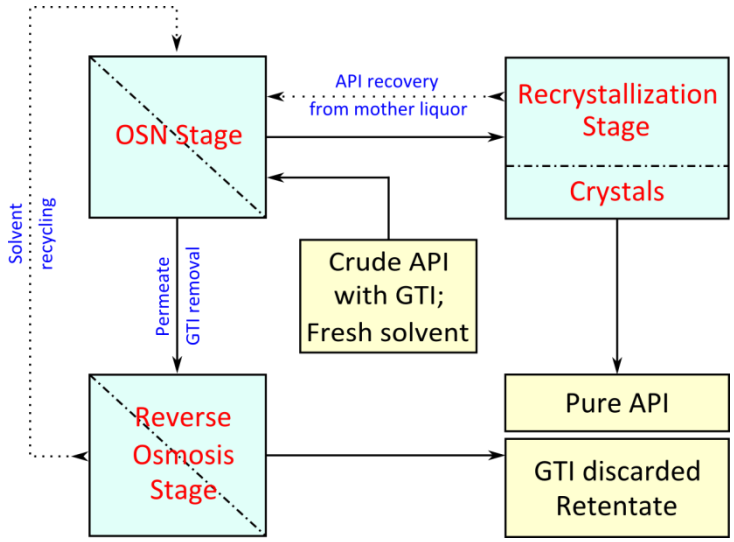

Figure 8 – Scheme of OSN based API purification, with potential use of organic reverse osmosis for solvent recycling

1.6. Molecular imprinting

The use of MIPs for separations in the pharmaceutical industry and in bio- and pharmaceutical analysis have been previously suggested[134,135]. Exploring the high specificity achieved by MIPs, several studies have evaluated their use for chiral separations[136,137,138]. Nevertheless, degenotoxification of APIs by means of molecular imprinting is currently being evaluated and the first publications on the topic are just recently materializing[62,139,140,141]. A possible limitation of the use of molecular imprinting for GTI removal is the need to develop specific MIPs for each individual GTI – or groups of GTIs – hence this technique has not become widespread at this time.

1.6.1. Concept of molecular imprinting

Molecular imprinting is a versatile technique for the preparation of intelligent materials featuring selective recognition behavior towards an analyte[142]. The active sites of the selective cavities are formed by monomers which can be specifically functionalized or by simple,

commercially available monomers. The most common types of MIPs have specific binding sites capable of reversible non-covalent interactions with target species. The formation of selective cavities is the result of the coordinating effect of the template molecule resulting from complementary functionalities and topographies.

The continuous development of molecular imprinting technology has been ascribed to several factors including (i) the wide range of chemical classes utilized as templates from acetamide[63], the simplest and smallest molecule to be imprinted through to the complex structures of proteins[143], and (ii) its diverse applicability to a number of research fields such as analytical[144], biocatalytical[145] and preparative purification[141,146] technologies. The most important factors affecting the success of imprinting have been recently reviewed[147] being temperature, pressure, type of initiation, magnetic field, solvent, dilution ratio, polymerization time and the pre-polymerization complex of which the latter is in focus during the molecular imprinting investigation part of the present thesis. 1,3-diisopropylurea (IPU), methacrylic acid (MAA), ethylene glycol dimethacrylate (EDMA) and 1,2,2,6,6-pentamethylpiperidine (PMP) were used during the preparation of the novel MIPs as potentially genotoxic template, functional monomer, cross-linker and base respectively (Figure 9).

Although the ingredients are all relatively simple organic molecules as depicted in Figure 10, the IPU-MAA-PMP pre-polymerization complex system is more intricate than it immediately seems. The principal interaction of interest among the ingredients is not of a simple acid-base nature and the formation of higher-order complexes was also observed by NMR, and for the first time in the imprinting field, it has been treated numerically. The latter, high order complexes lead to binding site heterogeneity, an important and often unwanted phenomenon in molecular imprinting. Exploring these properties is believed to be of significant interest to molecular imprinting research as they have consequences on binding site fidelity.

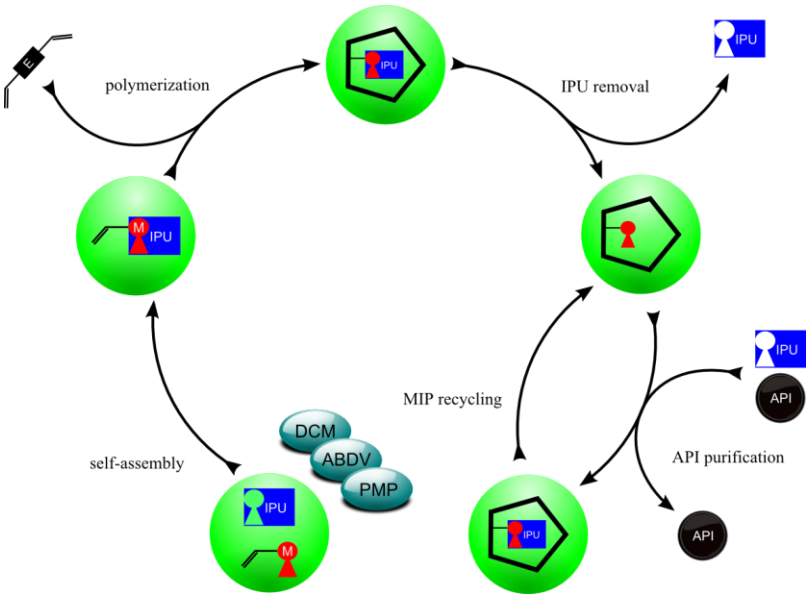

Figure 9 – The concept and application of IPU imprinting

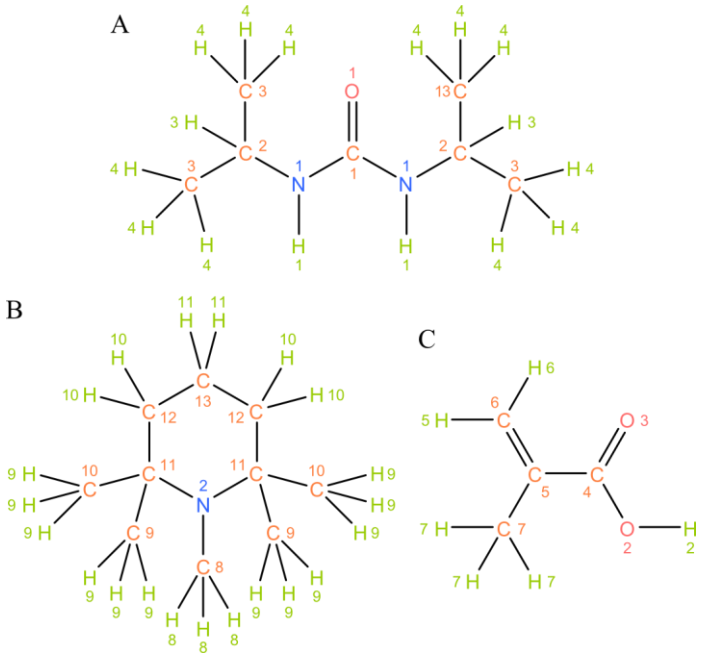

Figure 10 – Structure and atom numbering of the complexation system: IPU (A), PMP (B), MAA (C)

1.6.2. Investigation of complexes in the pre-polymerization solution

Investigation of the functional monomer – template complexes in the pre-polymerization solution and recognition phenomena of MIPs is of significant importance for a deeper understanding of the imprinting phenomena. Due to practical difficulties of molecular scale

investigation of MIP suspensions (solid-liquid interface) where the rebinding of the analyte takes place, the generally accepted procedure is to study the pre-polymerization solution. The basis for this simplification is based on the following. The nature of imprinting can be summarized in the statement that the strength and type of interactions between the functional monomers and template in the pre-polymerization mixture is preserved in the polymer matrix and will determine the recognition behavior of the scavengers so prepared. It is assumed that after the self-assembly, the pre-polymerization complexes formed will somehow survive the polymerization stage and their structure will be preserved in the scavenger, hence the name: molecularly imprinted polymer[148]. Therefore, it is important to investigate the crucial interactions between IPU, MAA and PMP in terms of binding strength, binding stoichiometry and geometry. DCM and chloroform were chosen as solvents for the present studies because (i) they do not interfere significantly with hydrogen bonding, (ii) DCM was used as a porogen for MIP preparation and (iii) the degenotoxification of APIs is also carried out in DCM. The importance of the cross-linking monomer and the initiator on host-guest complexation in pre-polymerization systems has been argued,[149] but for the simplification of the otherwise already complicated higher-order complex system, a decision to exclude the cross-linker and the initiator from the complexation study was made.

1.6.3. Role of NMR and FTIR in the imprinting field

NMR titration is a relatively common method for the determination of binding constants in the field of host-guest chemistry. In most cases due to fast-exchange complexation, NMR signals of the complexes and the initial compounds do not appear separately but as their average. Several tutorials, educational articles and some computer codes have been published on the evaluation of NMR titration data. Most of the articles focus only on 1:1 complexes[150,151,152] and the literature is limited on detailed studies of higher order complexes such as 1:2 complexes[153,154,155,156,157]. Furthermore, articles dealing with the recognition behavior of molecularly imprinted polymers tend to ignore higher order complexes and, even in those cases where the experimental data of the continuous variation method showed deviation from 1:1 complexes, the binding constant calculation methods were based on the assumption of a 1:1 complexes[158,159]. One of the main interests of the complexation study of the thesis is to study the strength and formation mechanism of 1:1 and 1:2 pre-polymerization complexes. The continuous variation method (CVM) – also called Job plot or Job's method)[150,160] – can only be applied to obtain the stoichiometry of a complex, without

introducing further approximations[161], in the case of a one-step complexation event. The evaluation of NMR titration data in most cases needs non-linear curve fitting methods and thus several approaches were proposed to address the challenge of high sensitivity to initial parameters. An insightful overview about such approaches was published by Fielding for 1:1 complexes[162]. The popular graphic methods for determination of association constants referred to as the Benesi-Hildebrand (Hanna-Ashbaugh) method[163,164]; the Scatchard (Foster-Fyfe) method[165] and the Scott plot[166] require not just 1:1 complexation but also a pseudo-first order reaction, which means that the compound with constant concentration during the titration should be in large excess compared to the titrating compound. The Rose-Drago method[167,168] anticipates only 1:1 complexation. NMR calculation methods for 1:2 complexes are scarce in the literature[169,170] and apparently have never been applied in the imprinting field.

Self-association of amides is a constraining factor in the interpretation of NMR data. These have been investigated by dielectric permittivity measurements, osmometric[171] and relaxation time NMR techniques[172], infrared spectroscopy[173] and modeling studies[174] focusing mainly on qualitative aspects. Although self association is rarely considered in the articles dealing with NMR titrations, in the present study it is an integral part of the NMR titration data evaluation. Given the fact that self association is noteworthy only at higher free IPU concentrations, it has an impact mostly at lower total MAA concentrations where the complexation reaction is not dominant.

It is worth pointing out the inconsistencies of host-guest denomination in the literature. The host and guest are denominated according to chemical aspects. Usually, these denominations are used in articles dealing with multidentate ligands (e.g. crown ethers) or molecules that are precursors of complex systems (e.g. receptors) and are considered the hosts. This type of denomination is not used in studies of lanthanide induced shifts. Some of the articles define guest as the compound whose chemical shift is followed during the titration[152,162] while other articles measure the chemical shift of the host whilst varying the guest concentration[150,169]. Host-guest denomination is not relevant for 1:1 complexation, however there can be ambiguities in the understanding of the difference between 1:2 or 2:1 complexes. In the present paper, since the MAA is the precursor of the imprinted scavengers, the IPU and MAA are considered to be the guest and the host, respectively.

Infrared spectroscopy is only partly applicable in the investigation of the binding properties of weak complexes, however it can provide useful information about the vibrations at the binding site, thus giving additional proof for the complexation. Hence, the measurement of the complex FTIR spectra and the FTIR spectra of the initial compounds were recorded and analyzed.

1.6.4. In silico approaches to understand molecular imprinting phenomena

As stated in the disclaimer, the quantum chemical calculations were carried out by Peter Pogány (Department of Analytical and Inorganic Chemistry, Budapest University of Technology and Economics) as part of a collaboration. Hence, the thesis discusses only the most important and relevant findings of his work related to the complexation event in the pre-polymerization solution. In recent years computational modeling has been developed to the point where a broad range of spectroscopic parameters such as vibrational frequencies, electronic transition energies and geometric structures can be computed with a high degree of accuracy. Parallel to these experimental methods, the interactions between the template and the functional monomer or the polymer were explored by simple statistical mechanics[175,176], molecular mechanics (MM) and semiempirical methods[177,178], density functional theory (DFT) and *ab initio* static methods[179,180,181,182] coarse grained molecular dynamics (MD)[183] and classical MD calculations[149,184]. In the earlier studies the statistical and the MM/classical MD studies are predominant and quantum chemical methods have only been applied in recent years, resulting from the rapid development in computational power. In silico studies on imprinted polymers themselves and not the pre-polymerization solution are scarce due to (i) high demand on computation and time because of the complexity of the system, (ii) the need for restrictive assumptions leading to the loss of information at molecular scale[183,184]. The *ab-initio* and DFT methods are suitable for modeling the chemical interactions between the monomers and templates, describing their binding properties and stability. In most of the articles this method was chosen for making a functional monomer screening.

The quantum chemical studies use mostly localized atomic orbitals, hence for calculating the complex formation energies for systems with weaker bonds (H-bonds, dispersion forces) the consideration of Basis Set Superposition Error (BSSE) is inevitable. Since the primary interest in the complexation study is the binding characteristics of the template-monomer system, which was studied also with NMR, static DFT was chosen to meet these expectations.

The effect of solvent is crucial in the complexation process, since it can change the interactions for the complex formation (H-bonds, ionic, hydrophobic interaction). The present study illustrates how theory can be used as a complement to spectroscopy and rebinding studies to enhance the accuracy of deductions.

2. Materials

Active pharmaceutical ingredients Sumatriptan, Prednisolone, Betamethasone, Halobetasole propionate, Mometasone furoate and Roxithromycin were provided by Hovione whilst Lacosamide and Keppra were kindly provided by UCB and Irbesartan was purchased from Jiacheng-Chem Enterprises Ltd. The potentially genotoxic impurities methyl tosylate, dimethylsulfate, acetamide, thioacetamide, dimethyl carbamoyl chloride, 1,3-dicyclohexylurea, acrolein and 2-bromoethanol were purchased from Sigma-Aldrich while ethyl tosylate and 1,3-diisopropylurea were purchased from TCI Europe and Hovione, respectively. Ingredients for the molecularly imprinted polymers such as methacrylic acid, ethylene glycol dimethacrylate and 1,2,2,6,6-pentamethylpiperidine were purchased from Sigma-Aldrich. Solvents dichloromethane, methanol, methyl isobutyl ketone, ethylacetate, methyl ethyl ketone and tert-butylmethylether were purchased from Merck. Deuterated chloroform was purchased from LaborSpirit. Hydrochloric acid, ammonium hydroxide, 4-dimethylaminopyridine, tetrahydrofuran and 2,2'-azobis(2,4-dimethylvaleronitrile) were purchased from Fluka and Wako, respectively. Methanol, TLC aluminium sheets (Silica Gel 60 F254) and Silica Gel 60 powder was purchased from Merck. Shirasagi DC32 charcoal was purchased from Mitsubishi.

Before use, EDMA was first washed with 10% aqueous NaOH, water, brine and then water in this order. The EDMA was then dried with $MgSO_4$ and distilled under vacuum. Anhydrous solvents used for MIP preparation, rebinding tests, NMR studies were stored over molecular sieves under inert atmosphere. HPLC grade water was obtained from a Millipore Milli-Q-Gradient ultrapure water system (Millipore, Billerica, MA, USA). The other chemicals were used as received and were of reagent grade or higher.

SolSep NF010206, GMT-oNF-2, MPF-44 were purchased as flat sheet nanofiltration membranes from SolSep, Borsig Membrane Technology and Koch Membrane Systems, respectively.

3. Methods

3.1. DoE approach for GTI quantification

3.1.1. Instrumentation LC-MS/MS

LC-MS/MS measurements were carried out on High Performance Liquid Chromatograph Waters model Alliance 2695 (Milford, MA, USA) equipped with gradient pump, autosampler and PDA Waters 2996 UV detector. Triple Quadrupole Mass Spectrometer for Liquid Chromatography Micromass model Quattro Micro (Manchester, UK) equipped with an electrospray source was employed as the MS detector. A LaPrep P206 VWR International LLC valve (Carnaxide, Portugal) was placed between the UV and MS detector as divert valve to avoid sending the highly concentrated API to the MS detector. The control of the system was carried out on MassLynx V4.1 acquisition software and data collection and processing was handled by QuanLynx module. Before use, tuning was carried out by flow injection analysis (FIA) in positive electrospray ionization (ESI) mode using Micromass ESI tuning mix part #700002646.

3.1.2. Operating conditions LC-MS/MS

Phenomenex Gemini-NX 3μm C18 110Å 50x2.00 mm column was used with a flow rate of 0.5 $mL.min^{-1}$, with detection in the range of 190 to 400 nm. Eluent A was 0.1% formic acid in water and eluent B was 0.1% formic acid in acetonitrile. The gradient was linear from 40% to 70% B in 4 min, followed by 70% B hold for a further 1 min and a re-equilibration period of 5 min. The column temperature was 25 ºC and injection volume was 26 μL. Electrospray in positive mode was used with MRM monitoring for m/z 123>107 transition for DMAP. The capillary (kV), cone (V), extractor (V), ion energy (V) and collision energy (eV) were 0.2, 35, 3, 0.3 and 30, respectively. The LM and HM resolutions were 13.5 for both quadrupoles. Ion energy for the second quadrupole was 1.5 V. The source temperature, desolvation gas temperature (ºC) and gas flow ($L.min^{-1}$) were 120, 500 and 350, respectively.

3.1.3. Standard solution and sample preparation

20 $mg.mL^{-1}$ concentrated stock solution of DMAP was prepared by dissolving the compound in acetonitrile. The 0.2 $mg.mL^{-1}$ diluted stock solution was prepared by diluting 100 μL of the 20 $mg.mL^{-1}$ concentrated stock solution to 10 mL with acetonitrile. The 0.5 $\mu g.mL^{-1}$ diluted stock solution was prepared by diluting 250 μL of the 0.2 $mg.mL^{-1}$ diluted stock solution to 100 mL with acetonitrile. The working standard solution was prepared by accurately weighing about 125 mg of Mometasone furoate into a 25 mL volumetric flask and making up the solution to the graduation mark after adding 250 μL of the 0.5 $\mu g.mL^{-1}$ diluted stock solution to give 5 $ng.mL^{-1}$ and 5 $g.L^{-1}$ DMAP and Mometasone furoate absolute concentrations respectively which correspond to 1 ppm DMAP contamination relative to the drug substance. The working standard solutions were shaken to dissolve the API and homogenize the solution and were always freshly prepared just prior to injection. The DMAP samples for validation at 0.01, 0.05, 0.1, 0.5, 1, 2 , 3, 5, 7, 10 ppm concentrations relative to the API were prepared in the same manner using the 0.5 $\mu g.mL^{-1}$ diluted stock solution. DMAP standard solutions are prepared in 5 $g.L^{-1}$ Mometasone furoate concentration. Although higher concentrations would further increase the DMAP detection limit, in order to prevent possible matrix effects such as analytical column overloading – which can cause loss of sensitivity – the 5 $g.L^{-1}$ concentration was maintained throughout the study.

3.1.4. Design of experiments

The software Modde 9.0.0.0 by Umetrics was used to generate the sequence of runs and the data collected were investigated using regression analysis. This gave a model – relating the changes in the factors to the changes in responses – which indicated the important factors and their combination in influencing the responses. All of the five factors were studied simultaneously, namely flow, gradient and injection volume as LC factors and cone voltage and collision energy as MS factors. The LC-MS/MS method was optimized with respect to four responses, namely separation between peaks (i.e. difference between the retention time of the API and DMAP), peak area, length of the analysis and the signal to noise ratio (S/N). A central composite face (CCF) design – with 26 runs and 3 center points – was created and the modeling results using a quadratic model were converted into response contour plots which were used to clarify where the best operating conditions are to be expected. After the

determination of the analytical method, its robustness around the optimal conditions was evaluated applying a fractional factorial (FF) of resolution III with 8 runs and 3 center points further taking into account column temperature as well as quadrupole resolution besides the five factors previously mentioned.

3.1.5. Validation study

To demonstrate the accuracy of the developed method, validation was performed. The assessed parameters during validation were limit of quantification (LOQ), limit of detection (LOD), linearity, system precision and DMAP recovery of spiked samples. LOQ was established by injecting in the LCMS system various DMAP concentrations ranging between 0.01-15 ppm and recording their S/N ratios. The lowest concentration corresponding to S/N ≥ 10 was selected as LOQ and LOD was considered as 3/10 of LOQ, since the adopted criteria for this parameter is S/N ≥ 3. To validate these concentrations, two independent sample preparations at LOQ and LOD concentrations were carried out and were injected three times. The average result (x) is calculated by summing the individual results and dividing this sum by the number (n) of individual values as shown in equation 1. The standard deviation (SD) is a measure of how precise the average is, i.e. how well the individual numbers agree with each other. It is calculated as shown in equation 2. The relative standard deviation (RSD) is defined in equation 3 and expressed in percentage and is obtained by multiplying the standard deviation by 100 and dividing this product by the average. The suitability of the method was assessed by calculating the RSD for the above mentioned consecutive six injections of LOQ and 10xLOQ concentration. Linearity was performed by determining the correlation factor for a six point calibration curve, ranging between LOQ and 10xLOQ concentrations. DMAP recovery in spiked samples was studied at three different concentration levels of the calibration curve corresponding to LOQ, 5xLOQ and 20xLOQ. For each concentration level independent sample preparations were carried out giving six samples at the LOQ level and three at the other two levels. The apparent recovery (AR) is defined in equation 4 and it was determined by comparing the concentration of the spiked sample obtained (observed value → Q_o) with the concentration of the spiking standard (reference value → Q_y). The definition of these analytical terms follows the recommendation of the International Union of Pure and Applied Chemistry[185].

$$\bar{x} = \frac{\sum x_i}{n} \quad \text{(eq. 1)}$$

$$SD = \sqrt{\frac{\sum (x_i - \bar{x})^2}{n-1}} \quad \text{(eq. 2)}$$

$$RSD = 100\frac{SD}{\bar{X}} \quad \text{(eq. 3)}$$

$$AR = \frac{Q_y}{Q_o} \quad \text{(eq. 4)}$$

3.2. NMR titrations, continuous variation method and FTIR

The ^{1}H NMR spectra were recorded on a Bruker Avance III 400 spectrometer operating at 25 ºC within a deviation of 0.2 ºC. Chemical shifts (δ) are reported in ppm, with respect to the solvent peak of deuterated chloroform being 7.26 ppm[186]. The following abbreviations are used in the discussion: s = singlet, d = doublet, t = triplet, q = quadruplet, m = multiplet, bs = broad singlet. The solvent was kept under molecular sieves and handled under inert atmosphere in order to avoid contamination of the system with water which disrupts the intramolecular hydrogen bonds. For the self-association NMR experiments 1 mM, 2.5 mM, 5 mM, 7.5 mM, 10 mM, 20 mM, 30 mM, 40 mM IPU working solutions were prepared in $CDCl_3$. Additionally, three sets of CVM were also performed for obtaining the stoichiometry of the complex. During the CVM, the host/guest molar ratio was varied between 0 and 1 while their total concentration was kept constant at 20 mM. In CVM1 the host was MAA, in CVM2 the host was MAA:PMP (1:1), while in CVM3 the PMP is proportional to IPU and not to MAA being MAA:PMP (1:1). Furthermore, four sets of NMR titrations were carried out where IPU was titrated with MAA: T1 (5 mM IPU) and T2 (10 mM IPU) were performed in the absence of PMP, while T3 (5 mM IPU) and T4 (10 mM IPU) were performed in the presence of PMP. In order to study the effect of concentration, the T1 and T3 were performed at 5 mM IPU concentration, while T2 and T4 were performed at 10 mM IPU concentrations. The solutions were agitated to dissolve the IPU and homogenize the solution and were always freshly prepared just prior to analysis. The room temperature Fourier transform infrared (FTIR) spectra of 20 mM IPU and corresponding 20 mM IPU:MAA (1:1) complex were measured in DCM, in the 4,000-400 cm^{-1} region at a resolution of 4 cm^{-1}, using an IRAffinity-1 spectrophotometer from Shimadzu (model 2011).

3.3. Solid phase characterization of the scavengers

Elemental Analysis was performed at the Department of Organic Chemistry, Johannes Guttenberg Universität Mainz using a Heraeus CHN-rapid analyzer (Hanau, Germany). The percentage by mass of carbon, hydrogen and nitrogen of the polymers were calculated by equation 5.

$$\text{Mass} = 100\text{Aw} \cdot \sum_{i=1}^{3}\left(\frac{N_i \cdot n_i}{\sum_{i=1}^{3} n_i}\right) \cdot \sum_{i=1}^{3}\left(\frac{Mw_i \cdot n_i}{\sum_{i=1}^{3} n_i}\right)^{-1} \qquad \text{(eq. 5)}$$

where Aw is the standard atomic weight of element C, H or N; N_i is the number of C, H or N atoms of the ingredient *i* in the scavenger; n_i is the number of moles of ingredient *i* and Mw_i is the molecular weight of ingredient *i*. Ingredients considered during the calculation were MAA, EDMA and 2,2'-azobis(2,4-dimethylvaleronitrile) ABDV. The morphological analyses were carried out on a Morphologi G2 Model MOR5110 equipped with a sample dispersing unit. Nitrogen sorption measurements were performed on a Quantachrome Autosorb 6B (Quantachrome Corporation, Boynton Beach, FL) automatic adsorption instrument. Prior to measurements, 100 mg samples were heated at 80 °C under high vacuum (10-5 Pa) for at least 16 h. The specific surface areas (A_{SS}) were evaluated using the BET method, the specific pore volumes (V_{po}) were evaluated following the Gurvitch method, and the average pore radius (r_{po}) was evaluated using the Barret-Joyner-Halenda (BJH) theory using the desorption branch of the isotherm. The calculations related to the BET theory are as follows:

$$\frac{1}{v\left[\left(P_0/P\right)-1\right]} = \frac{(c-1)\cdot P}{v_m \cdot c \cdot P_0} + \frac{1}{v_m \cdot c} \qquad \text{(eq. 6)}$$

is the BET equation where v is the adsorbed gas quantity, P and P_0 are the equilibrium and the saturation pressure of nitrogen at the temperature of adsorption, v_m is the monolayer adsorbed gas quantity and c is the BET constant. Total surface area (A_{total}) and specific surface area are calculated based on equation 7 and 8, respectively.

$$A_{total} = \frac{v_m \cdot N \cdot s}{V} \qquad \text{(eq. 7)}$$

$$A_{SS} = \frac{A_{total}}{a} \qquad \text{(eq. 8)}$$

were N is the Avogadro´s number, s is the adsorption cross section of the adsorbing species, V is the molar volume of nitrogen gas and a is the mass of nitrogen. The pore volume calculated using the BJH equation[187]:

$$r_{po} = r_K + t \qquad \text{(eq. 9)}$$

$$V_{po} = V_K + \frac{r_{po}^2 \pi}{r_K^2 \pi} \qquad \text{(eq. 10)}$$

where r_p is the pore radius, r_K is the Kelvin radius, t is the thickness of the film and V_K is the Kelvin volume.

Fourier transform infrared (FTIR) spectroscopy was performed using a NEXUS FTIR spectrometer, with samples prepared in KBr disks. Thermal stability tests of the polymers were performed by thermal gravimetric analysis (TGA) Q50 TA instrument. 10 mg samples were placed on a platinum pan, which was heated with a heating rate of 10 °C.min^{-1} from 25 °C to 1,000 °C, under N_2 atmosphere and the % mass loss measured along with the respective temperature. Microscopy was carried out for visualization of polymeric particles and morphology. To estimate the average circularity[I], spherical equivalent volume[II], convexity[III] and light intensity, mean[IV] morphological analyses were carried out on a Morphologi G2 Model MOR5110 equipped with a sample dispersing unit. Each sample was prepared using the sample dispersing unit of the equipment applying the following conditions: injection pressure: 2 bar, injection time: 0.4 seconds, total cycle time: 2 min, sample size: 5 mg. The samples were visualized applying several lenses.

[I] Circumference of circle of equivalent area divided by the actual perimeter of the particle. A circularity of 0 corresponds to a cubic shape and 1 to a perfect sphere.
[II] SE is calculated on the basis of the diameter of a circle with the area of the particle image projected area.
[III] Convexity is a measure of the surface roughness of a particle and is calculated by dividing the convex hull perimeter by the actual particle perimeter.
[IV] The intensity mean is the average of the pixel grayscale levels ranging from 0 (black) to 255 (white). The average number of particles analyzed with morphology is 3378.

3.4. Nanofiltration methods and mathematical framework

The METcell Cross-Flow System, purchased from Evonik MET, consists of high-pressure filtration cells suitable for reverse osmosis and nanofiltration, an organic solvent compatible gear pump and a tank base. A total of 500 mL of solution is circulated between the tank and the filtration cells and filtration takes place in cross flow mode. The appropriate pressure is insured by a Nitrogen cylinder and a fine tuning pressure gauge. An HPLC pump is connected to the tank during diafiltration in order to keep constant the volume of filtration. The membranes were preconditioned by filtering ~300 mL pure solvent through each membrane piece (52.8 cm^2), until a constant solvent flux was obtained. Rejections were estimated at 10, 20 and 30 bar using single solute solutions of API and GTI at concentrations of 10,000 ppm for the APIs and 1,000 ppm for the GTIs in the respective solvent (THF, MEK or DCM). Exceptions are CHU and Suma solutions in MEK, they were prepared at concentrations of 500 ppm and 2,000 ppm, respectively due to their lower solubility limits. Feed volumes of 500 mL were used. Duplicate assays were carried out using the same sheet of membrane to estimate each rejection and the values reported are averages of the two values obtained. Rejection values (R_x) were always calculated on the basis of the concentrations of compounds measured in the feed ($C_{F,x}$) and in the first 50 mL permeate ($C_{P,x}$) – based on equation 11 – which corresponds to a feed volume decrease of only 10% and thus no significant increase in solute concentration is expected on the retentate side during filtrations. Still, retentate concentrations ($C_{R,x}$), were also measured at the end of the filtrations to close the solute mass balance.

$$R_X = 1 - \frac{C_{P,x}}{C_{F,x}} \qquad \text{(eq. 11)}$$

Rejections were estimated based on bulk concentrations and thus rejections reported are apparent parameters that will vary with concentration and hydrodynamics, according with several factors, such as the existence of concentration polarization at membrane interface and activity constants of solutes. However, following the simplistic approach from the literature, rejections were assumed constant during the diafiltration in order to estimate the diafiltration performance. During the diafiltration assays, the feed solutions were API and GTI mixtures (two solute system) in the selected solvent at concentrations of 10,000 ppm and 1,000 ppm,

respectively. The HPLC pump rate was adjusted to add fresh solvent volumes (V_{ADD}) to compensate the permeate volume (V_P) by keeping the retentate volume constant at a value of 500 mL, equal to the feed volume (V_F) over the entire operation. $C_{F,x}$ were measured after thoroughly mixing the feed solution in the METcell system using a gear pump, just prior to the start of the nanofiltration. The diafiltration was interrupted periodically, at permeation of each 500 mL, to take aliquots of the retentate and permeate solutions. Mass balances were closed at each step and the API losses and GTI removals were estimated.

As mentioned earlier, in diafiltration operational mode V_R is kept constant and thus $V_P = V_{ADD}$. Therefore, assuming a constant rejection and simple mass balances the concentration of the solutes in the permeate and retentate can be calculated as function of the permeate volume. Taken into account infinitesimal small amounts of permeate volumes V^i_P and the respective concentrations of solute in such permeate volume, as well as retentate concentrations at such time period, the following equations are established:

$$C_{R,t=0} = C_F \qquad \text{(eq. 12)}$$

$$C^i_{P,x} = \left(1 - R_x\right) C_{R,x} \qquad \text{(eq. 13)}$$

$$V_F C^i_{R,x} = \frac{V_F}{C^i_{R,x}} - \frac{V^i_P}{C^i_{P,x}} \qquad \text{(eq. 14)}$$

Considering that (i) the total volume collected at each instant of the diafiltration is actually the sum of all the V^i_P that permeates through the membrane until that time, and (ii) the measured concentration of the permeate is the result of the solute content in each of the V^i_P elements, equation 15 and 16 can be derived in each point:

$$V_P = \sum V^i_P \qquad \text{(eq. 15)}$$

$$C_{P,x} = \sum V^i_P C^i_{P,x} \qquad \text{(eq. 16)}$$

On the other hand, since the volume of retentate is kept constant, the retentate concentration can be derived directly as given in equation 17.

$$C^i_{R,x} = C_{R,x} \qquad \text{(eq. 17)}$$

The API loss and GTI removal are estimated on the solute concentration in the feed solution and in the retentate as given in equation 18 and 19.

$$\text{API loss} = \frac{V_R \cdot C_{R,API}}{V_F \cdot C_{F,API}} = \frac{C_{R,API}}{C_{F,API}} \quad \text{(eq. 18)}$$

$$\text{GTI removal} = 1 - \frac{V_R \cdot C_{R,GTI}}{V_F \cdot C_{F,GTI}} = 1 - \frac{C_{R,GTI}}{C_{F,GTI}} \quad \text{(eq. 19)}$$

Diavolumes (D), reflecting the solvent intensity of the OSN process, are reported based on equation 20.

$$D = \frac{V_{add}}{V_F} = \frac{V_P}{V_F} \quad \text{(eq. 20)}$$

The higher the number of diavolumes, the higher the amount of GTI pushed thought the membrane, but also the higher the API loss and solvent used in the processes contributing to higher solvent consumption. Thus, the number of diavolumes should be selected carefully taken into account the required GTI removal by its toxicity limits and economically acceptable loss of API.

The calculated values based on the equation system above match the previously established analytical expression reported in the literature[188] as equation 21.

$$C_{R,x} = C_{F,x} \exp\left[\frac{-V_P\left(1-R_x\right)}{V_F}\right] = C_{F,x} \exp\left[-D\left(1-R_x\right)\right] \quad \text{(eq. 21)}$$

Solvent fluxes (Φ) were estimated on the basis of membrane area (A_m) and filtration time (t) in duplicated experiments as given in equation 22. From a process economics perspective, solvent fluxes define a compromise on membrane area to be applied and operation time, respective associated costs and logistics.

$$\Phi = \frac{V_P}{A_m \cdot t} \quad \text{(eq. 22)}$$

3.5. IPU selective MIP preparation

IPU was used as template during the preparation of MIPs, but absent during the preparation of control polymers labeled as non-imprinted polymers (NIPs). Table 3 summarizes the composition of the different scavengers prepared. MAA (1.2 mmol, 0.102 mL) was dissolved in DCM (2.25 mL), which functions both as porogen and solvent. PMP (0.3 mmol, 0.054 mL) was added to MIP2 and corresponding NIP2 polymerization mixtures. For the MIP preparation, the IPU template (0.3 mmol, 43 mg) was added to the MAA solution and left for 5 min. EDMA cross-linker (6 mmol, 1.133 mL) and the initiator ABDV (1 weight% of total monomers) were added to the polymerization solution, which was purged with a flow of dry nitrogen. The polymerization tubes were sealed and the polymerization was initiated by placing the tubes in a thermostat at 40 °C. After 12 hours the temperature was increased to 60 °C for an additional 12 hours to complete the polymerization. The polymerization tubes were then broken and the polymers gently mashed using a pestle and mortar. The template was thereafter extracted quasi quantitatively in a Soxhlet-apparatus with a solution of 0.1 M HCl in methanol for 48 hours. The remaining acid in the polymers was then washed out with methanol using a Soxhlet-apparatus during 24 hours. This was followed by further mashing and sieving (Resh stainless steel sieves), whereby the 25-50 μm fraction was used to evaluate the binding properties of the polymers. The polymers were dried under vacuum in the oven overnight at 40 °C. The same fraction was used for the chemical and morphological characterization of the scavengers. Quantitative analysis of the washing and extraction steps indicated almost complete template removal (>98%). The non-imprinted polymers were prepared in the same way as described above, but with the omission of the template molecule from the pre-polymerization solution.

Table 3 - Composition of IPU selective scavengers

	composition	stoichiometry	method	comment
MIP1	IPU/MAA/EDMA	0.1/0.4/2		with IPU
MIP2	IPU/PMP/MAA/EDMA	0.1/0.1/0.4/2	ABDV	with IPU and PMP
NIP1	MAA/EDMA	0.4/2	40-60°C	without IPU not PMP
NIP2	PMP/MAA/EDMA	0.1/0.4/2		without IPU but with PMP

3.6. Swelling experiments

Swelling is measured by allowing a given volume of dry polymer, with a known particle size and weight, to equilibrate in a solvent. For comparison purposes the swelling of all scavengers was estimated. 100 mg polymer with 25-50 μm diameter was placed in narrow vials, each was loaded with 2 mL of the following solvents: DCM, MIBK, MeOH and a solution of 0.1 M HCl in methanol. The mixtures were stirred and left to stand overnight to reach equilibrium at which point the polymer does not absorb more solvent. The bulk volumes of the dry and swollen particles were calculated based on the height and diameter of the particle bed in the vial, and used to estimate the volume swelling ratio (VSR) as given in equation 23.

$$VSR = \frac{V_{swollen}}{V_{dry}} \qquad \text{(eq. 23)}$$

Since the weight and the volume of the dry particles are known, an apparent density (d_{app}) can be calculated based on equation 24.

$$d_{app} = \frac{m_{dry}}{V_{dry}} \qquad \text{(eq. 24)}$$

Specific swelling volume was calculated from the volume swelling ratio and apparent density based on equation 25.

$$V_{swelling} = \frac{VSR}{d_{app}} \qquad \text{(eq. 25)}$$

3.7. Bulk rebinding tests

Bulk rebinding tests were carried out to (i) evaluate the IPU uptake by the scavengers in the presence of APIs and (ii) explore the effect of a deprotonating agent on the capacity and kinetics of the binding. Furthermore, a polymer titration was performed in a bulk rebinding test format in order to establish the optimal IPU/MIP ratio. All the assays were carried out in duplicates featuring 100 ppm IPU in DCM.

In order to evaluate the binding properties of the several scavengers prepared 50 mg of each polymer (MIP1, MIP2, NIP1 and NIP2) were placed in independent vials and NIP2 and MIP2 were preconditioned with 0.1 M PMP solution in DCM. The preconditioning solution was removed from the scavengers and the rest of the rinsing DCM was evaporated. 1 mL of loading solutions – consisting of 10,000 ppm Meta, Roxi or KP in DCM spiked with 100 ppm IPU – were added to each scavenger. The relative concentration of API and GTI aims to reflect the industrial scenarios where the API is highly concentrated compared to the IPU being present in lower concentrations, which makes selective removal more challenging. However, in order to evaluate the selectivity of the polymer, a solution with equimolar concentration of IPU (100 ppm, 0.7 mM) and Meta (362 ppm, 0.7 mM) was also loaded to 50 mg MIP2. During the polymer titration 1 mL of 100 ppm IPU solution in DCM was loaded on 10, 25, 50, 100, 250, 500 mg of MIP2 both in the presence and absence of PMP. When PMP was presence, the MIP2 scavenger was preconditioned as described in the previous paragraph. The bulk rebinding mixtures were gently shaken for 24 hours. Samples of the mixtures were taken before the addition of the scavengers and after 24 hours. During the kinetic studies, samples were also taken from the supernatants at 10 min and at 1, 2, 4 and 8 hours. The samples were filtered with Millipore syringe filters in order to remove any floating particles before analysis. The DCM was evaporated and the samples were dissolved and diluted using the solvent of the LCMS mobile phase. Control experiments were run as described above, but replacing the loading solution with DCM.

3.8. Solid phase extraction methods

Solid phase extraction (SPE) experiments were performed on Visiprep DL Vacuum Manifold equipped with 3 mL cartridges from Supelco (Germany) that were packed with 50 mg of MIP2 polymer between Teflon frits. Disposable liners were used in order to eliminate the possibility of cross-contamination when processing a new extraction on the same port. The scavengers were preconditioned with 1 mL 0.1 M PMP base in DCM. The mixture was left to stand for 5 min and then the preconditioning solution drained and 1 mL solution of the compounds of interest loaded on the polymers. The cartridge was sealed and the mixture was occasionally stirred during the 24-hour equilibration time. The compounds were selectively eluted from the polymers by gradient elution featuring DCM, MeOH and MIBK and the eluants were collected in separate vials. The loading solutions and eluants were analyzed by LCMS. MIP samples were regenerated by washing with 0.1 M HCl in methanol in a Soxhlet

extractor overnight. To confirm that no IPU leaches from the MIP scavenger, 50 mg MIP2 was weighed in an HPLC vial and 1 mL DCM was added and the mixture was stirred for 24 hours. The ExploraSep® SPE screening was performed based on this protocol but on the ExploraSep® Screening Plate A containing 32 scavengers and the loading solution was prepared in acetonitrile:toluene (5:95) and it was loaded to each polymer manually using multi-channel pipettes. Vacuum was gently applied to collect all the solutions. The solvent was evaporated in a Sigma Vacuum Centrifuge and the residue was taken up in the mobile phase of the LC-MS/MS. The free IPU and API content in the supernatants were determined by LC-MS/MS.

3.9. Recrystallization

10,000 ppm Meta in DCM was spiked with 1,000 ppm DMAP and MeMS, respectively. A comparative study was carried out using in each assay (recrystallization, chromatography and nanofiltration) 500 mL crude API solution. The 500 mL feed solution was submitted to recrystallization based on WO9800437 patent[92]. Before and after the purification process Meta and DMAP were quantified by HPLC and MeMS with GCMS. A 500 mL round-bottomed flask was pre-calibrated at 50 mL, and 500 mL feed solution was added in two portions. The solution was concentrated under reduced pressure to the pre-calibration mark. 100 mL methanol was added and the solution was heated to 50 ºC, and the mixture was concentrated to 50 mL. Precipitation occurred at the end of this step. Further 100 mL methanol was added, and the mixture was concentrated to 50 mL. The solution was slowly cooled to 23 °C over 1 hour and then cooled further to 10 °C, at which temperature it was agitated for 2 hours. The Meta was obtained as a crystalline solid and filtered off and washed with 2 x 20 mL methanol cooled to 10 °C. The wet cake was charged into a 500 mL round-bottomed flask pre-marked at 50 mL. 3 g of Shirasagi DC32 decolorizing charcoal, 100 mL methanol and 100 mL DCM were added, and the steroid was dissolved with stirring. The solution was heated to 50 ºC and then filtered. The flask and filter paper were rinsed with 2 x 20 mL DCM and the rinsings were combined with the solution. The combined solution was heated to 50 ºC then concentrated under reduced pressure to 50 mL yielding a slurry. 100 mL methanol was added and the mixture was concentrated under reduced pressure to 50 mL again. It was then cooled slowly to 23 °C over 1 hour and then cooled further to 10 °C, at which temperature it was agitated for 2 hours. Meta was obtained as a crystalline solid and

filtered off and washed with 2 x 20 mL methanol cooled to 10 °C. Meta was dried in a vacuum oven at 70 °C for 24 hours.

3.10. Flash chromatography

For efficient flash chromatographic separation first a thin layer chromatographic (TLC) separation was developed to obtain the desired retention factors (Rf) for Meta and the impurities i.e. to determine the eluent for flash chromatography. The optimization started with the eluent given in the US4472393 patent[93] and resulted in DCM:EtOAc (95:5) for Meta-DMAP separation where the Rf values are 0.34 and 0.05 for Meta and DMAP respectively. In pure DCM the Rf values for Meta and MeMS are 0.02 and 0.2 respectively, thus for Meta-MeMS separation a gradient elution was developed as described in Table 4. It should be noted that in the original patent chloroform was used instead of DCM, however the latter has one less chlorine per molecule and thus a lower environmental and toxic potential impact[189]. Additionally, the difference in boiling points of these two solvents is of about 12 ºC, which decreases energy requirements when recovering DCM by distillation. Notice, that chloroform has been banned in many applications, where the use of DCM is still allowed and since the dissolving power properties of these two solvents is in many cases similar, therefore replacement of chloroform by DCM is recommended[189].

Table 4: Gradient elution for the separation of MeMS and Meta

fraction #	eluent composition (DCM:EtOAc)	eluent volume (mL)
1-12	100:0	600
13-14	98:2	100
15-16	95:5	100
17-18	90:10	100
19-20	80:20	100
21-24	50:50	200

Clark Still's flash chromatographic technique was applied for the purification of the crude Meta[83]. 500 mL crude API solution was concentrated to 10% in volume, keeping the API in solution, then 10 g silica gel was added and the solvent was evaporated. A chromatography column with 50 mm diameter was filled with a slurry of 300 mL silica gel in DCM and the API-silica mixture was applied to the top of the column. Pressure was applied with Nitrogen to force the solvent through the column and keep a steady eluent flow of 50 mL.min^{-1}. 24x50

mL fractions were collected, analyzed by TLC and the ones containing mainly Meta were merged and the solvent was evaporated. Meta was dried in a vacuum oven at 70 °C for 24 hours.

4. Results and discussion

4.1. GTI analysis by LC-MS/MS via DoE approach

The model system for the present study consists of the potentially genotoxic DMAP impurity and Mometasone furoate glucocorticoid. In the absence of toxicological data for the impurity, the TTC for genotoxic impurities is used to set limits. Calculation of the limit to be applied for DMAP is as follows: the TTC value (1.5 $\mu g.day^{-1}$) divided by the maximum daily dose ($g.day^{-1}$) and the number of GTIs gives the limit in ppm to be applied to the active substance[190]. Notice, that the number of GTIs in this particular case is 2 due to the methanesulfonylation reaction step which can lead to the contamination of the API with not only DMAP but methyl methanesulfonate as well. Considering the worst case scenario where 1,000 $mg.day^{-1}$ daily dose is applied, the GTI is required to be controlled at 0.75 ppm relative in the API which determines the range in the linearity study during method validation to be 0.1-10 ppm. This analytical study aims to prove the applicability of DoE in the trace analysis of GTIs through the DMAP model impurity in glucocorticoids-type APIs, however the methodology can be applied to other type of impurities.

4.1.1. DMAP fragmentation and MS risk assessment for DoE

Trace analysis of potentially genotoxic impurities inevitably calls for high sensitivity detection which can be addressed by state-of-the-art instrumentation such as triple quadrupole mass spectrometers. Hence, MRM was selected as acquisition mode due to its high sensitivity and selectivity over conventional SIM mode. An MS detector featuring a triple quadrupole is capable of eliminating overwhelming background interference from the sample matrix which is referred to as MRM. Firstly, the target ion is selected and then further fragmented, allowing for a high degree of selectivity in which only the target ions from the potentially genotoxic impurity are detected. Although MRM acquisition results in a somewhat lower signal, the S/N ratio significantly improves due to the decrease in background interference and hence leads to much better sensitivity. Being a base, DMAP is easily protonated to give a quaternary ammonium cation, thus formic acid was added to the mobile phase as ionization agent to form the protonated species.

A Flow Injection Analysis (FIA) was carried out using a 50 ng.mL^{-1} DMAP solution in which the initial electrospray source conditions were determined for the DoE LCMS method development approach and $[DMAP+H]^+$ m/z 123 was successfully detected and selected as parent ion for MRM experiment and then fragmented in the product ion scan analysis. The FIA experiment was also used as part of the DoE risk assessment. For the successful application of DoE, it is crucial to get a response in each run, hence the operating range of the MS variables had to be chosen with care. During FIA the MS variables were varied and the product ion m/z 107 was acquired in order to establish the range of the variables where still acceptable analyte response can be detected. The quick manual tuning during FIA led to the establishment of the collision energy and cone voltage ranges as 20-40 eV, 20–50 V respectively. To address the industrial need for quick method development the number of DoE runs was limited thus the main MS parameters were chosen as DoE variables and the parameters were tuned during the FIA. Furthermore the product ion scan revealed ion m/z 107 as most favorable fragment thus transition 123>107 was selected for monitoring in MRM mode. DMAP mass spectra are displayed in Figure 11.

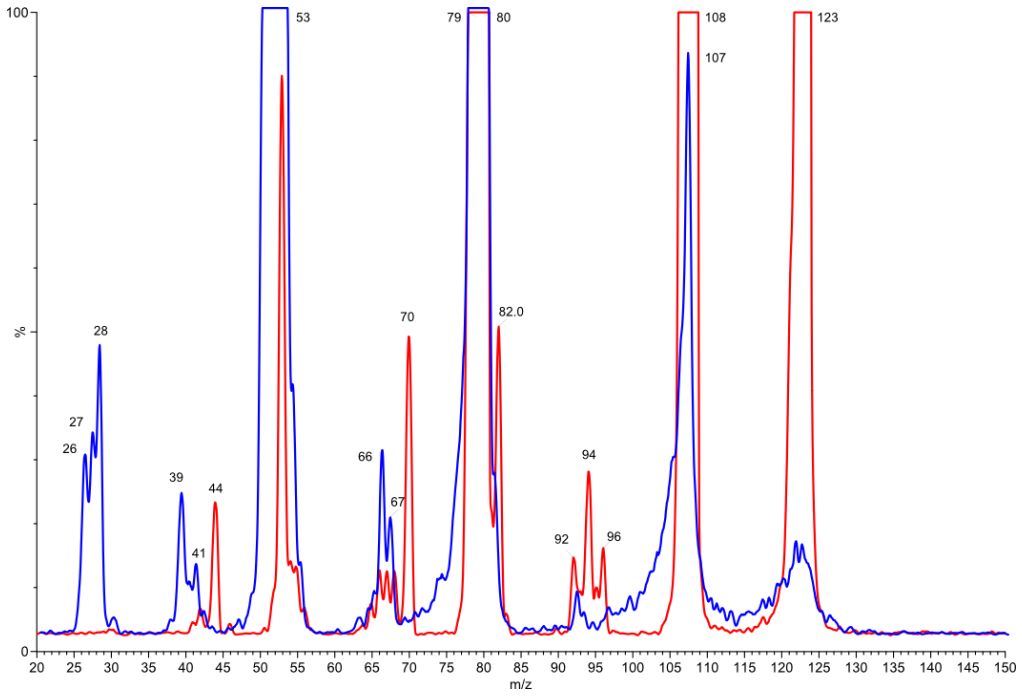

Figure 11 - Mass spectra of DMAP acquired at 20 and 60 collision energy (eV)

In Figure 12 the structures of the neutral fragment species are indicated above or below the arrows which show the resulting charged fragments and their m/z. DMAP, as an aminopyridine derivative shows both the aniline and pyridine type fragmentation routes.

Interestingly non-derivatized aminopyridines display fragmentation chemistry similar to aniline rather than pyridine, i.e. metastable HNC loss rather than stable neutral species HCN[191]. It was observed during product ion acquisition that varying the applied collision energy favors different fragmentation routes, hence 20 eV and 60 eV were chosen as representative collision energies to illustrate all the observed ions on fragmentation of m/z 123. DMAP can fragment directly in various ways giving rise to MS^2 product ions m/z 27, 79, 94, 96, 107 and 108, which are obtained when 20 eV collision energy is applied. On the other hand 60 eV favors the formation of MS^3 m/z 28, 66, 79 and 92. The observed 107>28 transition gives rise to neutral pyridine which is protonated in the collision cell due to high residence time. The protonated pyridine m/z 80 further fragments to aziridene- and cyclopropene type species as depicted in Figure 12.

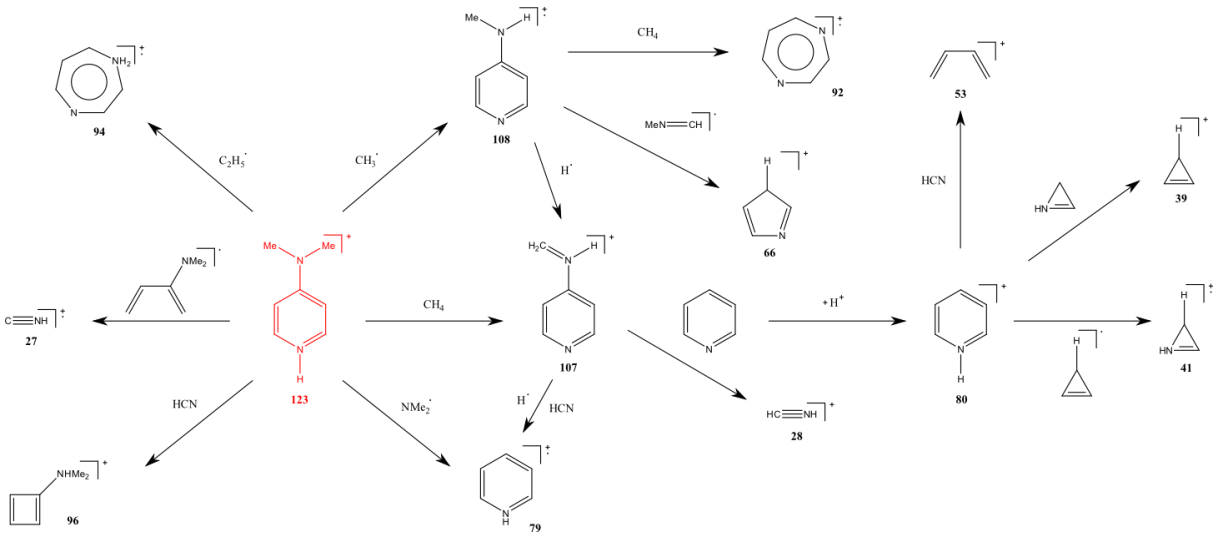

Figure 12 - Proposed fragmentation pathway of $[DMAP+H]^+$

4.1.2. Determination of the optimal LC-MS/MS method via DoE

The problems of a complex system such as LC-MS/MS influenced by many factors are handled more efficiently by DoE than the conventional COST approach thus the use of DoE for LCMS method development is proposed. The optimization of an analytical technique by the proposed approach is to determine which factors and combination of factors will result in optimal operating conditions. Note that prior to conducting any experiment, the analyst has to specify some input conditions: the number of factors and their ranges, the number of responses and the experimental objectives. The first step was to carry out a risk assessment to define the variables of the analytical method that could have impact on specific responses. As

described in chapter 4.1.1, 123>107 transition was selected to be monitored by the MS detector and during its determination the DoE ranges of the related MS factors were also established. The ranges of the LC factors and the analytical column were chosen based on the knowledge of experienced analysts and prior knowledge on the chromatographic behavior of glucocorticoids. The ranges of the variables chosen for the method development and the responses as well as their relation to the LCMS instrument are given in Figure 13.

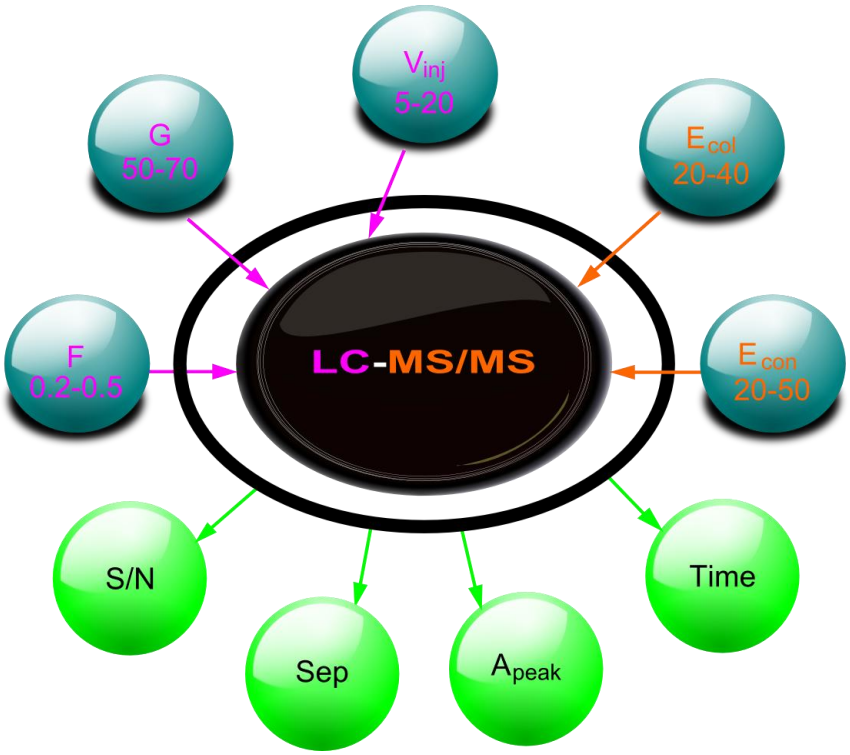

Figure 13 – Chosen factors with their ranges (blue bubbles), responses (green bubbles) and their relation to LC-MS/MS where the dimensions for F, G, V_{inj}, E_{col}, E_{con} are $mL.min^{-1}$, % eluent B, µL, eV and V respectively.

DoE is applicable to three types of problem solving: screening, optimization and robustness testing[192]. Optimization is more complex than screening (searching for relevant factors and identifying their ranges), thus optimization designs require more experiments per factor while the screening designs require few experiments in relation to the number of factors. Typically the first approach when using DoE is a screening method where a linear model is fitted. In this particular case a quadratic model was chosen as it could better fit the results without increasing the number of runs too much. Using the software Modde, a *Central Composite Face* (CCF) design with 26 runs and 3 center points was created to support such a model. The advantage of this approach is that it includes quadratic terms as well as interactions between variables. The LC factors chosen for the DoE study includes flow, gradient and injection

volume while cone voltage and collision energy were chosen as MS parameters. These factors were varied systematically in the defined ranges around the center-point experiment. The benefit of the described DoE approach is that it allows the simultaneous study of both the LC and MS factors rather than varying them in two, consecutive designs. This way the interactions between the LC and MS parameters are being considered. As for any analytical method development prior to conducting any experiments, the analyst has to specify the initial conditions. It has been decided to fix the column, the solvent and ionization agent of the eluent, while the initial MS parameters were identified by direct diffusion of the DMAP analyte (see chapter 4.1.1). On the other hand, the standard reference LC operating conditions were decided based on the general knowledge of a trained analyst. The runs selected by DoE are laid out in a symmetrical fashion around the standard reference experiment namely the center-point (Table A3-4 in the Appendix). Figure 14 shows the regression coefficients of the quadratic model and their confidence intervals for each response.

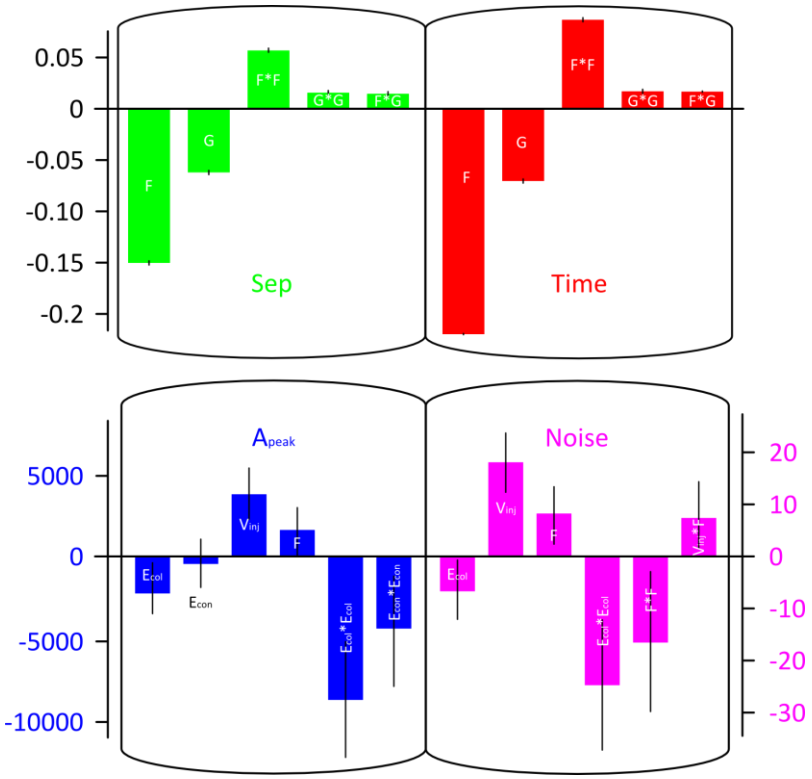

Figure 14 – Regression coefficient plot for the CCF design of method development

The coefficients representing one factor only are called linear terms while those squared are called quadratic terms. They reveal the real effects and importance of each factor. Since the response Sep is calculated as the difference between the retention times of the API and

DMAP, it shows similar behavior as the response Time itself F, F^2 and G being the most significant terms. Similarly, responses A_{peak} and S/N also share the most significant terms being E_{col}^2 and V_{inj}. However, the third most relevant term for S/N is F^2 but, on the contrary, for A_{peak} it is E_{con}^2. In other words, the noise of the measurement depends more on the flow while the peak area on the cone voltage. The coefficients representing the interactions among certain factors are called interaction terms and they show less relevance than the terms mentioned. Since the uncertainty of the coefficients is given by the confidence intervals, those with much higher uncertainties than the actual values themselves were eliminated leading to a better DoE model. In this sense better model means a higher Q^2 value. Note that however, E_{con} for the variable A_{peak} has no impact, it was still kept because its squared coefficient presents a significant factor. The summary of fit with the obtained model fit (R^2), predictability (Q^2), validity of the model (V) and reproducibility (R) values of the CCF model are shown in Figure 15.

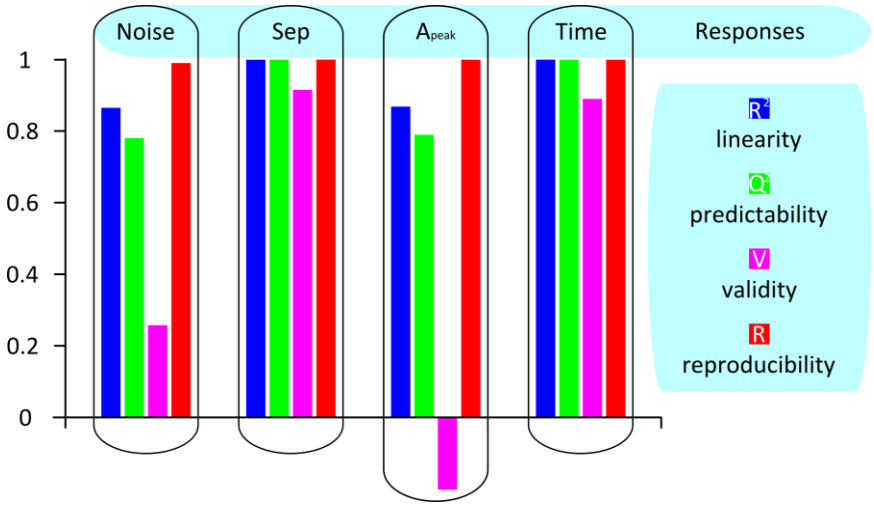

Figure 15 – Summary of fit for the CCF design of method development

The theoretical optimum value for all descriptive parameter is 1. The fit is over 0.98 for all responses, meaning that the model fits the data perfectly. Reproducibility is always higher than 0.8, meaning that under the same conditions the variation of all responses at the center point, compared to the total variation of the responses, are low. The most important descriptive parameter is predictability giving information about how accurately the model can predict the responses. The Q^2 value is higher than 0.7 for all responses, which is considered to be very good in DoE models. The validity of the model is good for Sep and Time, acceptable for S/N but the negative value for A_{peak} is caused by almost equal center points. Note, that the negative value means that the model error is larger than the replicate error which is only

acceptable if the response of center points is almost identical as in our cause. Figure 16 demonstrates the higher the V_{inj} and F the higher the A_{peak} while it reaches a global maximum as the MS variables, E_{con} and E_{col}, are varied. The descriptive statistics of the model can be found in the Appendix (Table A5).

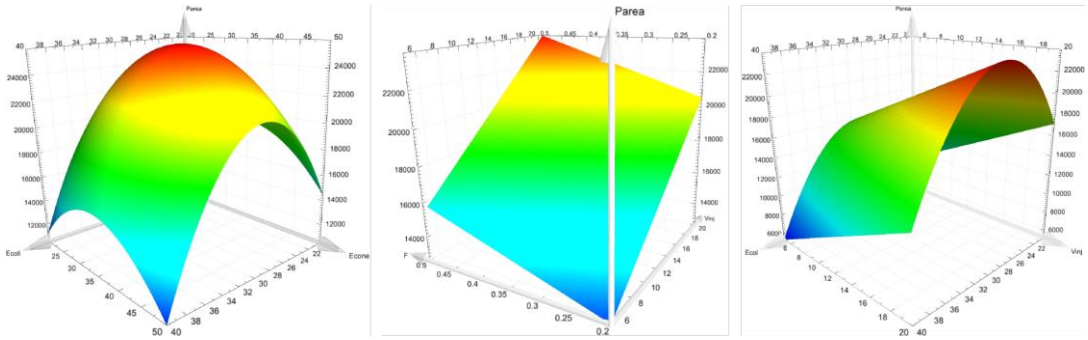

Figure 16 – Dependence of A_{peak} on E_{con}, E_{col}, V_{inj} and F

After defining the relationship between the variables of the method and the outputs using a quadratic model and establishing the design space – which is the ranges of the variables giving acceptable results – the optimum point was determined. Data evaluation was done by the optimizer function of Modde which is based on a simplex approach. The criteria for the responses were systematically aggravated in order to narrow the range of the so-called sweet spot where all the previously set criteria are met (Figure A1 in the Appendix). The optimum method parameters were determined using the optimizer function of Modde which gave 30 V, 35 V, 26 µL, 0.5 $mL.min^{-1}$, 70% eluent B for E_{col}, E_{con}, V_{inj}, F and G respectively. The software can automatically calculate the optimum parameters based on the model built on the relations among factors determined from the DoE method development runs. The DoE approach resulted in a general method for the trace analysis of DMAP which was investigated with glucocorticoid matrices such as Meta, Beclometasone Dipropionante, Fluticasone Propionate and Holobetasole proprionate resulting in 4.05, 4.47, 4.08, 3.88 min retention time respectively. The corresponding chromatograms are presented in Figure 17 where DMAP elutes at 0.61 min – detected by MS – and Meta elutes at 4.08.

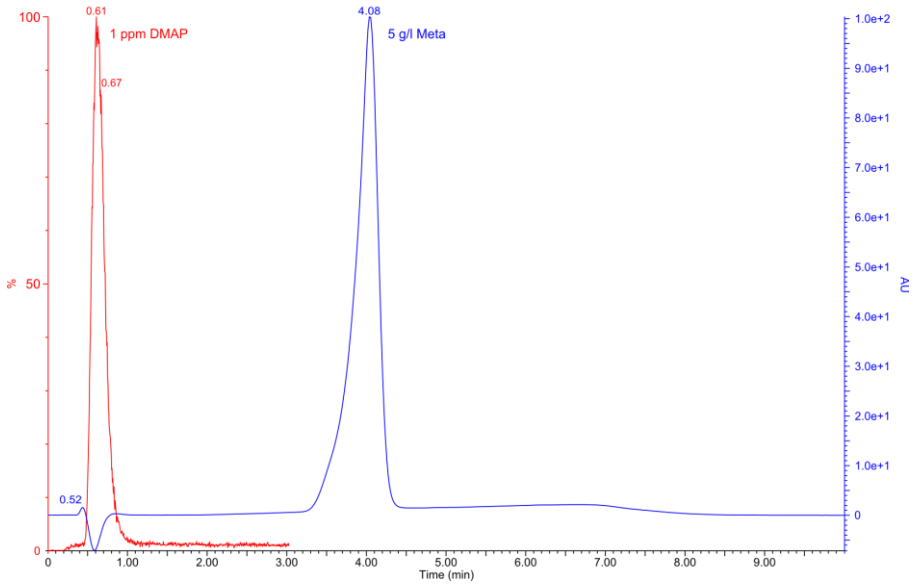

Figure 17 – Chromatogram of DMAP and Meta separation

Given the fact that the retention time of DMAP is always around 0.6 min and the APIs elute at least 3 min later, it is concluded that all of the glucocorticoids tested are chromatographically separated from the analyte. Since there is no API/DMAP interference the method can be used to determine DMAP contents in the above mentioned steroids. Additionally, a switch valve was fitted between the UV and MS detectors in order to avoid overloading the electrospray source with highly concentrated API solutions by sending the eluent to waste after 2 min. Although the method can be used with various glucocorticoids it was validated only for the quantification of DMAP in Mometasone furoate.

4.1.3. Robustness of the method

Demonstrating robustness of a particular analytical method is of high importance in order to meet regulatory and manufacturing standards. Although FDA and EMA as pharmaceutical regulatory authorities do not require robustness evaluation, it is implied in the scope of good manufacturing practices. Similarly to analytical method development, robustness studies were conventionally performed via COST approach providing limited data. However, DoE assisted multivariable testing is a newer approach to in depth robustness studies. The aim during the robustness study was to determine the sensitivity of the method to small changes in the factor settings. In LC-MS/MS such small changes usually correspond to fluctuations in the factors occurring due to electrical and mechanical errors and deviations.

In addition to the first CCF design used for the LCMS method development, variables such as column temperature and quadrupole resolution were considered in the robustness study. The rationale behind the expenditure of the number of variables lies in the change of the DoE design and objective. The CCF design which was used originally for the method development is capable of providing thorough relations between the factors and its purpose is to create a model, hence it requires more runs and thus analysis time. On the other hand, the objective of a robustness testing is not to build a model but to check the sensitivity of the obtained method to parameters that may fluctuate during the analysis, a simpler model can be applied requiring smaller number of runs and thus allowing a larger number of variables to be tested while still being time-efficient. An FF of resolution III design with 11 runs including 3 center points was applied for the evaluation of robustness where the focus is on evaluating the effect of small changes in the factors on responses and not in depth interaction analysis (Table A6 in the Appendix). A rapid robustness evaluation was achieved by increasing the number of factors in a decreased number of runs because of the new FF design.

The regression coefficient plot of the robustness testing indicates the factor induced fluctuations of the responses (Figure A2 in the Appendix). E_{col} and G have effect on A_{peak} and Sep respectively, while Time is affected by G and F. On the other hand, no factors have significant effect on the S/N. Note that in robustness testing only the effect of small changes in factors are studied. Assessing A_{peak} fluctuations, the highest deviation is 23% compared to the average of the 3 center points meeting the corporate operating procedures' criteria of 30%. Fluctuations observed in Time resulted in 16% highest deviation. On the other hand, the remaining studied factors have negligible influence on the responses due to high uncertainty/value ratio. The results show some sensitivity of the attributes to changes in some of the variables of the method but the overall results indicate that the obtained method is robust. Although it is of interest to note, that contrary to our expectations, the method is not sensitive to fluctuation in the injection volume, whilst this was one of the key factors during the DoE method optimization. The summary of fit of the FF model (Figure A3 in the Appendix) also confirms that the factors have no significant and predictable effect on the responses, as the V and Q^2 for S/N and Sep is low meaning that the model is not capable of describing the relationship between these attributes and the LC and MS variables. Note that an acceptable model was only built during the robustness testing for Time indicating that the relationship between time and the studied factors can be described by a quadratic model. It is in correspondence with the coefficient plot (Figure A2 in the Appendix) revealing the relevant

factors being F and G. The high variation of predictability among the responses and the low model validity values are consistent with the fact that the ideal results of a robustness testing model refinement is that no model is encountered.

4.1.4. Validation of the method

Validation of the instrumentation and the methods are additional requirements to ensure their intended purposes. The extent of the method validation will vary with the stages of drug development, becoming more rigorous as the drug progresses to marketing. Validation should cover sensitivity, specificity, accuracy, linearity and precision in order to prove the method is capable of its intended use.

4.1.4.1. LOD and LOQ assessment

Analyses of two independent DMAP spiked 5 $mg.mL^{-1}$ Mometasone furoate glucocorticoid solutions were carried out to determine detection and quantification limits, thus ensuring that API presence in the chromatographic system does not interfere with analyte detection. Note that a concentration of 5 $g.L^{-1}$ API constitutes a lesser risk of overloading the chromatographic column and a consequent loss of sensitivity. Tested concentration levels of 0.03 and 0.1 ppm relative to the API (0.15 and 0.5 $ng.mL^{-1}$ respectively) were established as LOD and LOQ since S/N results obtained from QuanLynx software successfully meet the acceptance criteria for those parameters. Also, the two independent API solutions spiked at LOQ level when injected three times each, demonstrate that the method is repeatable at 0.1 ppm concentration level and can be used as a limit test. The results are presented in Table 5.

Table 5 – LOD and LOQ summary of results

Samples[a]	A_{peak}	S/N[c]
LOD#1	n.a.[b]	4, 4, 4
LOD#2		3, 4, 4
LOQ#1	2410,2749,2767	11, 11, 11
LOQ#2	2988, 2893, 2889	11, 11, 12
RSD	7%	n.a.[b]

a) Independent preparations per concentration level
b) Not applicable
c) S/N = Signal to noise ratio

4.1.4.2. System precision

An API spiked sample at 1 ppm DMAP was injected six times to evaluate the precision of the LC-MS system and the peak areas recorded. An RSD of 0.02% was obtained which is considered an acceptable value.

4.1.4.3. Linearity

A range from 0.1 ppm to 10 ppm was considered since the TTC level is about 1 ppm. Determining DMAP content accurately above this value is not of great interest for pharmaceutical companies so ten times the TTC level was decided as upper range limit for academic quantification purposes. For DMAP concentrations above 10 ppm the authors suggest to dilute the solution accordingly in order to work within the validated concentration range. This parameter was assessed using spiked API solutions at six different concentration levels, yielding a correlation factor of r=1.000 (r^2=0.999).

4.1.4.4. Repeatability

Quantification of six independent spiked sample preparations was carried out at the LOQ concentration level to assess the method's ability to quantify samples in this level. The DMAP content for the six preparations was determined by the least squares method. The calculated RSD for the six concentrations is 1%, which represents an acceptable value for an absolute concentration of 0.5 ng.mL^{-1}.

4.1.4.5. DMAP recovery in Mometasone furoate

A total of twelve independent recovery determinations were performed, distributed over three concentration levels: LOQ (six preparations), 0.5 ppm (three preparations) and 2 ppm (three preparations). Sample quantification was performed by the least squares method. Table 6 displays obtained AR. Given that the absolute DMAP concentration range is 0.5-10 ng.mL^{-1} the obtained recoveries are considered acceptable.

Table 6 – DMAP recovery in Meta at three different concentration levels

preparation	A_{peak}	concentration (ppm)	AR (%)
LOQ#1	2410	0.083	83
LOQ#2	2749	0.096	96
LOQ#3	2767	0.096	96
LOQ#4	2988	0.104	104
LOQ#5	2893	0.101	101
LOQ#6	2889	0.101	101
0.5ppm#1	15618	0.567	113
0.5ppm#2	15620	0.567	113
0.5ppm#3	15624	0.567	113
2ppm#1	52642	1.924	96
2ppm#2	52616	1.923	96
2ppm#3	52629	1.923	96

4.2. Comparison of conventional and nanofiltration API purifications

The schemes of the three purification processes including inputs, outputs, sources of energy consumption and waste formation are illustrated in Figure 18.

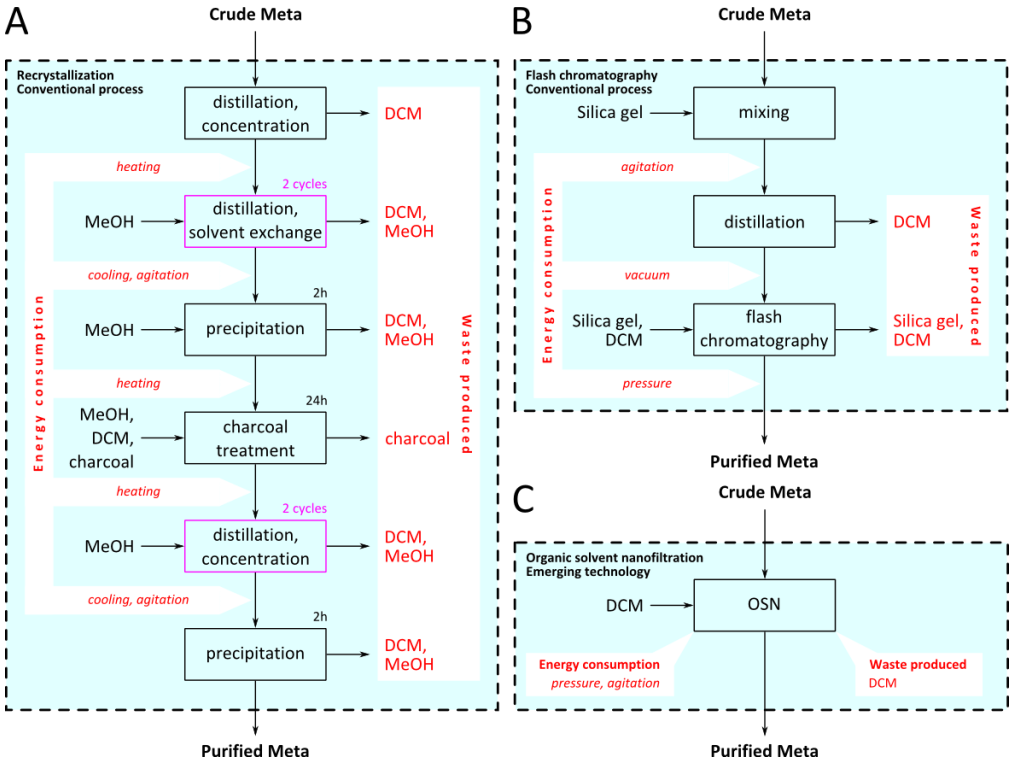

Figure 18 – Comparison of purification processes under investigation: recrystallization (A), flash chromatography (B) and organic solvent nanofiltration (C)

4.2.1. Overall process performance comparison

Selection of purification technologies for GTI removal from API post reaction solutions is not trivial: industrial feasibility, economic and environmental impact, achievable purity grade and API loss have to be evaluated individually to make a reasonable decision leading to a viable manufacturing process. Degenotoxification of APIs is fundamental to decrease toxicological risk to patients. GTI limits in APIs are calculated as follows: the TTC value (1.5 $\mu g.day^{-1}$) divided by the maximum daily dose ($g.day^{-1}$) gives the limit in $mg.dm^{-3}$ to be applied to the active substance[190]. Considering 500 $mg.day^{-1}$ daily dose of Meta the GTI is required to be controlled at 3 $mg.dm^{-3}$, relative to the API. Consequently, a post-reaction stream containing 10 $g.L^{-1}$ Meta and 1 $g.L^{-1}$ GTI requires an impurity removal higher than 99.7%. Since the higher the desired purity, the higher the API loss, and compromise between level of purity and API loss has to be made for any purification process whilst taking into account the threshold limit of impurities. Figure 19 demonstrates API recovery versus GTI removal for each process.

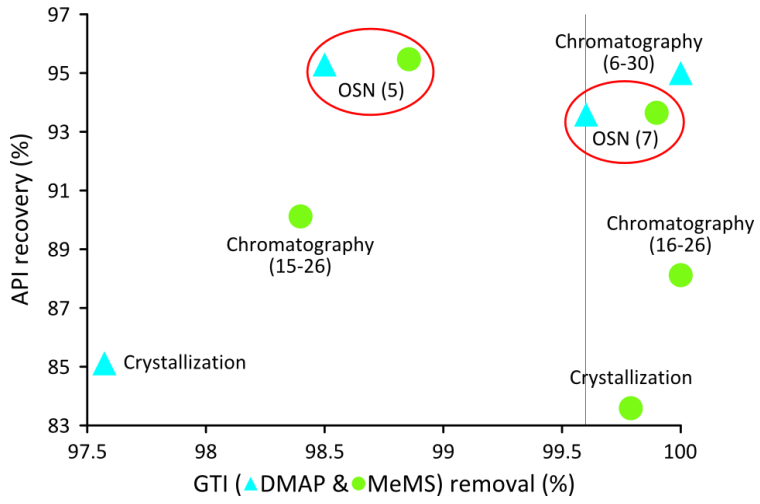

Figure 19 – Process performance comparison for two case studies: Meta/DMAP and Meta/MeMs

Regarding the model GTI, recrystallization shows higher API loss without acceptable compensation in the API purity achieved. Despite its drawbacks, such as impurity carryover and API loss in the mother liquor and washing solutions, recrystallization is a widely used purification process due to the fact that it delivers the API in the desired crystallographic form. Regarding the removal of DMAP, flash chromatography shows an ideal, almost 100% purification level, at the cost of only a 5% loss of Meta. On the other hand, the same level of

GTI removal by OSN incurs significant Meta loss. Notice that 98.5% DMAP removal implies a loss of 4.7% Meta at 5 diavolumes. MeMS is a smaller molecule compared to DMAP and thus permeates through the membrane slightly easier. Hence, at the same diafiltration volumes, whilst the same API recovery is observed, a slightly higher amount of GTI is removed by OSN. MeMS removal by OSN provides an efficient route when compared with chromatography. About 4.5% of the API is lost during the removal of 98.9% of MeMS at 5 diavolumes and further purification up to virtually 99.9% GTI removal is achieved with a loss of 6.3% API showing the robustness of this simple technique. Recrystallization is one of the oldest and common processes employed in pharmaceutical industry for API purification. Although in the current study the performance of this technique seems inferior, one should note that recrystallization is easily scalable and has the advantage of presenting the API in the required crystallographic form. In order to highlight the different operational steps of the processes to be compared and map API loss as well as GTI removal, the data obtained at each particular step, process performance, solvent and energy used, as well as key process costs are described in details in the following chapters.

4.2.2. Stepwise process performance comparison

A detailed discussion and analysis of each step of the experimental trials follows. Flash chromatography was performed collecting fractions of 50 cm^3 of eluent. Removal of DMAP from crude Meta proved to be straightforward with an isocratic elution described in the experimental section of the thesis. Notice that silica gel has a slightly acidic nature which causes partial protonation of the basic DMAP, hence its retention on the stationary phase is very high (Rf = 0.05). Meta is not detected in the first 300 cm^3 (fraction 1 to 6). 95% being continuously eluted without contamination by DMAP in the following 1200 cm^3 (fractions 7 to 30) as monitored by TFC and confirmed by HPLC-UV quantification. A higher EtOAc content in the eluent facilitates the elution rate of Meta resulting in lower operational time and solvent consumption but this option was rejected since DMAP leakage was observed contaminating the API and thus severely affecting purification efficiency. MeMS and Meta show reciprocal affinity for the stationary phases with a faster elution rate for MeMS (Rf = 0.2) than Meta (0.02) in pure DCM. Therefore, a gradient elution (Table 4) was applied with initial elution with 600 dm^3 pure DCM to elute MeMS first (fractions 1-13), followed by progressive increase of EtOAc to recover Meta. Results of the MeMS removal and corresponding Meta loss are shown in Figure 20A. Most of Meta was recovered in fractions

16-26 representing 90.1% of the total applied to the column. Note that these fractions correspond to the part of elution gradient where EtOAc content is higher than 5%. Intermediate fractions with eluent containing EtOAc between 0 and 5% (fractions 14 and 15) feature Meta with low MeMS contamination. Accordingly, fractions 14 and 15 were also combined with the main stream (fractions 16-26), thus the MeMS-Meta case study involves two analyses values: fractions 16-26 and 14-26. By collecting fraction 14-26 it is possible to remove 98.4% of MeMs at a cost of 9.9% API loss. Alternatively, if fractions 16-26 are collected up to 100% GTI removal (below LOD) can be achievable at a cost of 11.9% API loss, which is not significantly higher than when fractions 14-15 are included. Therefore, concerning further analyses, this study focuses on the best scenarios with 100% removal of both for MeMs and DMAP.

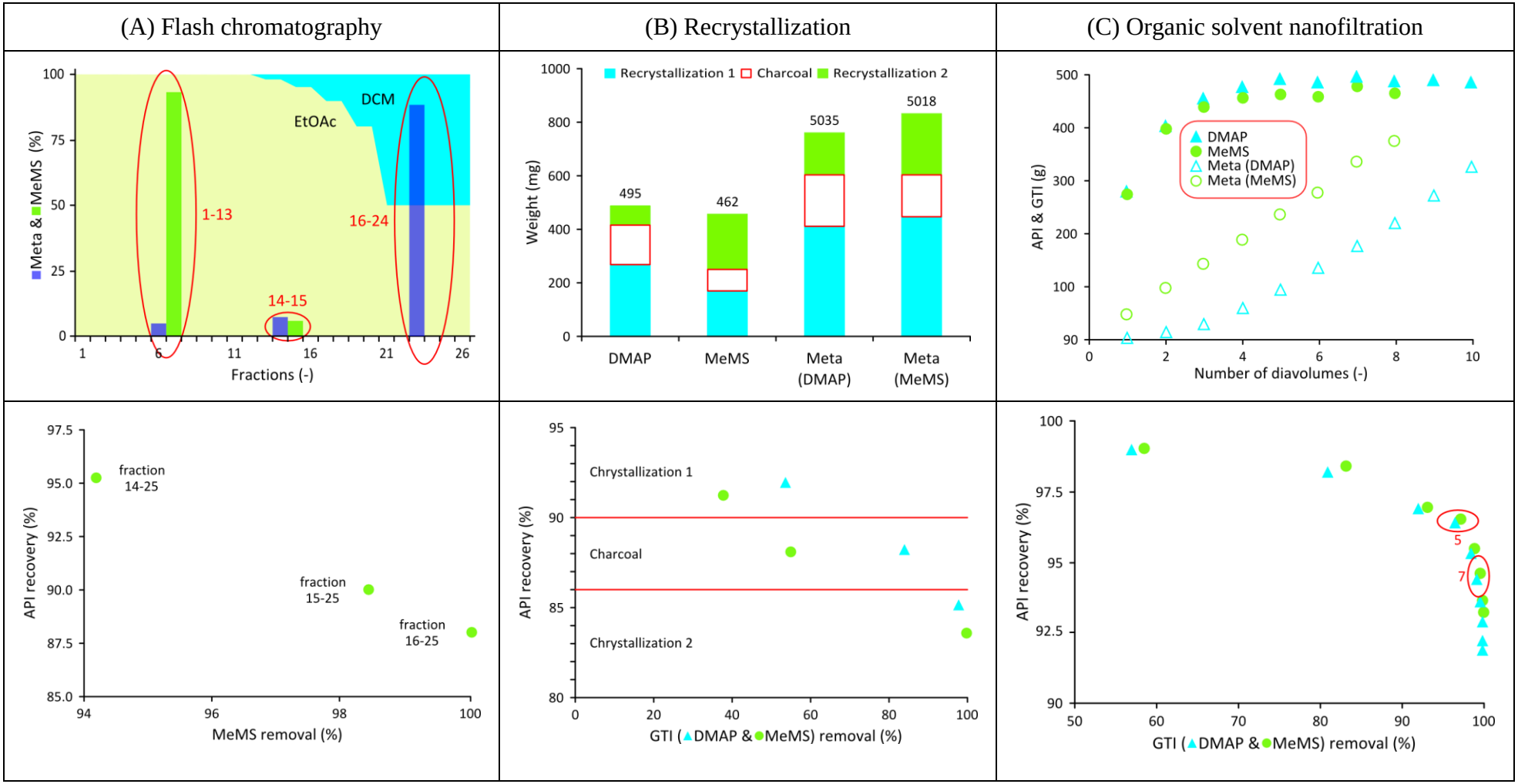

Figure 20 – Experimental evaluation of Meta and MeMs and/or DMAP separations. Distribution of API and GTI is shown in top panels (A) in groups of fraction for flash chromatography, (B) crystallization and adsorption stage in recrystallization process and (C) in function of diavolume in OSN. API recovery versus GTI removal for each stages are shown in bottom panels.

The recrystallization procedure – illustrated in Figure 18 – includes three main stages: (i) first recrystallization from methanol, (2) charcoal adsorption and (3) second recrystallization. Firstly, the API precipitates during distillation assisted solvent exchange from DCM to methanol enriching the mother liquor in the impurity. In the second step charcoal adsorbs the impurity and the API remains dissolved in the DCM:MeOH solution. Altogether four distillations are required during the two solvent exchanges from DCM to methanol. In order to consequently map both GTI removal and API loss during each steps, the amounts were quantified in the mother liquors, crystalline solids and charcoal filtrate as illustrated in Figure 20B. The amount of API and GTI leaving the system through the adsorption to charcoal was estimated by component mass balance. Mass balances for crystallization close within 2.5% for both API and GTI. The largest fraction of API loss was observed in the first recrystallization, representing 9% and accounting for half (53%) of the total API loss over the 3 steps. API loss on charcoal and second recrystallization accounts for about one quarter (19-27%) each of total API loss. Although GTI removal cannot be assigned preferentially to any of the steps, it can be concluded that DMAP has a higher affinity to charcoal than MeMs, similar to that previously observation with adsorption on silica gel.

Discrimination of API and GTI during purification by diafiltration featuring nanofiltration membranes is mainly based on their molecular size, and consequently membrane rejections of these species are different. The nanofiltration membrane chosen for the present application is GMT-oNF-2 showing good stability in DCM. The flux across the membrane was determined for different applied pressures between 5 and 45 bar, with incremental steps of 5 bar. A linear relation of flux with pressure, with a correlation factor of 0.97 was found up to 30 bar of applied pressure, corresponding to a membrane permeability for DCM of 4.7 $L.m^2.h^{-1}.bar^{-1}$. Experimental DCM fluxes through the membrane were 55 $L.m^2.h^{-1}$. The membrane rejections obtained at 10 and 20 bar, presented in Table 7, show that the API, with a molecular weight of 521.44 $g.mol^{-1}$ is effectively retained by the membrane as both GTIs, DMAP and MeMs, respectively, with molecular weight of 122.16 and 110.14 $g.mol^{-1}$, cross the membrane easily. Since the difference in the rejection of Meta at 20 and 10 bar is negligible, but higher amounts of GTI crosses the membrane at 10 bar, the latter pressure was selected for experimental evaluation of diafiltration. Since MeMS is only a slightly smaller molecule than DMAP, its average rejection is not significantly lower than DMAP rejection. Note that not only molecular size rules solute transport through membranes but other factors such as membrane solute interactions and polarity may also play important roles. The results represented in

Figure 20C show that the higher the number of diavolumes, the higher the API loss, but on the contrary the increments in GTI removal become less significant. On the basis of GTI removal versus API recovery (Figure 20 – bottom panels) one can consider two scenarios concerning diavolume selection. GTI removals superior to 98.5 or 99.5% can be achieved at the cost of lower than 5% or 7% API loss at diavolumes of 5 and 7, respectively. Despite the higher purity of API achieved, higher diavolumes not only lead to higher API loss but also increases the solvent consumption and operation time. To be consistent with the flash chromatographic study, a diavolume of 7, representing the purest API, was selected for further analysis.

Table 7 – Rejection of DMAP and MeMS impurities and Meta drug substance

	rejection (%)	
	10 bar	20 bar
MeMs	13.0±0.1	15.0±1.1
DMAP	15.1±0.3	16.5±0.4
Meta	99.0±0.1	99.1±0.1

4.2.3. Scale-up considerations

The experimental trials at a laboratorial scale were performed using 500 cm^3 solutions with API and GTI concentrations of 10 $mg.dm^{-3}$ and 2 $mg.dm^{-3}$, respectively. In order to provide an environmental and economic analysis, an inventory of materials and energy of the different steps was prepared for the different processes (chapter 4.2.4). Furthermore, the assumptions and estimations applied to elaborate inventory in a scale-up scenario are also included in Table A7 which can be found in the Appendix. Scale-up was calculated for a factor of 2,000, maintaining API and GTI concentrations, corresponding to average steroid batches of 1 m^3 featuring 10 kg of API. Production of 10 batches per annum was considered, satisfying a demand of about 100 kg API.

(A) Flash chromatography	(B) Recrystallization	(C) Organic solvent nanofiltration
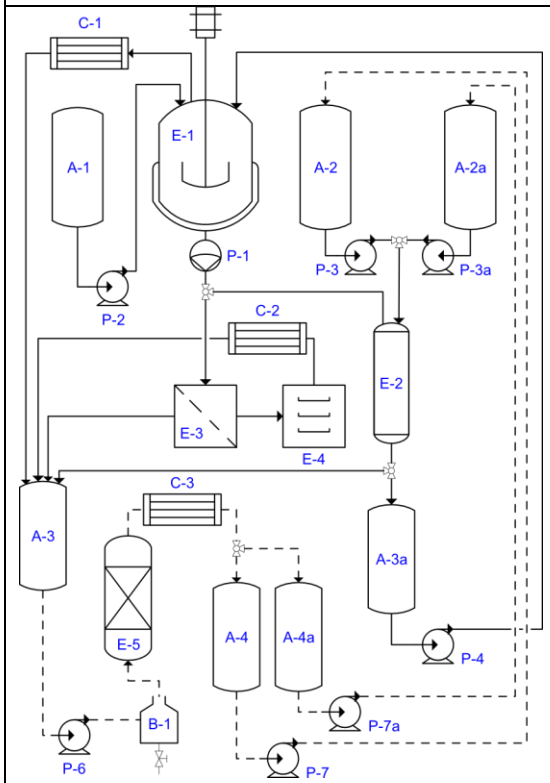	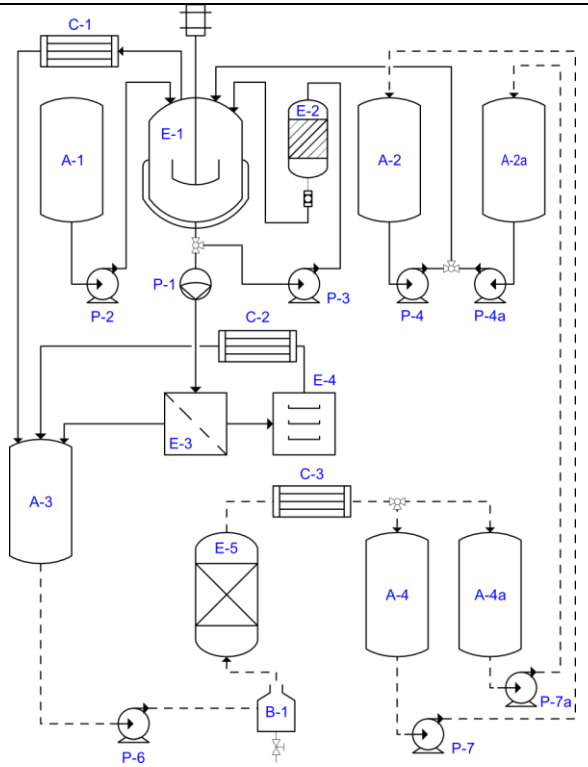	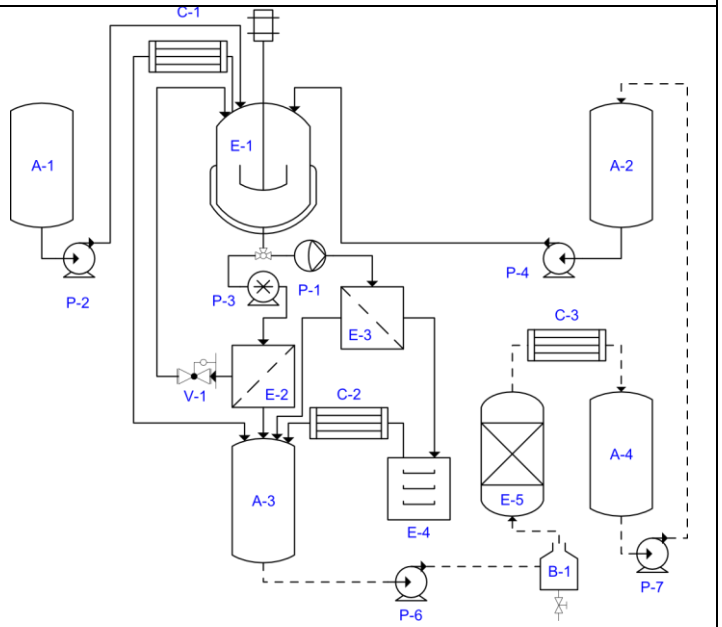

Main equipment: (i) E-2 is the silica gel column, active carbon column or OSN membrane housing for flash chromatography, recrystallization and OSN process respectively; (ii) E-1 vessel with jacket and stirrer, E-3 filter, E-4 dryer, E-5 distillation column; and (iii) C-1 condenser of the stirred vessel, C-2 condenser of the dryer, C-3 condenser of the distillation column, B-1 boiler of the distillation column. **Tanks:** A-1, auxiliary tank for API feed, A-2 auxiliary tank for approved DCM, A-2A auxiliary tank for approved EtOAc or MeOH, A-3 auxiliary tank for waste solvent to be recycled or disposed, A-3A auxiliary tank for diluted pure API, A-4 auxiliary tank for DCM to be approved, A-4A auxiliary tank for EtOAc or MeOH to be approved (A-3A is only required for Flash Chromatography. A-2, A-4 are not required for the OSN process). **Pumps:** (i) P3 is a centrifugal pump for solvent elution through silica and charcoal columns for flash chromatography and recrystallization process, but a high pressure pump in OSN; (ii) P-2 pneumatic diaphragm pump for slurry transportation, P5 Vacuum for filtration P-1, P4, P4A, P6, P7 and P7A are centrifugal pump for solvent transportation. (P4A and P7A are not required for OSN process)

Figure 21 – Idealized process diagram for the three processes

Figure 21 represents the process scheme diagrams of the envisaged processes. The multi-propose reactor E-1 is comprised of a vessel with jacket and stirrer and coupled with a condenser C-1 in all of the processes, allowing an internal loop for removal of solvent from API solutions by distillation. This is required since both flash chromatography and recrystallization require a reduction of 90% of the volume of DCM. The slurry obtained is fed to the main process, i.e the silica column E-2 for flash chromatography or remains in reactor E-1 for solvent exchange (DCM → methanol) for recrystallization. Note, that at the end of each process, including OSN, the purified API solution is fed to E-1 for concentration by distilled to 90% in volume in order to obtain a slurry that can be sent to E-3 for filtration. The wet cake obtained is dried in E-4. The specific assumptions for the main steps of each process which take place in E-1 and E-2, are discussed below. Note, that the scale-up data is only indicative, with the objective of rational selection of the best purification process in terms of sustainability and green aspects. The scale-up of the process would require experimental justification and adjustment of parameters once the lead process has been selected.

At a lab scale, increase of scale for Flash Chromatography is usually performed by increasing column diameter while maintaining both its height and the linear elution solvent velocity. However, such an approach can only be followed to a certain extent without compromising homogeneous plug flow through the column at large diameters. Ideally the column diameter should remain below 63 cm. Therefore, for a significantly large scale-up it is inevitable that the column high increases. The higher the column, the higher the contact time between the solutes and the stationary phase promoting better solute separations, i.e. a higher number of theoretical separation plates is verified at the same linear velocity. However, a conservative approach was taken in which a potential increase in number of theoretical plates was not considered and a silica to API ratio of 1.1 was applied. The ratio of column height to diameter was kept at a value of about 3.1, corresponding to a column diameter and height of 63 cm and 2 m respectively. A linear velocity of 2.55 $cm.min^{-1}$ was considered regardless of the scale, corresponding to a flow rate of about 475 $m^3.hour^{-1}$. Solvent volumes and fractions enriched in API or discharging GTI were directly scaled up by a factor of 2,000. Figure 21A illustrates a process scheme for the chromatography process. The 100 dm^3 pre-concentrated API solution is loaded onto silica gel column E-2 for purification. The eluent fractions comprising pure or GTI contaminated solvent are collected in tank A-3. The eluent fractions enriched in the purified API are collected in tank A-3B and then transferred to E-1 in order to be concentrated to yield a slurry with a volume of 100 dm^3 whilst the distilled solvent is

collected in tank A-3. The slurry is transferred to filter E-3 using a diaphragm pump and the wet cake is manually transferred to E-4 for drying. Tank A-3 contains large amounts of solvent and GTI.

Scale-up of the recrystallization is estimated based on volume and masses, using a scale-up factor of 2,000 and an assumption of maintaining same performance level. Charcoal to API mass ratio is maintained at a value of 0.6 while filters are scaled on the basis of solution volume to filter membrane area. Figure 21B represents the process scheme diagram of the recrystallization process. The 1 m^3 API crude solution is loaded to E-1 and *solvent exchange I* (DCM → methanol) is carried out in parallel with the concentration of the solution to 100 dm^3 by distillation at 50 ºC of the solvent in two cycles of addition of fresh methanol to tank E-1 followed by distillation of the same volume, thus obtaining the API in 100 dm^3 methanol. In *recrystallization I* the API mixture is cooled down to 10 ºC at a rate of 30 $ºC.h^{-1}$, and maintained at 10 ºC for 2 additional hours. The precipitated API is then transferred to filter E-3 where a further 80 dm^3 of methanol at 10 ºC is used to wash the crystals beore manually transferring to E-1, where a mixture of 400 dm^3 DCM:MeOH (1:1) is used for complete dissolution of the API. The charcoal operation stage is carried out by recalculation of the solution obtained at a flow rate of 1.5 $m^3.h^{-1}$ through charcoal column E-2 and reactor E-1 during 3 hours (>10 volumes). The charcoal column is washed with a further 80 dm^3 of fresh DCM. *Solvent exchange II* is carried out by concentration of the solution to 100 dm^3 by distillation at 50 ºC and addition of 100 dm^3 fresh methanol followed by distillation until the original volume is achieved. The mixture is then submitted to *recrystallization II*, following the procedure of *recrystallization I* where after, the crystals are manually transferred to dryer E-4. All the distilled and filtered solvents are collected in tank A-3.

The OSN process scale-up assumes constant ratio of load volume to membrane area, a diavolume of 7 and the use of 0.5 m^3 of solvent for preconditioning/cleaning the membrane between batches. An operation time of 7 hours was estimated, corresponding to a membrane area of 20 m^2. Note however that shorter operation times can easily be achieved by increasing membrane area, e.g. an increase in membrane area from the 20 to 35 m^2 l corresponds to an operation time of less than 4 hours. Figure 21C represents the OSN process scheme diagram. The crude API solution is loaded to tank E-1 and then circulated between tank E-1 and the OSN membrane modules E-2. E-1 and E-2 are pressurized to 10 bar using a high pressure pump, P-3. The diafiltration is carried out by pumping additional DCM from tank A-2 into the

pressurized vessel E-1 while the permeate is collected in tank A-3. At the end of the operation the retentate volume is further reduced by distillation and the distilled solvent collected in tank A-3, whilst the resulting slurry is transferred to E-3 for filtration and finally, the wet cake is manually transferred E-4 dryer.

At the end of each process, the use of an additional 0.5 m^3 of solvent to clean the vessels E-1, E-3 and A-3 and respective connecting pipes is considered. All the solvents removed from the main stream – e.g. (i) internal loop distillations from E-1 for volume reduction of initial crude API and final purified API solution, as well as API solvent exchange in recrystallization, (ii) eluent or permeate solutions containing GTI resulting from the silica column or OSN membrane, (iii) solutions from E-3 obtained from filtration of crystals and final slurry filtrations in E-3 and wet cake drying trough C-2, and (iv) vessel and pipe washings – are collected in tank A-3 to be eventually recycled. At the end of the API purification, pump P-6 can be used either to transfer solvent for off- or on-site disposal, e.g. by incineration or recovery by distillation. An optional distillation unit (E-5/C-3) is suggested with this aim in each of the processes. This alternative implies additional capital and operating costs for the different processes. Continuous lines represent pipes connecting equipment used in the main process and dotted lines represent pipes connecting equipment only needed when solvent is recycled. The effect of solvent recovery on the costs and environmental impact are discussed in chapter 4.2.4 and 4.2.5, respectively.

4.2.4. Inventory and cost analysis

Capital costs estimated in the current analysis include (i) main equipment costs based on process schemes established in Figure 21 and (ii) indirect capital costs based on multiples of main equipment costs as suggested in the literature[193], which includes additional costs such as for assembling piping, instrumentation, electrical installation, process buildings, utilities, storage, site development and ancillary buildings (respectively at ratios of 0.4, 0.7, 0.2, 0.1, 0.15, 0.5, 0.15, 0.5, and 0.15 of total main equipment cost) as well as design, contractors fees and contingency (at a ratio of 0.60)[194]. Therefore, the total capital cost can be calculated as 3.95 times the main equipment costs. The annual capital costs takes into account a 10 year amortization period. Operation costs, annual maintenance costs and insurances are then calculated as 10%, 5% and 1% of total capital costs. Comparison of capital costs is shown in Figure 22.

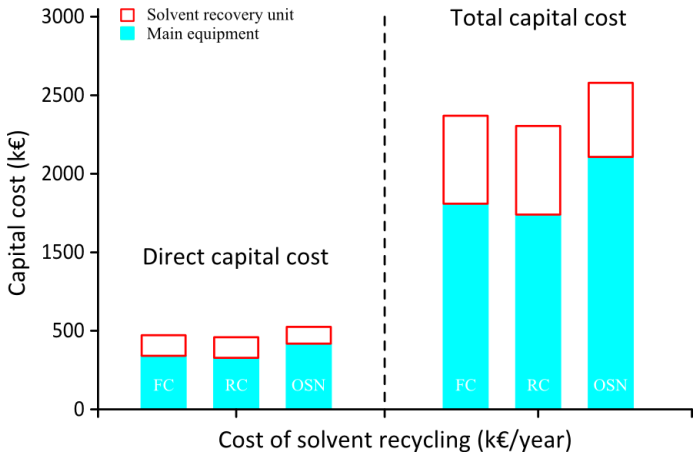

Figure 22 – Comparison of capital costs

Inputs and outputs of the process are represented in Figure 23. Particular attention is given first to solvent and energy consumption with the respective CO_2 footprint and waste generated and secondly to process time and full time equivalent labor, which is estimated for the three alternative processes.

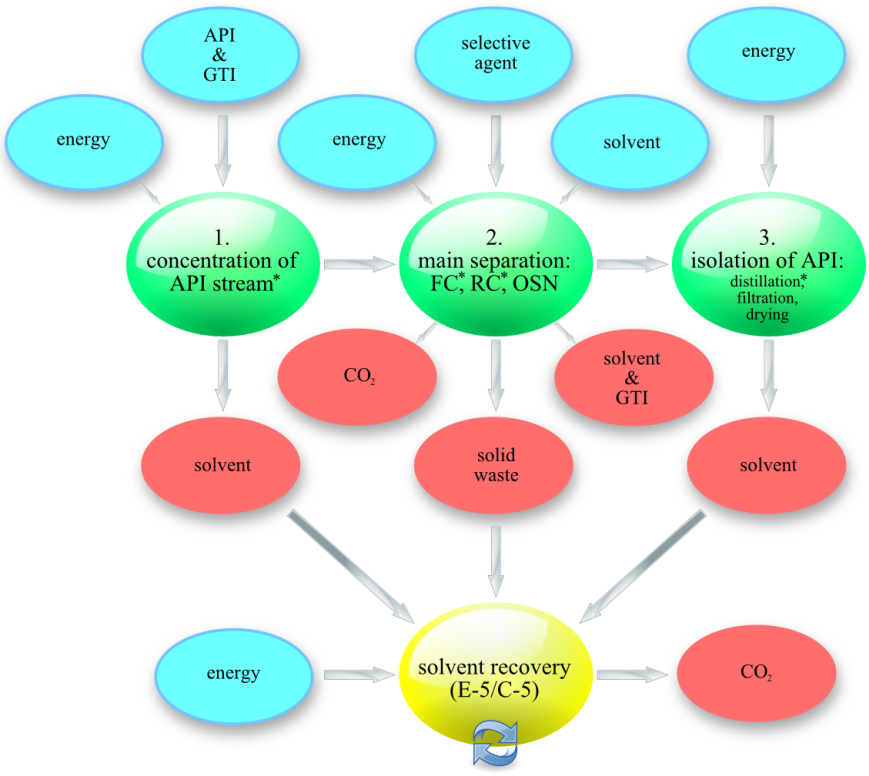

Figure 23 – Inputs and outputs of the purification processes where the blue, green, red and yellow bubbles represent the input, process, output and solvent recovery respectively (* including E-1/C-1 internal distillation)

The selective agent and solvent requirements per batch are shown in Figure 24 where DCM, EtOAc and methanol costs are assumed as 998, 1039 and 340 €.m^{-3}. Silica and activated carbon costs considered were 31.4 and 18.7 €.kg^{-1} and membrane cost was 2,000 €.m^{-2}. The process generating the largest amount of solid waste is flash chromatography with the disposal of 330 kg silica gel per batch (31.4 €.kg^{-1}). On the other hand, recrystallization resulting in 6 kg charcoal per batch (18.7 €.kg^{-1}) and the disposal of OSN membrane modules every two years are both negligible. The solvent in tank A-3 for disposal or recycle includes fresh solvent added during the process and the solvent from the crude API solution (1 m^3). OSN is clearly the most solvent intensive process, recrystallization requiring the lowest amount of solvents. As described in Figure 22, the processes include an internal distillation stage for API concentration and solvent exchange, which takes place at E-1/C-1. Such distillations are energy intensive, thus the amount of solvent distilled at these steps in each of the processes is also shown in Figure 24A.

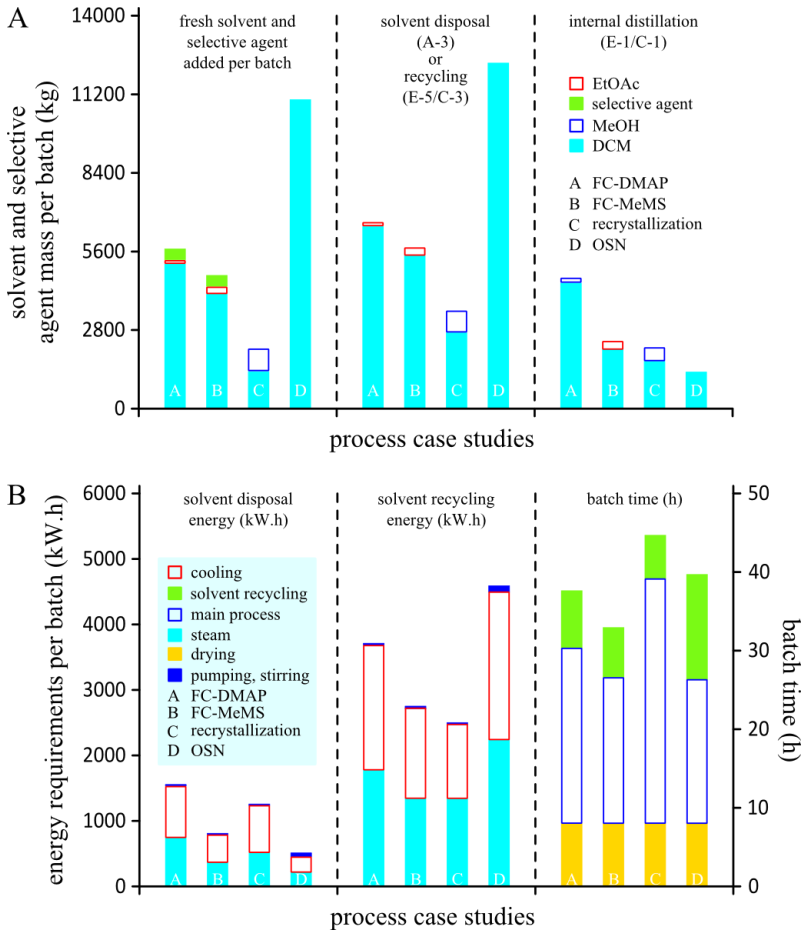

Figure 24 – Solvent and energy consumption comparison of the processes

The energy requirements for heating (steam) and cooling (brine) in the internal distillation stage (E-1/C-1), in the condenser C-2, in the cooling ramps of the crystallization (E-1) and for the external distillation unit (solvent recovery) were calculated taking into account solvent heat capacities and heat of vaporization. The outcome is shown in Figure 24B. Energy requirement calculations for pumping and stirring take into account power, time and volumes. All the pumps (P-1, P-4, P-4A, P-7 and P-7A) used to fill and empty tanks were assumed to be set to a flow rate of 5 $m^3.h^{-1}$ while P-6 is set to the corresponding distillation flow rate. During OSN and flash chromatography the operation time of the diaphragm pump (P-2) and vacuum filtration (P-5) is estimated to be 2 hours, while recrystallization calls for 4 hours due to the fact that the respective operations are repeated twice. Estimated flow rates of P-3 are 0.475, 1.5 and 1.1 $m^3.h^{-1}$ for flash chromatography (5.5 and 7 hours/batch for MeMs and DMAP removal, respectively), recrystallization (3 hours/batch for charcoal) and OSN processes (7 hours/batch), respectively. The volume of multipurpose reactor E-1 is 1 m^3 for OSN and 0.5 m^3 for flash chromatography and recrystallization. Stirring times were estimated based on filling, emptying and cleaning tank E-1 (3.5 to 5.5 hours), internal loop distillations for solution concentration and solvent exchange and main operations (1 to 4.5 hours), and main operations (i) two crystallization and charcoal adsorption (about 12 hours) for the recrystallization and (ii) membrane preconditioning/cleaning and diafiltration (7 hours) for the OSN process. Additional times considered include 8 hours for final drying of API, 3 hours for changing silica and charcoal replacement between each batch and 1 working shift for membrane replacement/maintenance every 5 batches (1.6 hours per batch).

Total batch times with and without the option of solvent recovery are considered and are shown in Figure 24B. Taking into account, main operation times, which include set up, cleaning and shut down times, but not drying time, between 2 and 3 shifts are required. Shifts for flash chromatography and OSN process with two FTE are allocated for each shift for operational work. Recrystallization, on the other hand, given that it is a more time consuming process is given 4 shifts and since these include operations that are more labor intensive, e.g. more handling slurries and solids, 4 FTE are allocated for each shift for operational work. OSN is more solvent intensive, therefore for additional solvent recovery additional FTEs were considered being 2 for the OSN process, but only one for the other two processes. An average wage cost of 30,000 € per annum was considered for operators. Total labor costs were calculated on the basis of 10 batches per year using the, operating labor mentioned. Additional costs for supervision and analytical laboratory costs were calculated as 20% of

operating labor costs; plant overheads being calculated as 50% of operating labor costs. Total yearly costs for the three processes are represented in Figure 25.

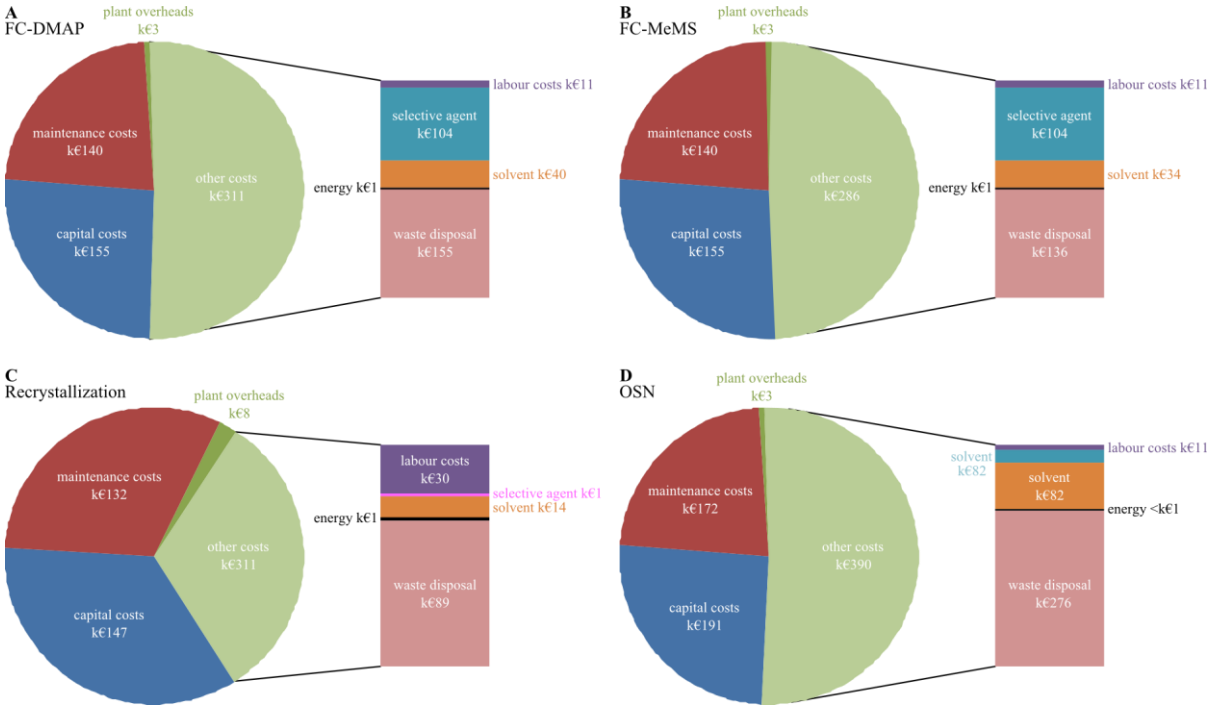

Figure 25 – Economic comparison of the processes

4.2.5. Environmental and economic impact

The three processes are conceptually quite different, however for cost comparison the variable costs, the inventory of inputs and outputs had been organized in four categories: (i) process performance indicators related to the API loss and GTI removal; (ii) mass intensity related to solvent consumption, discharged materials, selective agent input and solid disposal; and (iii) energy intensity and (iv) carbon footprint. Further qualitative analysis was carried out related to (v) operation time and labor requirements; and (vi) process complexity and scale-up complexity. Process performances are estimated as API loss and GTI removal and are illustrated in Figure 19. Note that as scale increases, the fraction of API lost in a recrystallization process tend to decrease[195]. The detailed data for the evaluation of mass and energy intensity are illustrated in Figure 24. GSK suggests a metric system for assessment from 1 to 10 (the higher the better) of the impact of solvent use based on four vectors (i) waste, considering solvent recycling, incineration, VOC and biotreatment issues; (ii) environmental impact addressing solvent fate and effect on the environment; (iii) health -

acute and chronic effects and exposure potential; and (iv) safety, which considers explosivity, flammability and operational hazards. According with the GSK methodology[97], use of solvents categorize between 1 and 3 (red flag) is associated with major issues to which appropriate control procedures have to be implemented, between 4 to 7 (white flag) some issues have been identify and control procedures should be considered, and for values higher than 8 there are no issues identified. The mass intensity is dominated by the use of DCM, however it would be interesting to have an insight into the mixtures with solvents of lower impact. EtOAc and methanol used in flash chromatography and recrystallization are used in high enough quantities to alter the weighted average of such impacts. The calculated values are presented in Table 8, where it is shown that only in the recrystallization process the use of higher fractions of methanol improves both the health vector to a value of 2, which is still flagged red, and the environmental impact to a value of 4, in the white flag region.

Table 8 – Solvent impact on waste disposal, environment, health and safety

	Waste	Environment	Health	Safety
DCM	3	3	1	10
EtOAc	4	9	7	4
MeOH	3	8	4	8
FC-DMAP	3	3	1	10
FC-MeMS	3	3	1	10
RC	3	4	2	10
OSN	3	3	1	10

The batch time required for each process is illustrated in Figure 24B. Note that all the processes have an 8 hour final drying step that is low labor intensive. Recrystallization is the most time consuming process and given the nature of the separation steps, strategies to decrease batch time are more challenging. However, scaling up of this process often results in a decrease of API losses and, due to the familiarity that regulator authorities have with API crystallization it is often a choice of preference. Scaling up flash chromatography implies a larger risk, with probable losses in efficiency. Reduction in the batch time would also be difficult without additional equipment or without losses in efficiency of the separation. OSN is regarded as a technique easily scaled up on the basis of membrane area. Batch time can be reduced by increasing membrane area. However, as OSN uses larger amount of solvents with the option of solvent recovery significant amount of time needs to be allocated and additional distillation units deployed.

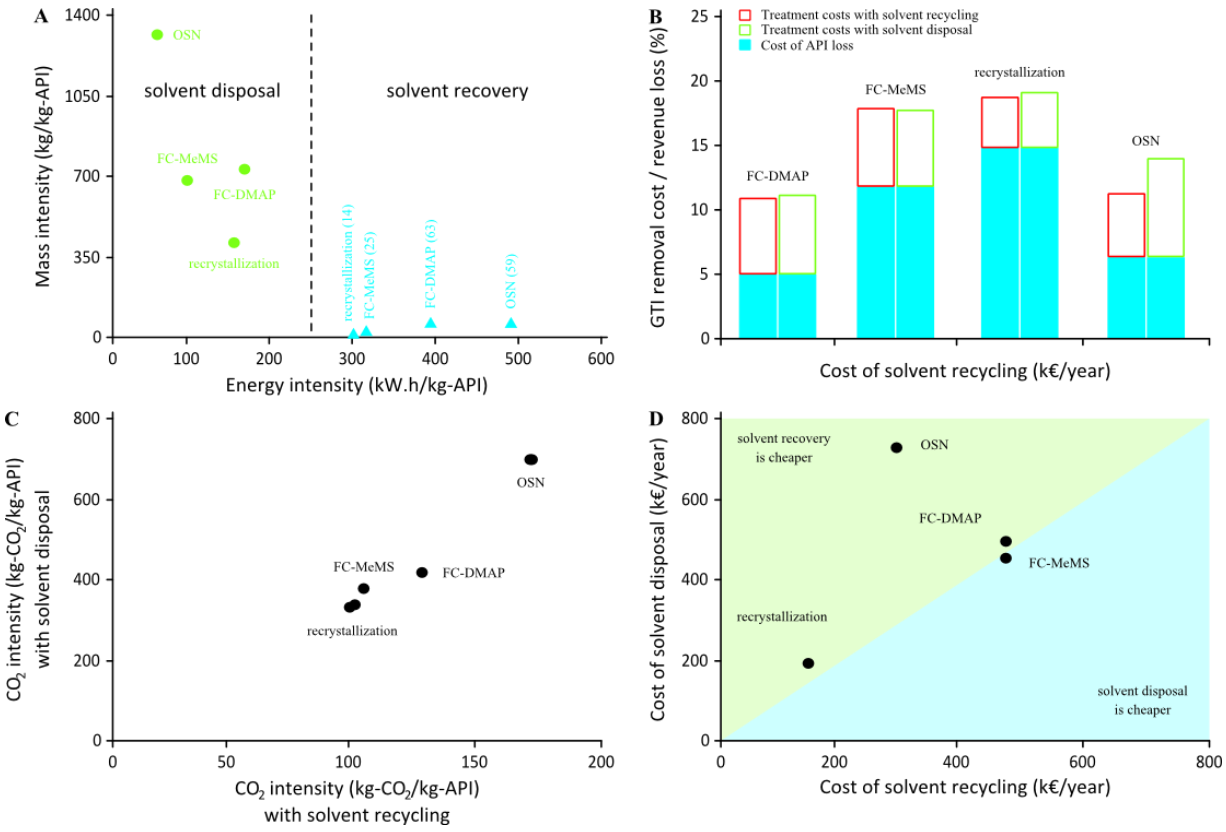

Figure 26 – Effect of solvent recycling on the environmental impact of the processes

Figure 26A shows mass intensity vs energy intensity for each of the processes and with disposal or recycling of the solvent (a 5% make up of the solvent is considered for each of the batches). It is clearly possible to dramatically reduce mass intensity by recycling the solvent but at the cost of an increase in energy intensity, particularly for the OSN process, which is the process with the highest solvent requirements, and therefore with highest energy requirements, when the option of recycling the solvent by distillation is followed. However, since mass and energy intensity are not directly comparable, those options were also evaluated using an economic and environment metric, cash and CO_2 intensity, respectively. In the calculations of energy intensity, costs and associated carbon intensity, the source of energy was taken into account at 203.7 or 369 kg of CO_2 and 27.4 or 93.5 €.MWatth^{-1}, for steam and electricity, respectively. Solvent incineration is considered for solvent disposal. Interestingly, following the option of recycling narrows down process CO_2 intensity to a range of about 100 kg of CO_2 per kg of API (80 to 180 kg-CO_2/kg-API), which implies a large reduction of CO_2 footprint for the OSN process (Figure 26C). Figure 26D shows that the cost options for solvent disposal (considering the costs of 1.35 and 3 €.kg^{-1} of chlorinated solid and liquid waste, respectively) and solvent recycle it is fairly similar for flash

chromatography and recrystallization but not for OSN. In the case of OSN the option of recycling is cheaper than disposal, with a yearly gain of €275,000. The DCM used in the OSN (123 ton per year) is about double that used for flash chromatography, and thus well above the critical point at which it becomes cost effective to have a DCM in-site recovery unit (directed investment cost of €150,000), with savings in solvent and waste treatment costs of €78,000 and €234,000. These figures are aligned with previous literature, a case study for reducing waste by DCM distillation in pharmaceutical processes by Dow Chemical Company[194], which aimed at an initial recycle of 50% of the DCM for a total use of 124 tonnes of DCM, and with a final aim of recycling 95%. The projected initial investment was $140,000 and reported savings of raw materials and waste treatment costs were €105,000 and €335,000 respectively. Overall costs are very much dependent on the total API loss and Figure 26B illustrates calculated values for the scenarios considered in the current study assuming an API value of 100 €.kg^{-1} using the values described above for the costs of API losses in addition to the GTI removal process costs.

4.3. Screening of OSN membranes

4.3.1. API and GTI rejections and fluxes

The solvent fluxes for pure solvent were firstly estimate for pure solvent fluxes at different pressures, as resumed in Figure 27. The maximum applied pressures indicated by the suppliers were 35 and 20 bar for GMT-oNF-2 and for SolSep NF010206, respectively. In this study we did confirm experimentally that Solsep NF010206 membrane was damaged, with the flux increasing rapidly, at 30 bar and 40 bar, when permeating THF and MEK, respectively. For the permeation of the 300 mL assessed in this experiment, the GMT-oNF-2 membrane was stable up to 45 bar. Diafiltrations were carried out for longer periods, up to 2 days at 10 and 20 bar, and both membranes were stable for such periods.

Flux was stable for all the membranes after permeation of the first 50 mL of solvent and permeability was calculated from the linear section of the curves obtained between 5 and 25 bar applied pressure at a value of 3 Lh^{-1}m^{-2}bar^{-1} for permeation of THF in both membranes and MEK in SolSep NF010206.

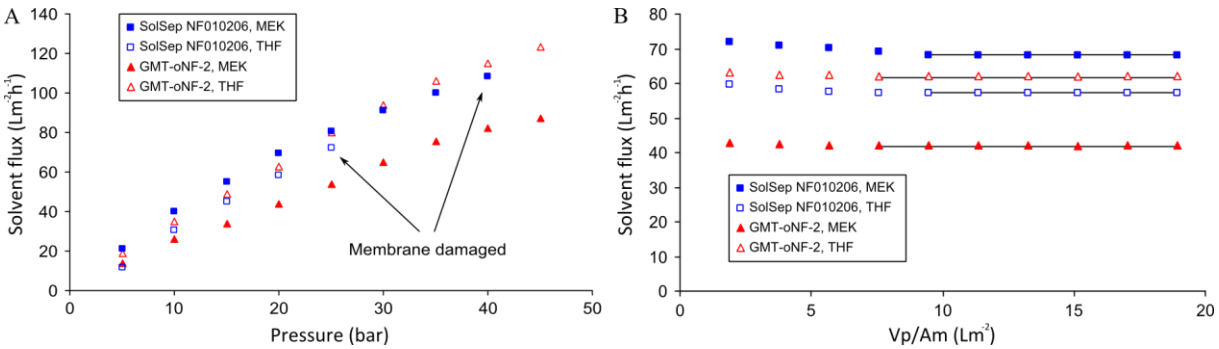

Figure 27 – (A) comparison of solvent fluxes at different pressures, (B) changes in solvent flux at 20 bar until steady-state is reached

However the permeability value was 2.1 $L.m^{-2}.h^{-1}.bar^{-1}$ for permeation of MEK in GMT-oNF-2. The experimental rejections obtained for the APIs and GTIs in both solvent systems and membranes obtained at 10 and 20 bar are resumed as function of compound Mw in Figure 28 and the values are summarized in Table 9 where the different cases further evaluated by diafiltration are highlighted.

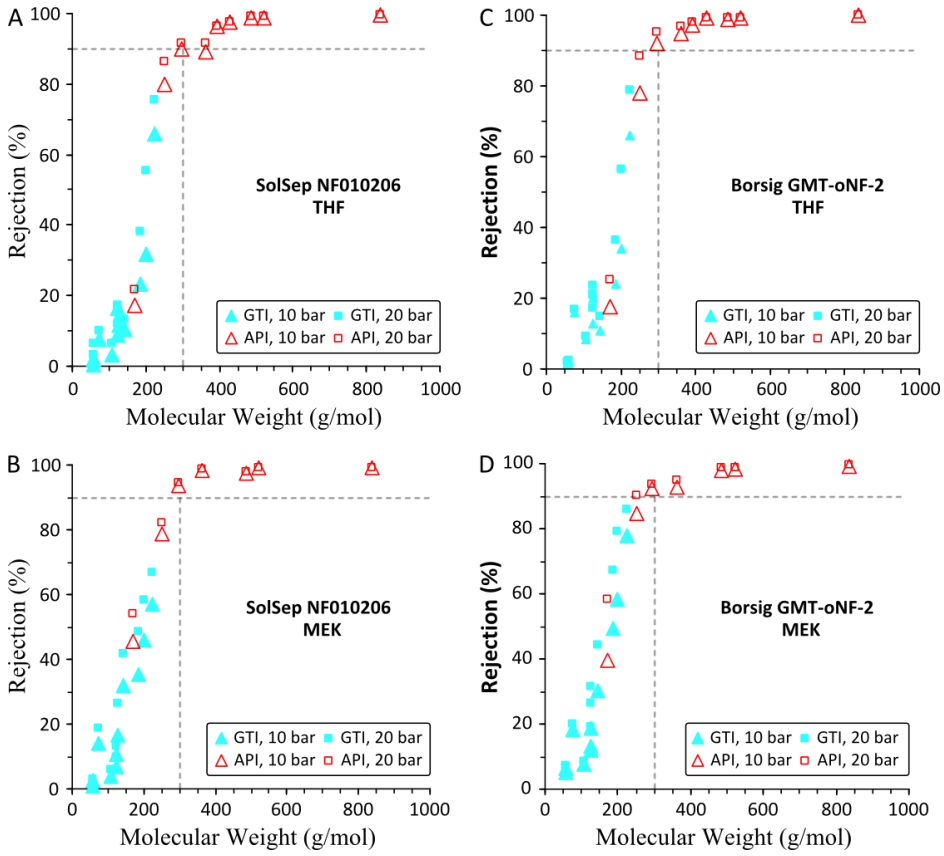

Figure 28 - API and GTI rejections for SolSep NF010206 in THF and MEK; Borsig GMT-oNF-2 in THF and MEK are shown in chart A, B, C and D respectively.

Table 9 – Rejections of APIs and GTIs

Membrane	SolSep 206				GMT-oNF-2			
Solvent	THF		MEK		THF		MEK	
Pressure (bar)	10	20	10	20	10	20	10	20
ACR	0.6	6.4	2.5	2.9	1.6	2.2	5.2	6.9
AA	2.2	3.2	0.9	1.3	2.1	2.5	6.3	7.2
TA	7.7	10.0	14.1	18.8	16.0	17.0	18.2	20.0
DMCC	3.4	6.4	3.9	5.8	8.5	9.3	7.6	8.7
EtMS	16.7	17.4	7.0	9.9	20.1	21.2	18.7	31.6
BE	8.9	12.0	10.7	13.2	12.6	17.1	12.1	19.3
DMS	11.6	14.1	16.4	26.4	21.4	23.7	13.3	26.5
IPU	10.4	13.4	31.9	41.9	10.8	14.9	30.3	44.3
KP	17.4	21.5	45.7	54.0	17.8	25.4	41.0	58.9
MeTS	23.3	38.4	35.2	48.4	23.9	36.6	49.4	67.3
EtTS	31.8	55.5	45.9	58.5	33.9	56.5	58.3	79.4
CHU	65.8	75.4	56.9	66.7	66.2	79.0	77.8	85.8
LA	80.1	86.5	78.6	82.1	78.0	88.6	84.9	90.2
Suma	90.0	91.7	93.5	94.4	91.9	95.2	92.2	93.6
Pred	89.0	91.7	98.2	98.6	95.0	97.0	92.8	95.0
Beta	96.4	96.6	-	-	97.1	98.0	-	-
Irb	97.4	97.7	-	-	99.2	99.3	-	-
Halo	99.0	99.3	97.3	98.0	99.0	99.3	97.9	98.9
Meta	98.9	99.1	99.1	99.3	99.1	99.2	98.4	98.9
Roxi	99.4	99.6	99.3	99.3	99.8	99.9	99.2	99.5

Case A	GTIs
Case B	APIs
Case C	

There is only a slight increase in rejection, as pressure is increased from 10 bar to 20 bar (Figure 29A), which is explained by a decrease in free volume of the active layer due to higher compressibility, as consistent with a TFC membrane with a active layer relatively thick. This effect is less pronounced in the tails of lower and higher rejections on the MWCO curve, but become visible for intermediate rejections: the gap between rejections can be as large as the one observed for EtTS. This phenomenon occurred in both membranes and solvent systems (e.g. EtTS 58.3% vs. 79.4%, GMT-oNF-2 in MEK or 31.8% vs. 55.5%, SolSep NF010206 in THF). MEK promotes lower permeability and higher rejections (Figure 29B) for GMT-oNF-2 than SolSep NF010206, whereas the same high permeability and similar rejections were estimated for both membranes in THF. These results could be explained with identical slight swelling degree of the active layer of the membranes in THF,

but different ones for MEK, with GMT-oNF-2 swelling less than SolSep NF010206 in this solvent, which leads to lower free volumes, higher rejections and lower permeability. Overall, rejections in MEK are higher than in THF (Figure 29C) which is the more apolar solvent. Further and more detailed studies are required to analyze these results.

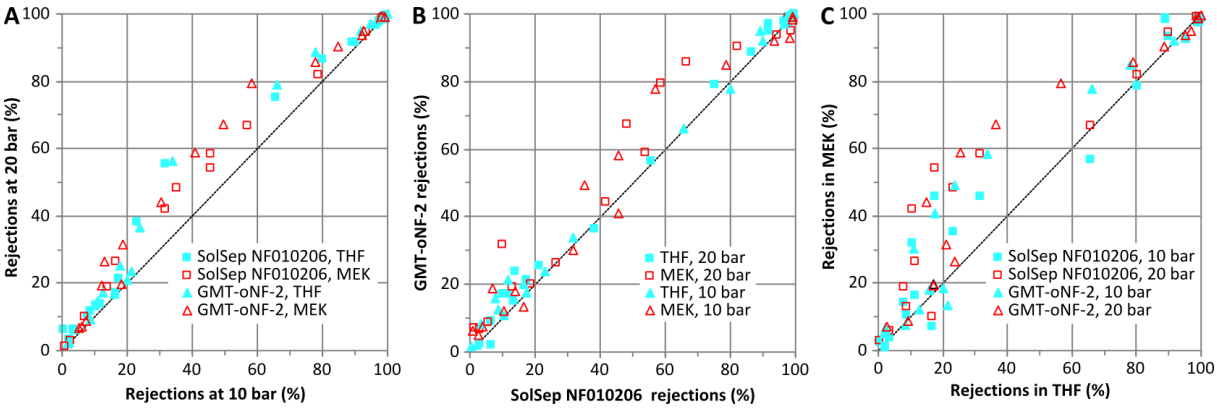

Figure 29 – Rejection comparisons at 10 vs. 20 bar; SolSep NF010206 versus GMT-oNF-2 and MEK vs. THF are shown in chart A, B and C respectively.

The performance of the two OSN membranes are quite similar, providing similar rejections for the same compound in filtrations performed under same conditions (Figure 29B). This observation is in accordance with the SEM analyses (Figure 30) that show for both membranes an active layer of similar thicknesses (5 μm), and most probably of the same material, silicone rubber polydimethylsiloxane (PDMS). Further amplifications, within the resolution limit of the SEM used do not capture an asymmetric structure of the active layer, indicating that most probably, this layer is comprised by a homogenous phase, such as the ones obtained using silicone rubber. Still it is interesting to note that in the MEK system, for a few compounds with intermediate Mw, there is a shift to lower rejections when SolSep membrane is used instead of the GMT-oNF membrane. This information is important for GTI removal: the SolSep membrane can provide desirable lower rejections than GMT-oNF. For example MeTS, EtTs and CHU have 20% lower rejection in MEK applying SolSep membrane compared to GMT-oNF. Notice as well that API retention is similar for both membranes.

Interestingly, the shape of the MWCO curves is quite different (Figure 28). However, the interpolation of the rejection curves obtained with a rejection of 90% is similar for the 2 membranes and solvent system, at a value of 275 Da; consisting with the estimation of similar MWCO estimation (based on 90% rejections), the rejections, at their higher Mw range are virtually independent of the solvent used (Figure 29C). In the lower range of rejections, MEK promotes predominantly higher rejections for GMT-oNF membrane, which turns more challenging to remove the corresponding GTIs (IPU, MeTS, EtTS) when dissolved in MEK.

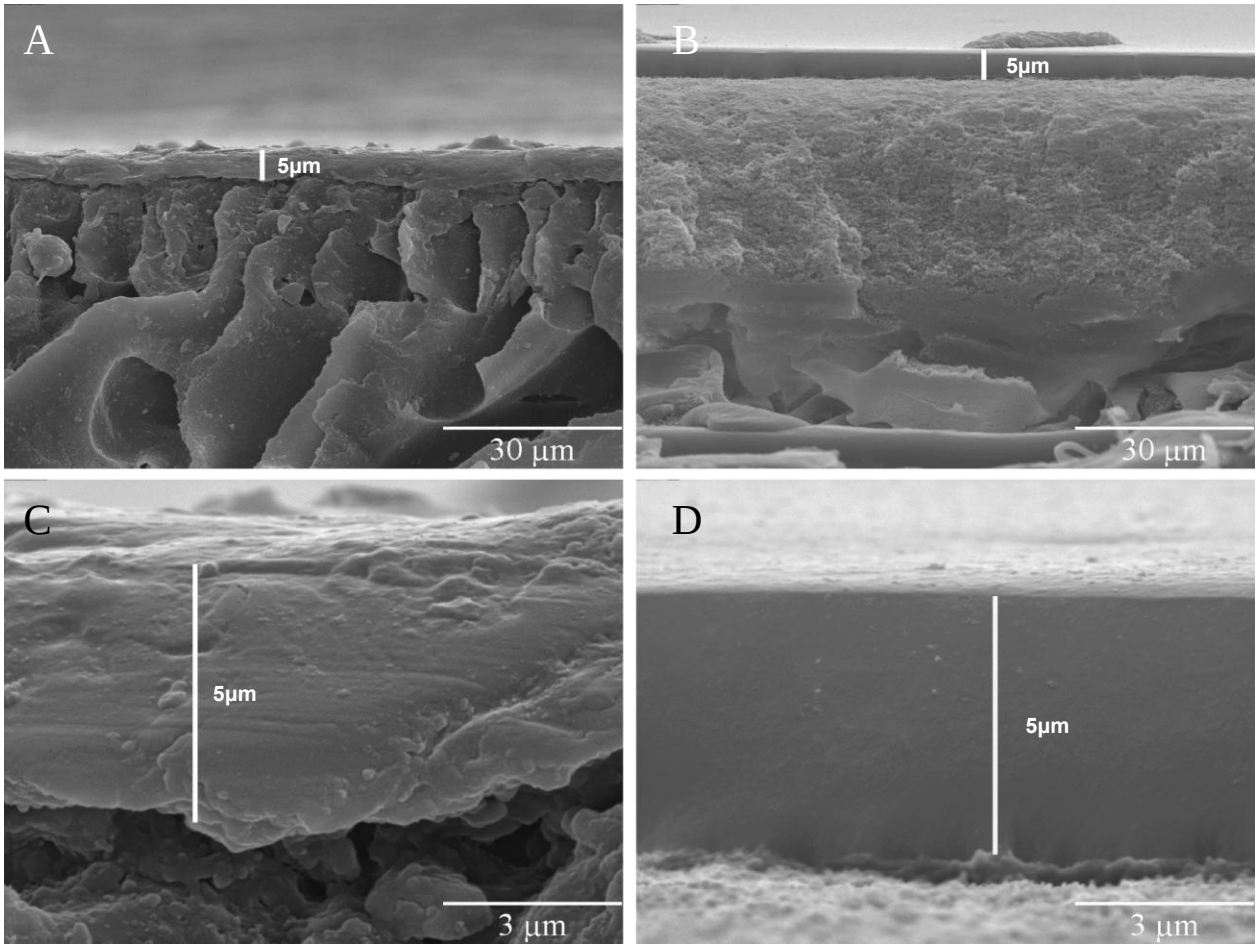

Figure 30 – SEM images obtained for the membranes: left panels (A and C) refers to SolSep NF010206 and right panels (B and D) to Borsig Membrane GMT-oNF-2; bottom panels (C and D) show amplifications of the top active layer of the membranes

4.3.2. Membrane stability test with peroxide

An additional concern for membrane users is membrane stability: THF usually contains traces of peroxide which can damage the polymeric membrane, promoting pinholes and leakages (Figure 31).

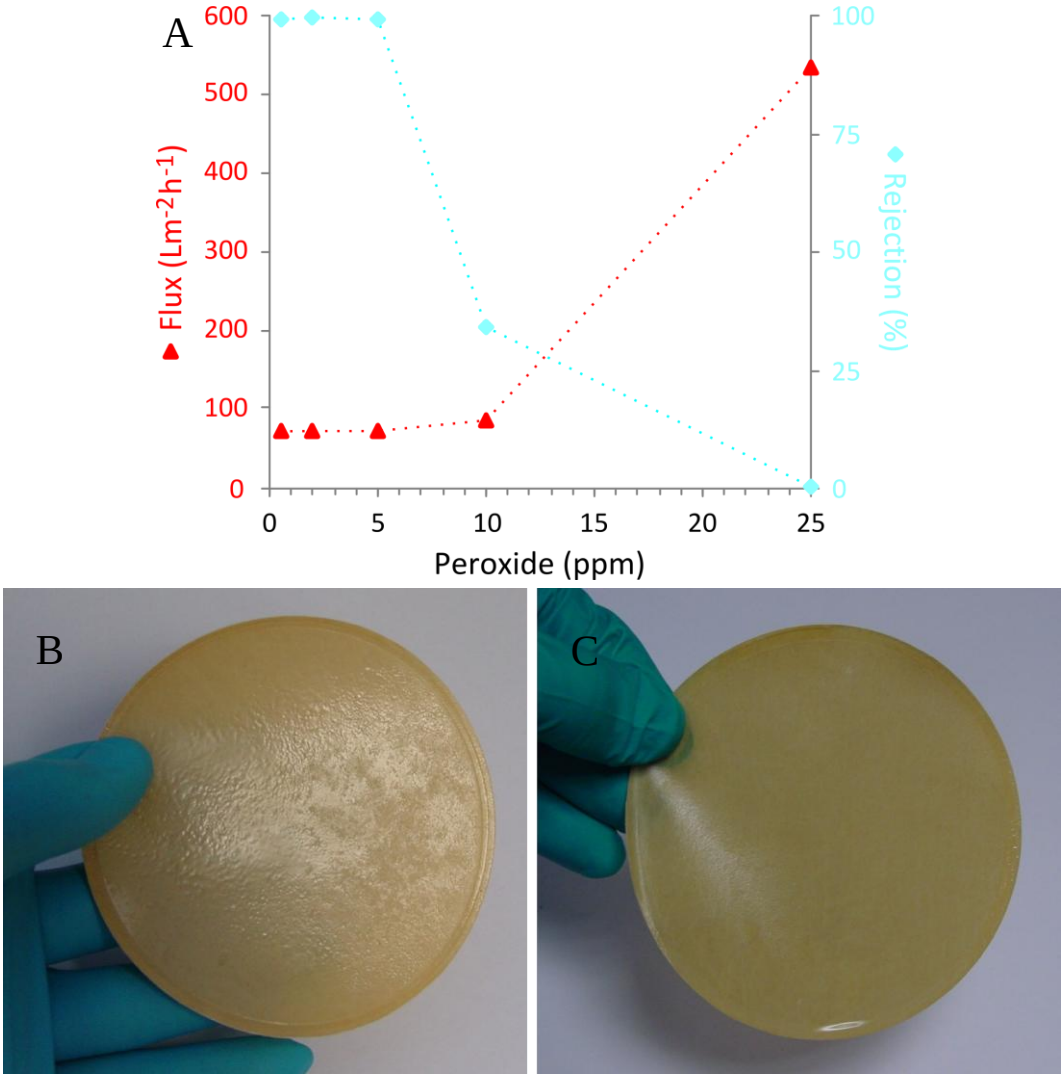

Figure 31 – A: Flux and rejection at various peroxide spiking levels, B: Damaged SolSep membrane after THF filtration in the presence of peroxide, C: Intact SolSep membrane after THF filtration in the absence of peroxide

The amount of peroxide depends on the purity grade of the solvent, the peroxide content increases with time (long and/or inappropriate storage!). Furthermore, API post reaction solutions may contain residual peroxide when it was used as an oxidizing agent during API

synthesis, for instance in Beta production[196]. Thus an additional experiment was performed to the SolSep membrane. Roxi, the API with the largest molecular weight (and thus rejection) was used in this study as a marker during the filtration to check the integrity of the membrane. Peroxide free THF was spiked with increasing amounts of peroxide from 0.5 to 25 ppm and used to prepare 10,000 ppm Roxi solutions. These solutions were left in contact with the membrane for 60 minutes and then solvent flux and Roxi rejections were estimated applying 20 bar. The results indicate that up to 5 ppm of peroxide the membrane is stable, but it is attacked at concentrations of 10 ppm and higher. These effects, flux increase and observable differences on the membrane surface, were not present on the GMT-oNF-2 membrane, and thus this membrane is apparently stable to peroxide in the concentration range usually present in THF.

4.3.3. Diafiltrations

Ideally the rejection of an API and GTI would be 100% and 0% respectively, thus the API loss would be zero. In a diafiltration of a given volume of post reaction solution, several equivalent volumes of fresh solvent are added and permeate, and one can easily calculate that for the ideal case described the GTI removed after permeation (and addition) of 1, 2, 3 and 4 of equivalent volumes (D=1, 2, 3 and 4), 50%, 75%, 87.5% and 93.75% of the GTI would be removed. Unfortunately such ideal case is statistically impossible, since the membrane selectivity follows a probability curve. The success of the OSN separation is mainly defined by the gap between the rejection values of the API and GTI pairs, which is function of molecular size, among other chemical and physical properties. Therefore to probe OSN stage feasibility several experimental diafiltration assays were performed (Figure 32).

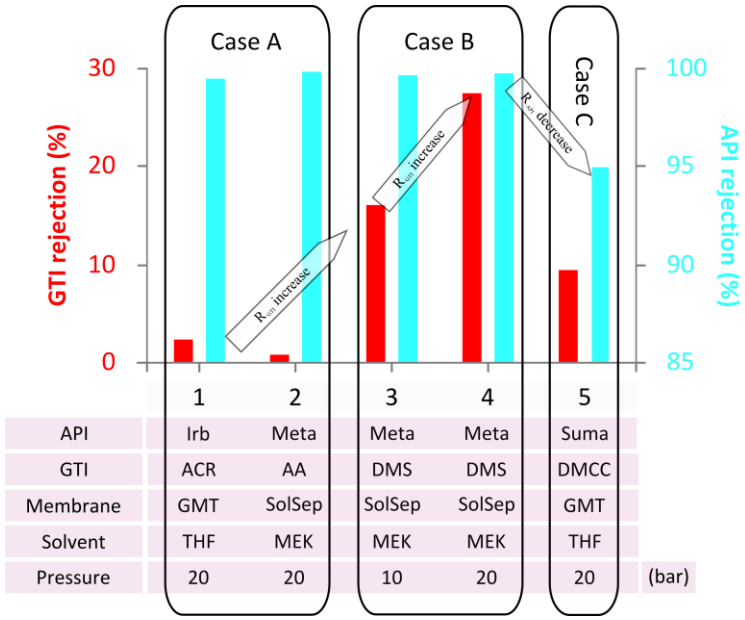

Figure 32 – Diafiltration case studies: resume of input parameters

Table 10 – Diafiltration case studies

Cases	API vs GTI	Rejections (%)		Conditions: membrane, solvent, pressure (bar)
		API	GTI	
Case A: Easy	Irb vs ACR	99.3	2.2	GMT-oNF-2, THF 20
	Meta vs AA	99.2	1.3	SolSep, MEK, 20
Cases B: High GTI rejection	Meta vs DMS	99.1	16.4	SolSep, MEK, 10
	Meta vs DMS	99.3	26.4	SolSep, MEK, 20
Case C: Low API rejections	Suma vs DMCC	95.2	9.3	GMT-oNF-2, THF, 20

Three cases were selected in order to illustrate the opportunities and challenges of the use of diafiltration (Figure 32, Table 10), in all the cases an initial GTI/API ratio was set to 10wt%, with an API concentration of 10,000 ppm. Case A illustrates a scenario where OSN is particularly adequate for the separation, since API and GTI rejections approach the ideal case. Different solvent and membrane combinations were selected (SolSep, MEK, 20 bar AA 1.3%, Meta 99.2% and GMT-oNF-2, THF, 20 bar Acr 2.2%, Irb 99.3%). Cases B shows how higher GTI rejections can present additional challenges to OSN, and how the effect of pressure was explored to improve GTI removal, without increasing API loss. Two examples, both using the same membrane, solvent and solutes, but two different pressures applied, were selected for this case (SolSep, MEK, 20 bar DMS 26.4%, Meta 99.3%and SolSep, MEK, 10 bar DMS

16.4%, Meta 99.1%). Case C illustrates that a slight decrease in API rejection represents a dramatic increase in API loss, limiting the maximum operating dilution (GMT-oNF-2, THF, 20 bar DMCC 9.3%, Suma 95,2%).

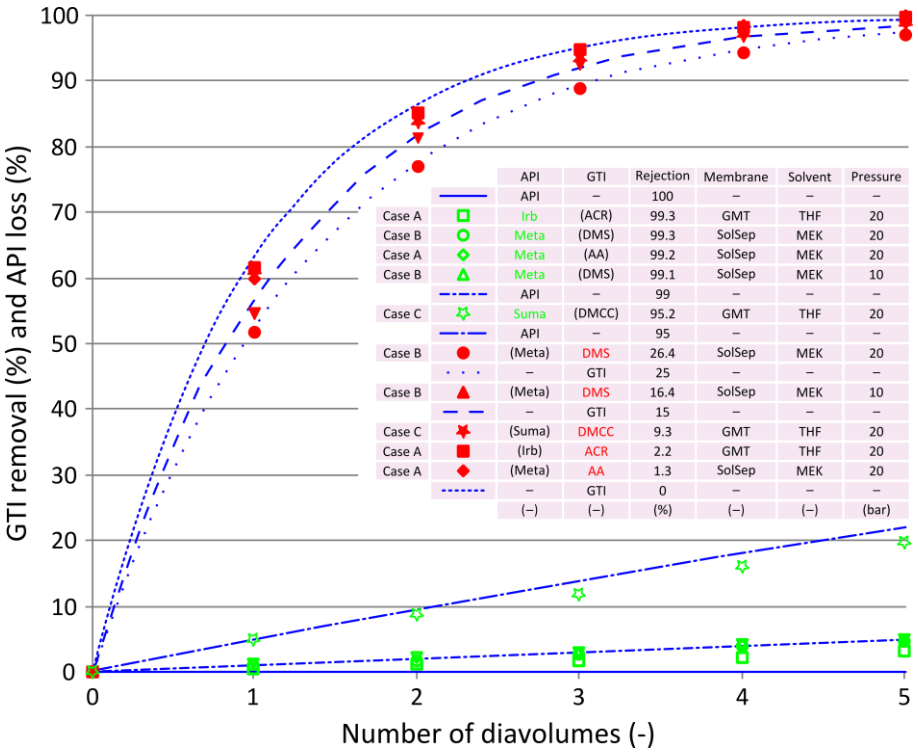

Figure 33 – Diafiltration results: lines correspond to calculated values based on estimated rejections, markers correspond to experimental results. When reporting GTI removals or API losses, the corresponding co-dissolved API or GTI is indicated in the legend between brackets

The examples within Case A show that is feasible to remove virtually all the GTI (more than 99.5%) using a diavolume of 5, with API loss below 5% (3.2% and 4.5%). The data are initially presented as API loss and GTI removal percentages (Figure 33). However, it is actually GTI per API amounts that will dictate drug safety. In the present experimental study, model systems with initial concentrations of API were always 10 $g.L^{-1}$ and the GTI 1 $g.L^{-1}$, corresponding to initial GTI/API mass ratio of 10 wt%. These are quite high initial GTI/API ratios compared with the usual values find in real synthetic routes, usually in the range of 1-5wt%. It is still worth to report the GTI content present on the final solution and the respective final GTI/API ratios (Figure 34).

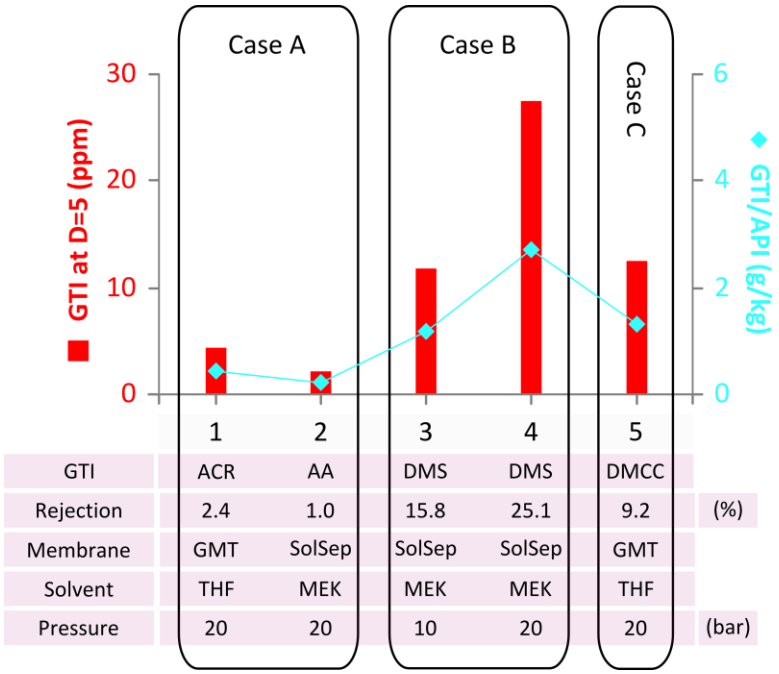

Figure 34 – Resume of diafiltration results obtained in the case studies when the number of diavolumes was 5

Notice that in Case B, changing the pressure from 20 to 10 bar, it was possible to decrease to more than half the final GTI level in the API. Also in the examples of Case B the rejections of GTIs are significantly high which makes GTI removal challenging, even though the API rejections are quite high at values of about 99%. Therefore higher numbers of diavolumes (above 5) were also tested in order to evaluate if further API purification is feasible without significant API loss. The results in Figure 35 show that complete GTI removal, below the detection limit of 0.5 ppm, were indeed achieved with API loss of about 9%.

Removal of DMS from a Meta solution has been chosen as an example, which falls in Case B, to calculate the effectiveness of OSN in API detoxification. Steroids, such as Meta and Pred, are often used to treat dermatologic diseases. These can be used as oral tablets where 5, 30 and 100 mg per day are generally considered low, moderate and high doses[197].

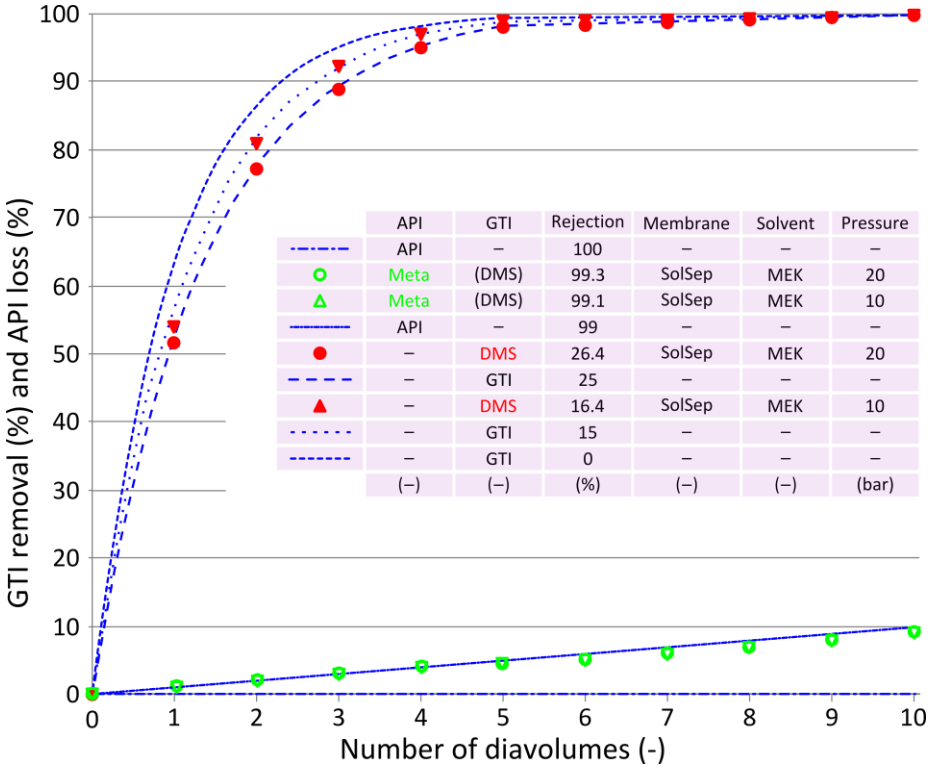

Figure 35 – Examples of diafiltration at higher numbers of diavolumes, effect of pressure: lines correspond to calculated values based on theoretical rejections; markers correspond to experimental results

In the absence of toxicological data for the impurity the TTC for genotoxic impurities should be used to set limits. Calculation of the limits to be applied for DMS is as follows: the TTC value (1.5 μg.day^{-1}) divided by the maximum daily dose (g.day^{-1}) gives the limit in ppm to be applied to the active substance[190]. For diafiltration Case B, where DMS was removed from Meta in MEK at 20 bar, the maximum limit of the impurity is calculated and the numbers of diavolumes needed to achieve sufficiently pure API and the corresponding API loss are given in Table 11. Notice, that regardless the daily dose considered, for the calculated case, taking into account the particular conditions used, such as API concentrations and TTC value, the allowable concentration range of the impurities is always higher than 5 ppm.

Table 11 – Dependence of diafiltration effectiveness on the API daily dose

	API daily dose (mg.day^{-1})	Impurity limit (ppm)	Number of diavolumes (-)	API loss (%)
Low dose	5	300	2	1.8
Moderate dose	30	50	5	4.6
High dose	150	10	7	5.5

Case C represents a boundary for the application of OSN in degenotoxification of pharmaceuticals, in which about 99% of the GTI is removed using a diavolume of 5, but at a cost of 20% of API loss, which is a similar value for the phase exchange stage in a conventional process.

4.4. Screening and designing molecularly imprinted scavengers

4.4.1. In search for IPU selective scavengers – ExploraSep® screening

The aim of the screening was to rapidly identify a hit scavenger capable of selectively binding IPU in the presence of an API. All the scavengers are re-usable when clean solvents are used – in the absence of surfactants and proteins – and can be regenerated by an elution step. All scavengers found in ExploraSep® plates are commercially available both in pre-packed SPE columns and as bulk adsorbents. This has the advantage that once a hit scavenger is found by screening (i) optimization of the separation process can be easily assessed and (ii) the scale-up for pilot plant and industrial scale is assured. The basic principle behind the ExploraSep® screening is the cross-reactivity of the scavengers: molecules having similar functional groups and framework to the template molecule can also be captured by the binding sites due to having a degree of flexibility in their recognition properties[198]. This approach is referred to as selectophore concept[199]. The work was carried out at MIP Technologies, part of Biotage AB, Sweden[200]. ExploraSep® Screening Plate A was chosen to be screened since its scavengers feature different hydrophobic and carboxylic acid moieties that can possibly bind IPU. The screening was carried out on a multiwell plate containing 16 MIPs – and the corresponding reference NIPs – generated against many different templates and comprising different monomer chemistries. Note, that the composition of the scavengers is confidential. The binding percentage values of IPU and Meta on Plate A in acetonitrile:toluene (5:95) loading solvent are shown in Figure 36A. The selectivity (S) of the scavenger can be calculated based on equation 26 and the results are summarized in Figure 36B.

$$S = \frac{B_{IPU} - B_{Meta}}{B_{IPU}} \cdot 100 \qquad \text{(eq. 26)}$$

where B_{IPU} and B_{Meta} are the binding percentage of IPU and Meta respectively. The highest selectivity of IPU over Meta was achieved by the scavenger labeled as EA088 corresponding

to 94% IPU binding. Interesting to note that the hit scavenger is a NIP and not a MIP. On the other hand, the corresponding MIP – labeled as EA087 – has 15% higher binding of IPU but a significant amount of Meta is also bound to the extraction phase (Figure 36).

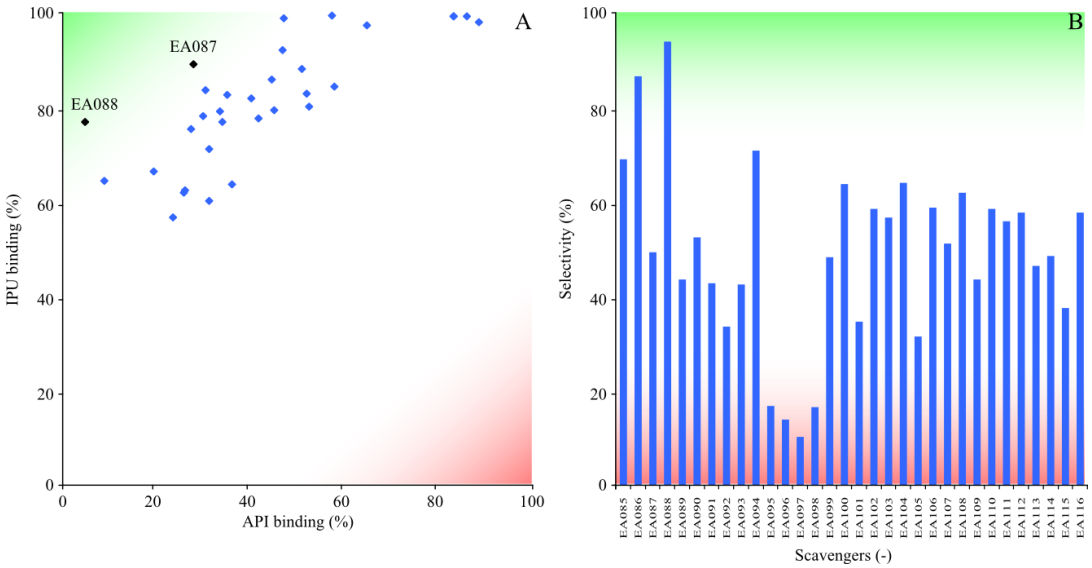

Figure 36 – Binding (A) and selectivity (B) of the IPU-Meta system on ExploraSep® Screening Plate A

In order to adjust to the current industrial needs a solvent swap was necessary from acetonitrile:toluene (5:95) to DCM resulting in 29% IPU and 2% Meta binding on EA088. The decreased capacity of the scavenger in DCM called for a specifically designed MIP featuring IPU as the template.

4.4.2. Design and characterization of the novel scavengers

Two IPU-imprinted polymers (MIP1-2) and two corresponding non-imprinted polymers (NIP1-2) were prepared in the absence (MIP1 and NIP1) and in the presence (MIP2 and NIP2) of the deprotonating agent PMP (details in chapter 3.5, Table 3). The model functional monomer selected for IPU scavenging is MAA being often used in non-covalent imprinting protocols. Usually the non-covalent molecular imprinting protocols are preferred due to the relative ease for preparation, template removal and recovery. Particularly, the non-covalent strategy involves the self-assembly of the IPU template and the MAA functional monomer via non-covalent interactions to form IPU-MAA complexes in DCM, a typical non-polar porogen for molecular imprinting. MAA features a carboxylic acid moiety which can act as a host and form complexes in two different ways: (i) as an acid it can protonate the target analyte

resulting in an ionic interaction or (ii) as a conjugate base it can attract protons from the guest. Despite of the fact that MAA has been applied in molecular imprinting as a functional monomer since the establishment of the field, up until this point in time, relatively few investigations have addressed (i) the mechanisms underlying the molecular recognition of methacrylate based MIPs, and (ii) the role of template-MAA complex formation during the self-assembly process in the pre-polymerization mixtures. Furthermore, the effect of a deprotonating agent on the complexation mechanism and strength has never been thoroughly investigated. In the present thesis NMR, FTIR and DFT were applied to study the complexation mechanism both in the presence and absence of PMP deprotonating agent. Note that the quantum chemical calculations were done by Peter Pogány (Budapest University of Technology and Economics) as part of a collaboration. Besides the complexation in the pre-polymerization solution, the effect of a deprotonating agent on molecular recognition of the scavenger itself was also studied and novel indicators are proposed to numerically describe the effect on MIP performance. It is interesting to note that Hall *et al*. used a diaryl substituted urea derivative in anion recognition receptors whilst the present work discusses MIPs featuring anionic binding sites for scavenging a urea derivative[201].

The novel IPU imprinted polymers were characterized by elemental micro-analysis, FTIR and TGA to gain information on polymer composition and to confirm removal of the target molecule. BET was carried out to estimate the pore size distribution of the prepared polymers, as well as their specific pore volume and surface area, whereas the polymer particle size and shape was characterized by microscopy. The percentage by mass of carbon, hydrogen and nitrogen of the solvent extracted polymers determined by elemental analysis, as well as the expected values predicted from the feed ratio are given in Table 12 and the corresponding calculation is presented in chapter 3.3 under equation 5. Apart from the nitrile containing initiator, which when fully incorporated would give a nitrogen content of 0.15%, the only source of nitrogen is found in the presumed extractable IPU and PMP, which prior to extraction would result in a %N of 1.04. The nitrogen content is hence informative of the extent template removal. MIP1 and NIP1 exhibit a %N close to 0.15 indicating an effective removal of IPU if it is assumed that the initiator was incorporated 100%. This contrasts with MIP2 and NIP2 which both display elevated nitrogen content. Interestingly the values observed (0.45% and 0.42%) are in close agreement with the presumption that the IPU is completely removed whereas PMP is not fully extracted as would be the case where this

amine is ionically bound to the carboxylate of the polymer. Additional evidence for the presence of PMP in the polymer came from the thermal gravimetric analysis.

Table 12 – Measured percentage by mass of carbon, hydrogen and nitrogen of the scavengers. The expected elemental composition assuming an exhaustive removal of IPU and PMP was as follows: %C=60.31; %H=7.15; %N=0.15. In the case of only partial removal of IPU or PMP the following N percentage can be expected: %N=0.46 (IPU removed, no PMP removed); %N=1.04 (no removal of IPU and PMP).

	Carbon (%)	Hydrogen (%)	Nitrogen (%)
MIP1	59.37	6.89	0.19
MIP2	59.53	7.02	0.45
NIP1	59.39	6.92	0.15
NIP2	59.63	6.81	0.42

All the polymers show similar thermograms. All start to lose mass at 250 ºC, which is closely followed by the degradation of the material from 450 ºC onwards. Figure 37 shows the thermogram of the scavengers.

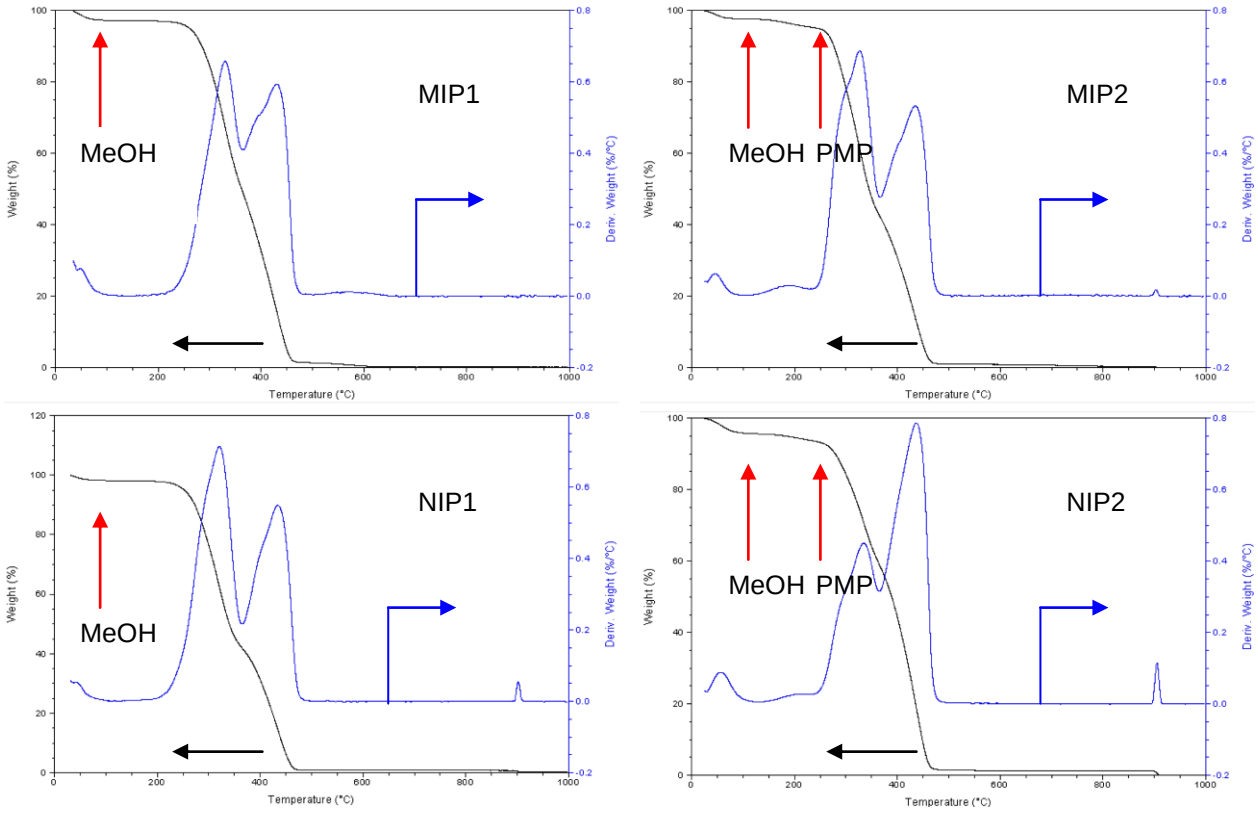

Figure 37 – Thermograms of the scavengers demonstrate the presence of a small amount of PMP and methanol, driven from the synthetic and washing steps, respectively

A 2% mass loss was observed at 50 ºC presumably due to the adsorbed methanol, carried on from the washing step to remove the template. It is interesting to note that the imprinted polymers adsorb slightly more methanol than the non-imprinted polymers. A 5% mass loss, with an onset at 150 ºC, was observed for both MIP2 and NIP2 polymers, but not for the MIP1 and NIP1, which show no weight loss at that temperature. This result agrees hence with the elemental analysis, confirming that, despite the intensive solvent extraction procedure after the MIP preparation, the PMP base used in the synthesis of MIP2 and NIP2 is still present in the final polymer samples.

Apart from the differences described above, FTIR (Figure 38) and nitrogen sorption analysis (Table 13) indicated that the materials were nearly identical in terms of chemical composition and dry state morphology. As expected, the typical characteristic peaks of carboxylic acids (from the MAA functional monomer) are clearly identified corresponding to the strong and broad band for the O–H stretch in the region 3,300-2,500 cm^{-1}, centered at about 3,000 cm^{-1}, which are superimposed with sharp C–H stretching bands of the alkyl groups, visible in the same region. The carbonyl stretch C=O from the saturated and unsaturated aliphatic esters from the EDMA cross-linker and the MAA carboxylic group corresponds to the intense band at 1750 cm^{-1}. The typical carboxylate C–O stretch (1300 cm^{-1}) and O–H bends (1430 cm^{-1}, 950 cm^{-1}) were also observed.

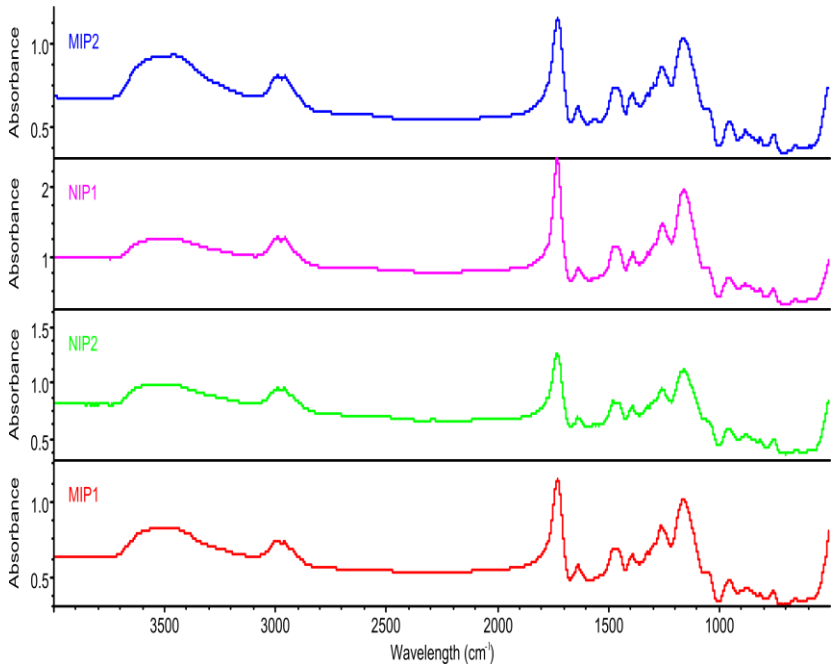

Figure 38 – FTIR spectra of the novel scavengers

Table 13 – BET and morphological characterization of the novel scavengers

	V_{po} (ccg^{-1})	A_{SS} (m^2g^{-1})	r_{po} (nm)	V_{SE} (μm^3)	Circularity (-)	Convexity (-)	Intensity (-)
MIP1	0.969	850	0.193	43.25±5.25	0.67±0.24	0.90±0.11	134±15
MIP2	0.953	855	0.195	40.95±4.85	0.89±0.21	0.99±0.03	108±13
NIP1	0.879	801	0.195	42.94±3.91	0.74±0.24	0.95±0.08	128±13
NIP2	0.922	820	0.196	42.41±7.06	0.93±0.21	0.98±0.058	107±17

The nitrogen sorption analysis revealed a mesoporous morphology with an exceptionally high specific surface area (A_{SS}) and pore volume (V_{po}) by the BET method[202,203]. This permanent porosity we anticipated to be important for a broad applicability of the materials in a wide range of organic solvents. The properties of the imprinted and non-imprinted polymers are shown in Table 13. The specific surface area and pore volume increase in the following order: MIP2 > MIP1 > NIP2 > NIP1 but the values are similar, with a respective experimental error of 0.04 ccg^{-1} and 25 m^2g^{-1}. V_{po} and A_{SS} of about 0.9 ccg^{-1} and 850 m^2g^{-1} was estimated. The shape of isotherms resembled *Type II* according to IUPAC classification (Figure 39)[204]. The high slope and the lack of rounded knee below a relative pressure of 0.4 P/P_0 indicates that the formation of multilayers after the monolayer is immediate. Hysteresis indicates capillary condensation in meso- and macropores and closes at a relative pressure of 0.4 P/P_0 (indicating the presence of small mesopores).

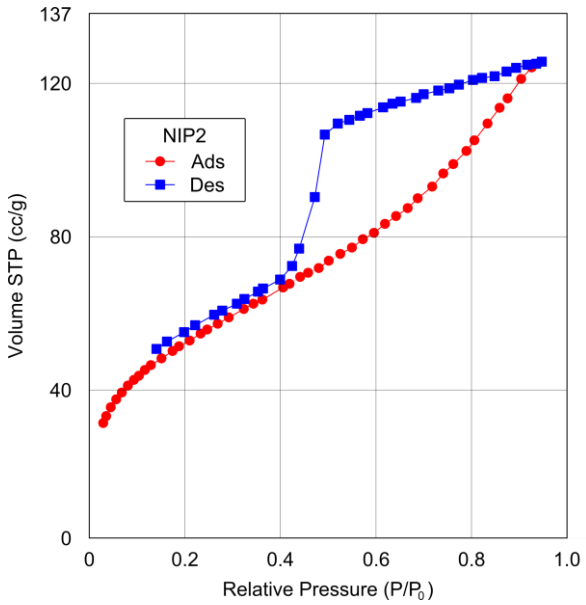

Figure 39 – The isotherms observed show a typical BET isotherm for a poly(MAA-co-EDMA) based monolith (illustrated through NIP2)

The present study does not aim to optimize the morphological properties of the polymer particles in terms of their controlled size and shape distribution, but to focus on the molecular recognition properties. Hence, simple "bulk" polymerization was applied in the presence of a porogen which can result in macroporous materials containing very large pores. Further work, such as suspension polymerization[205] may be applied in subsequent studies to obtain monodispersed particles of several microns in diameter. Nevertheless, the particles of the polymer scavengers were visualized by microscopy and the resulting images can be seen in Figure A4 in the Appendix. The particles were similar with respect to shape and size (Table 13) with an average circularity around 0.8, an average spherical equivalent volume (V_{SE}) around 42 μm^3, and the majority of the particles with high convexities in a range of 0.9 to 0.985. The light intensity mean reflects the particle compactness, with less light crossing more compact particles. Particles corresponding to MIP2 and NIP2 prepared in the presence of PMP were more compact than those prepared in the absence of PMP (MIP1 and MIP1), with differences of intensity means in the range of 15-18 % (Figure A5 in the Appendix).

4.4.3. Molecular recognition dependence on deprotonating agents

4.4.3.1. Geometrical parameters of the pre-polymerization complexes

The theoretical calculations of the IPU and MAA showed that the most stable conformers of these two compounds are IPU[a] and *trans*-MAAH (Figure 40), both for gas phase and implicitly treated DCM solution. The latter has already been established by several previous articles[206,207]. The difference of the ground state structure and the other two IPU conformers is significant with a value of 23 kJ.mol^{-1} in gas phase and 25 kJ.mol^{-1} in DCM for IPU[b] and 8 kJ.mol^{-1} in gas phase and 13 kJ.mol^{-1} in DCM for IPU[c]. However the energy difference between *trans*-MAAH and *cis*-MAAH is only marginal, being 1-2 kJ.mol^{-1}. The complexes were constructed considering all the sterically different structures.

The observed difference in the stability of the conformers in gas phase and DCM solution is insignificant. Figure 41 shows the most stable structures of the complexes in DCM solution. The structures of IPU:MAA$^-$ (1:1) complex in both gas and liquid phase show high similarity (Figure 41B). The only difference in the complex structure is that the MAA$^-$ moiety is more bent relative to IPU in DCM than in the gas phase, however this causes an energy difference of around 1 kJ.mol^{-1}. Note that this structure is not symmetric due to the non-symmetric

MAA^- molecule (C11 and C12 are sp^2 and sp^3 carbon atoms respectively – for the numbering see Figure 41B).

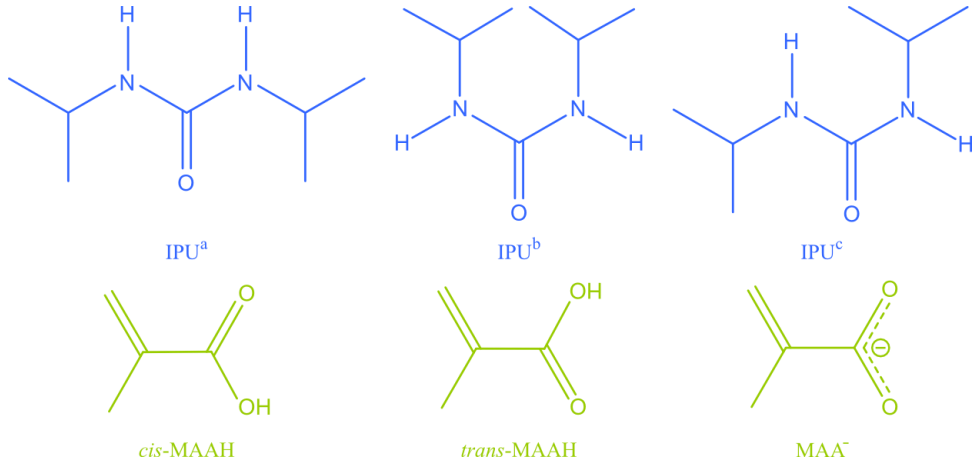

Figure 40 – Schematic representation of the initial conformers of IPU and MAA for the DFT calculations

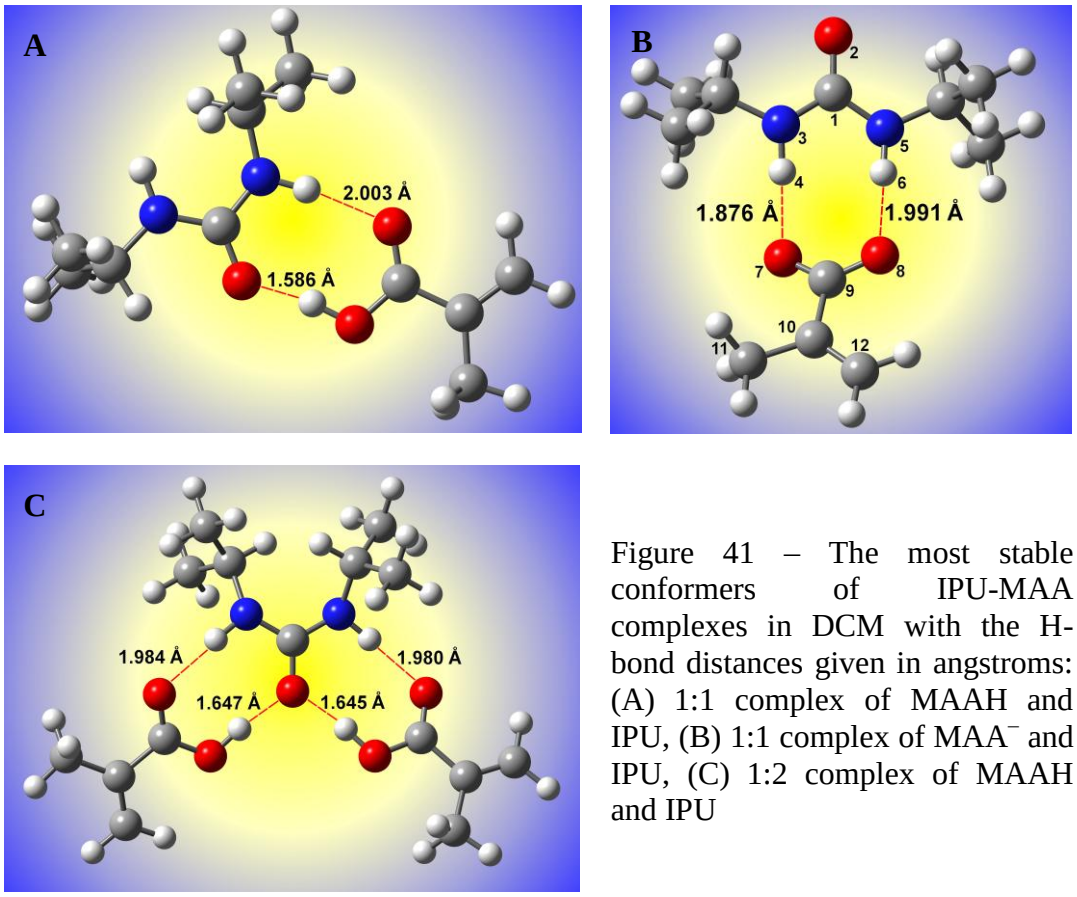

Figure 41 – The most stable conformers of IPU-MAA complexes in DCM with the H-bond distances given in angstroms: (A) 1:1 complex of MAAH and IPU, (B) 1:1 complex of MAA^- and IPU, (C) 1:2 complex of MAAH and IPU

To explain this phenomenon better NBO analysis was applied. The electrostatic effects were, unexpectedly, not important in this asymmetry. Table 14 shows that the symmetry of charges

in IPU did not change with complexation, however N5, N3 and O2 gained some negative charge (all together 0.084 e), whilst H4 and H6 lost some charge (0.054 e). Some smaller changes of the charges occur on the isopropyl part of the molecule. These charge changes show, that significant charge transfer should occur in the system. The charge transfer from the IPU N3-H4 bond and the N3 lone pair to MAA^- C9-O7 is around 11 $kJ.mol^{-1}$, whilst from N5-H6 to C9-O8 it is only 5 $kJ.mol^{-1}$. However the charge transfer in the other direction is expected to be much larger due to the lone pairs of O atoms. Two delocalized electron system can be found in MAA^-: O7-C9-C10-C12 and O7-C9-O8. O7 is present in both of these, therefore O7 can donate more electrons to H4 of IPU than O8 to H6. This is justified by the NBO charge transfer analysis. The N3-H4 bond and the H4 atom receives electrons from O7 lone pairs, O7-C9 bond and C9-C10 bond, on the contrary the N5-H6 bond and H6 atom receives electrons only from the O8 lone pair. The total energy of the charge transfer in the first case is 76 $kJ.mol^{-1}$ and in the second case 41 $kJ.mol^{-1}$. The higher charge transfer accounts for the shorter bond distance in the complex. The gas and liquid phase structures of MAAH:IPU (1:1) complex differ in the mutual position of the MAA sp^2 and sp^3 carbons, which are reversed in the gas phase in comparison with the structure in DCM, thus making a *trans*-MAAH-IPU[c] more stable in gas phase compared with the *cis*-MAAH-IPU[c] in DCM (Figure 41A). However this change also causes an energy difference of 1-2 $kJ.mol^{-1}$.

Table 14 – NBO charges in MAA^-, IPU[a] and 1:1 complex of IPU and MAA^-

	MAA^-	IPU[a]	IPU:MAA^- (1:1)
C1		0.819	0.818
O2		-0.752	-0.788
N3, N5	–	-0.673	-0.697
H4, H6		0.405	0.432
O7	-0.821		-0.798
O8	-0.832		-0.802
C9	0.745		0.755
C10	-0.107	–	-0.102
C11	-0.604		-0.602
C12	-0.378		-0.376

For IPU:MAA (1:2) complexes, results were obtained only for MAAH. Unexpectedly, the charge density in case of two MAA^- would be so large, that the 1:2 complex spontaneously decomposes, although some higher energy minimum-type structures were found, which can be formed and preserved in solution for a limited time. On the other hand, a stable IPU:MAAH (1:2) complex was observed and its structure is depicted in Figure 41C. The

energy differences between the most stable complex structure observed – featuring one *trans*-MAAH and one *cis*-MAAH conformers – and the less stable structures having two *trans*-MAAH and *cis*-MAAH conformers are 1 $kJ.mol^{-1}$ and 2-3 $kJ.mol^{-1}$ respectively. It is interesting to note that the IPU:MAAH (1:2) complex incorporates IPU^b conformer while the IPU:MAAH (1:1) complex features IPU^c conformer. Despite of the fact that IPU^b is higher in energy than IPU^c by a value of 12 $kJ.mol^{-1}$, the former conformer allows a better access to the NH and C=O moieties which are the active sites of the complexation.

The FTIR experiments confirmed the existence of these binding sites. The FTIR spectra of the IPU and the complex were both measured and calculated. The observed FTIR spectra can be found in the Appendix (Figure A6). Detailed FTIR studies of MAA in halogenated solvents can already be found in the literature (see Table A8 in the Appendix)[206,207]. The comparison of the calculated and measured spectra of IPU is summarized in Table 15. The self-association of IPU was not taken into account in FTIR studies, since at the value determined for the association constant (chapter 4.4.3.3) at the measured IPU concentration (20 mM) the dimer concentration was around 1% compared to the initial IPU. The FTIR is usually insensitive to these trace amounts. The negative or noisy peaks at 706-739, 896 and 1266 cm^{-1} are assigned to the DCM solvent and the peaks at 2342 and 2359 cm^{-1} correspond to the asymmetric stretching vibration of CO_2 present in the air.

The measured and calculated spectra are in a good agreement with an average difference between the measured and calculated frequencies of 38.8 cm^{-1}. It is worth mentioning that consideration of anharmonicity or employing scaling factors could further improve the accuracy of calculations, although all the important signals are yet easily assigned. The biggest differences are observed in the stretching vibrations of both the CH_3 and NH groups. In case of the complex in the absence of PMP), mainly the strongest bands of MAA can be found in the spectrum of the complex (951, 1204, 1300, 1375, 1454, 1636, 1697, 1730 cm^{-1}) whilst only some CH vibration bands appear from the IPU (2872 and 2972 cm^{-1}). There are however three bands which do not appear in either spectrum of the individual compounds (1177, 1423, 1541 cm^{-1}). The assignment of these bands is summarized in Table 15. All three bands which differ in the complex are assigned to characteristical vibrational modes of complex NH…O and OH…O vibrations, thus giving a further evidence for the binding along with binding site characteristics.

Table 15 – Measured and calculated FTIR spectrum of both IPU (#1-18) and the complex (#19-21) in absence of PMP, different from the MAA and IPU spectra)

#	measured		calculated		Assignment[b]
	ν [cm^{-1}]	Intensity[a]	ν [cm^{-1}]	Intensity [$km.mol^{-1}$]	
1	1128	w	1139	75	δCNC, γC-CH_3
2	1167	m	1178	172	νNC, γC-CH_3
3	1229	s	1247	286	δ_rCNC
4	1325	w	1351	16	γCH
5	1368	m	1382	26	γCH
6	1385	m	1394	29	$\delta_s CH_3$
7	1423	w	1413	13	$\delta_s CH_3$
8	1466	m	1492	47	$\delta_{as} CH_3$
9	1524	vs	1549	813	γNH, δNCN
10	1670	vs	1669	557	νCO, δNCN
11	2342	m	-	-	$\nu_{as} CO_2$
12	2359	s	-	-	$\nu_{as} CO_2$
13	2872	w	3013	30	$\nu_{sy} CH_3$
14	2932	m	3017	67	$\nu_{sy} CH_3$
15	2972	s	3086	147	$\nu_{as} CH_3$
16	3046	w	3099	85	$\nu_{as} CH_3$
17	3339	w	3397	14	ν_{as}NH
18	3429	m	3411	189	ν_{sy}NH
19	1177	m	1181	83	βNH…O, βNH, νNC
20	1423	m	1413	150	βOH…O, νNC, $\delta_s CH_3$
21	1541	m	1509	119	βNH…O, νCO

[a] The abbreviations vs, s, m, w and sh mean very strong, strong, medium, weak and shoulder, respectively. The calculated data were obtained at the B3LYP/6-311++G** level.

[b] The abbreviations s, as, ν, δ, β, sci, r mean symmetric, asymmetric, stretch, deformation, bend, scissoring and rock, respectively.

4.4.3.2. Effect of the deprotonating agent on the complexation mechanism

PMP is a highly basic tertiary amine (pKa = 11.25)[208], which can deprotonate MAA forming methacrylate anion. First, the continuous variation method (CVM) was applied, where IPU mole fraction × Δδ (chemical shift change) is plotted as a function of IPU mole fraction. The

points of this curve are proportional to the concentration of the complex assuming solely 1:1 complexation. The first set of experiments (CVM1) were performed in the absence of PMP while two more sets of CVM (CVM2, CVM3) experiments were performed in the presence of PMP. In the case of CVM2 PMP was proportional to MAA while in case of CVM3 the PMP was proportional to IPU. The results obtained from the three sets of CVM experiments are shown in Figure 42. The global maximum of the fitted curves occur at about the same mole fraction of IPU for both CVM1 (x_{IPU} = 0.57) and CVM2 (x_{IPU} = 0.59). This corresponds to a complex ratio of IPU:MAA (1.33:1) and (1.44:1), respectively. These results show two important findings. Firstly, there is no significant difference between the complexation mechanism of methacrylic acid and methacrylate anion with IPU. Note, that the binding strength can still be different as referred to in chapter 4.4.3.3. Secondly, either in the absence or in the presence of PMP the system is more complex than in a one-step complexation event, suggesting (i) the formation not only of 1:1 but 1:2 and 2:1 complexes as well as (ii) the self association of IPU. Given the proportion of IPU:MAA (1:4) in the pre-polymerization solution the presence of IPU:MAA (2:1) complex can be considered as negligible. Hence, the present study focuses only on the IPU:MAA of (1:2).

In order to investigate the importance of the amount of deprotonating agent on the complexation mechanism, the PMP:MAA ratio was radically perturbed in CVM3. Hence, PMP was set to be proportional to IPU (1:1) instead of MAA, the PMP:MAA ratio varied throughout experiment CVM3 (Figure 42C). Up until an IPU mole fraction of 0.5 the PMP is in excess compared to MAA, resulting in mainly deprotonated MAA, whilst when the IPU mole fraction reaches levels of more than 0.5 the MAA is in excess compared to PMP, leading to mainly protonated MAA. The continuous variation of the PMP:MAA ratio during CVM3 leads to an unusual Job plot having a maximum at an IPU mole fraction of 0.7. At low IPU mole fractions the shape of the curve is similar to the CVM2 curve. This indicates an acid-base equilibrium reaction between PMP and MAA. Thus both methacrylic acid and the conjugate base are present, forming complexes with IPU, and resulting in anomalous behaviors of the chemical shifts. These results indicate that the proper choice of the concentration of the deprotonating agent is crucial for the pre-polymerization solution of MIPs, since when in excess this can hamper the binding of the target molecule by the functional monomer. It is interesting to note, that the H3 and H1 (Figure 10) signals of IPU change compared to the other signals. The explanation of this phenomena was aided by DFT calculations, since in some non-ground state but minimum-type complex structures the MAA

O3 (both as MAAH and MAA^-) can form weak H-bonds with H3 and H4 of IPU, indicating also that the effect is much weaker for H4 than for H3. These structures have energies in the range of 20-50 $kJ.mol^{-1}$ above the ground state.

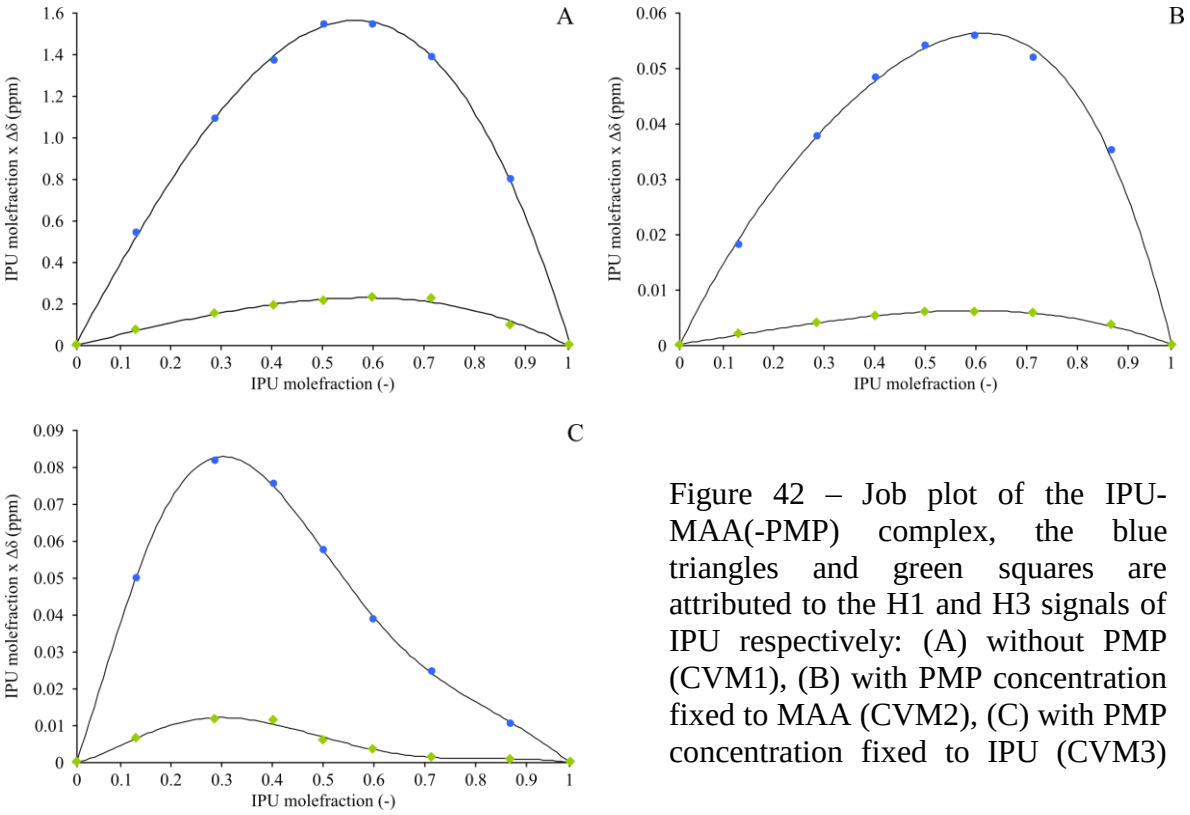

Figure 42 – Job plot of the IPU-MAA(-PMP) complex, the blue triangles and green squares are attributed to the H1 and H3 signals of IPU respectively: (A) without PMP (CVM1), (B) with PMP concentration fixed to MAA (CVM2), (C) with PMP concentration fixed to IPU (CVM3)

IPU is the observed species for all NMR experiments (titration and CVM) and its H1 and H3 proton were chosen to be followed throughout the NMR studies. The rational behind the selection of the H1 proton is as follows: (i) no peak overlapping occurs throughout the titration, (ii) the proton is directly involved in the complexation under investigation. To confirm that the observed chemical shifts are due to complexation between IPU and MAA, two additional studies were carried out: (i) self-association of IPU; (ii) the effect of PMP on the IPU signals in the absence of MAA were assessed. Although the two H1 signals of IPU were found to be identical while being titrated with MAA irrespectively of the presence of PMP, during the self-association experiments at higher concentrations the H1 signal splits. Figure 43 shows the downfield shift (0.201 ppm) and splitting of the H1 signals as well as the upfield shift (0.009 ppm) of the H4 doublet. This can be explained by the different behavior of the two H1 groups in the dimer as opposed to the IPU-MAA(-PMP) complex. The latter contains the flexible MAA structures, while the dimer has only IPU molecules which are more rigid due to their two isopropyl groups promoting steric hindrance. Despite of the low

solubility of IPU (50 mM in $CDCl_3$) thus making it difficult to reach the saturation of the self-association curve, the self-association constant was estimated to be 0.485 $dm^3.mol^{-1}$. As predicted, a small association constant was obtained, which is only significant at high IPU concentrations or in the presence of low concentrations of MAA, i.e. at the initial points of the NMR titrations. Although the H3 signals of IPU continually change during the titration with MAA irrespective of the presence of PMP, during the self-association experiments, the H3 signals did not shift. This observation corresponds with the low value of self-association constant. Furthermore, neither the H1 nor the H3 signals shift during the titration of IPU with PMP in the absence of MAA, confirming that complexation only occurs in the presence of MAA whilst the PMP is present only as a deprotonating agent.

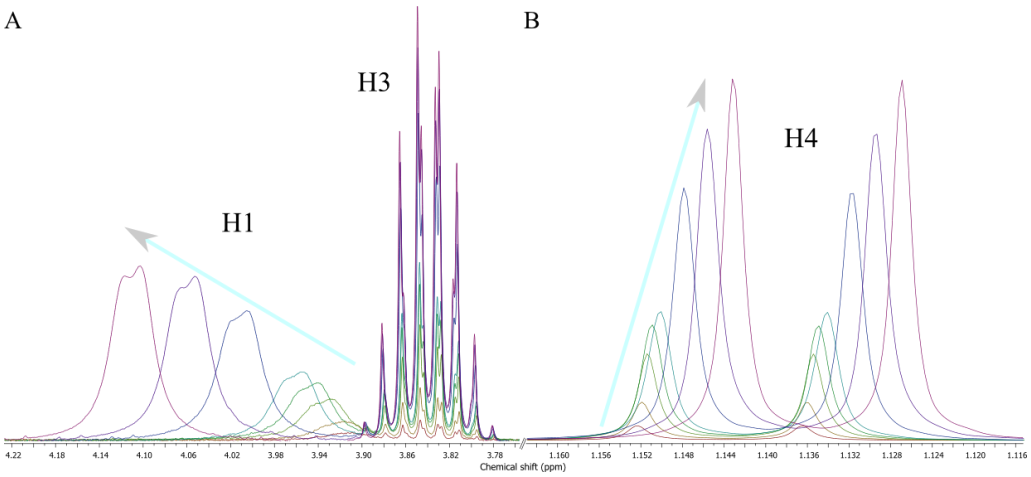

Figure 43 – Self-association of IPU in the concentration range of 1-40 mM in $CDCl_3$ indicating the (i) upfield shift of H4, (ii) the downfield shift of H1 as well as its split and (iii) the no-shift of H3 – the arrows indicate the increase of concentration

4.4.3.3. Effect of the deprotonating agent on the complexation strength

In order to investigate the effect of the deprotonating agent on the binding strength between the IPU and the functional monomer, four sets of NMR titrations were carried out both in the absence and in the presence of PMP at concentrations of 5 and 10 mM IPU. The observed chemical shifts are shown in Figure 44 whilst a typical spectrum indicating all the chemical shifts of the system studied can be found in the Appendix (Figure A7). For the calculation of the IPU-MAA(-PMP) binding constants, the self-association constant of IPU was considered only for the H1 signals, since the H3 signals do not shift due to the self-association of IPU – vide supra. In the case where 5 mM IPU was titrated with MAA(-PMP) the fitting was carried

out considering only a single-step complexation with the formation of 1:1 complexes. On the other hand, when 10 mM IPU was titrated with MAA the IPU:MAA (1:2) complex was also considered due to the higher final proportion of MAA/IPU. The association constants and chemical shifts of the pure compounds obtained are summarized in Table 16.

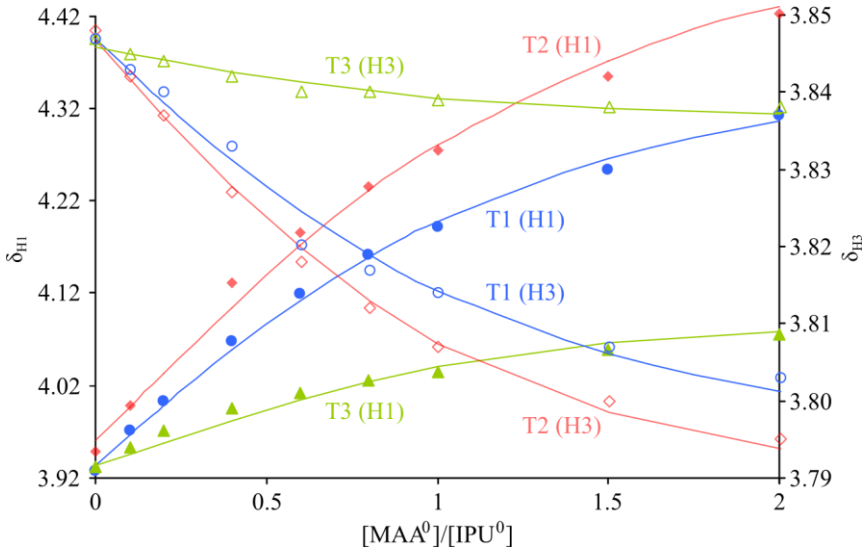

Figure 44 – Measured chemical shifts of H1 (filled signs) and H3 (empty signs) and the fitted curves (lines) for the NMR titration of IPU-MAA(-PMP) system where the red rectangular, blue circular and green triangular data sets represent titration T2, T1 and T3 respectively where T1 (5 mM IPU) and T2 (10 mM IPU) were performed in the absence of PMP, while T3 (5 mM IPU) was performed in the presence of PMP.

According to the conclusions drawn from the Job plot, the IPU-MAA complexation is multi-step. At higher IPU ratios the IPU:MAA (2:1) complex is dominating, while at higher MAA proportions the prevailing complex is IPU:MAA (1:2). Therefore, only 1:1 complexes were considered for the calculation of the binding constant where the relative quantities of MAA were lower (IPU titrated up to 2 equivalent MAA). As expected, this approach did not result in acceptable fitting for the set of NMR titrations where the relative MAA quantities were higher (IPU titrated with 5 equivalent MAA). For the latter experiments either 1:2 or 2:1 complexes were considered to fit the experimental data, both giving similar results. Due to the high excess of MAA in the pre-polymerization solution, the results are given only for IPU:MAA (1:2). The calculated average values for the association constants and the standard deviations are summarized in Table 16.

Table 16 – Calculated association constants and observed chemical shifts of the H1 of IPU during the titration experiments

	T1 (H1)	T1 (H3)	T2 (H1)	T2 (H3)	T3 (H1)	T3 (H3)
K_1	555	537	556	482	1144	1133
K_2	-	-	1.12	0.78	-	-
δ_{IPU}	3.905	3.847	3.905	3.847	3.905	3.846
δ_{C_1}	4.423	3.787	4.450	3.785	4.104	3.836
δ_{C_2}	-	-	9.383	3.692	-	-
K_1 average	532±35				1138±8	
K_2 average	-		0.95±0.24		-	

However, the addition of PMP results in the formation of methacrylate anion which is expected to form a stronger complex with IPU than the free methacrylic acid. The expectations are in correspondence with the results of the bulk IPU rebinding studies (see chapter 4.5.2.1, Figure 52), where MIP2 (prepared in the presence of PMP) showed 26% higher rebinding of IPU than MIP1 (prepared in the absence of PMP). This significant improvement of binding is consistent with the results shown in Table 16, indicating that the binding constant between IPU and MAA is 2.1 times higher when PMP is used.

In order to prove the importance of considering the higher order complexes and the self-association, the T1 and T2 NMR data representing the 5 and 10 mM IPU titrations were, in addition, evaluated in a conventional fashion. Assumptions are often made in the literature during the evaluation of complexation studies of MIPs wherein higher order complexes and self-association are neglected[158,159]. Following this approach and the widely applied Rose-Drago method the calculated K^{-1} is depicted as a function of the chosen set of $\Delta\delta_{max}$ values. At different $\Delta\delta_{max}$ values different lines are obtained which have a common intersection point giving the value of K^{-1}. Association constants of 525 $dm^3.mol^{-1}$ and 437 $dm^3.mol^{-1}$ were obtained with standard deviations being 195 $dm^3.mol^{-1}$ and 574 $dm^3.mol^{-1}$ for the T1 and T2 datasets, respectively. The Rose-Drago plot can be found in the Appendix (Figure A8). It should be noted that (i) the standard deviations are of the same order of magnitude as the association constants themselves and (ii) the calculation resulted in a negative association constant. Evaluation of this data hence demonstrates that for higher concentrations one has to consider self-association as well as higher order complexes.

The reactions leading to complex formation were also investigated and the corresponding reaction energies are summarized in Table 17. Note that in solution, due to both the existence of configurations with close lying energy levels and the presence of thermal perturbation, the simultaneous appearance of more complex structures is expected. Hence, the measured association constants cannot be assigned to one, well-defined structure. The reaction energies related to the formation of the most stable conformers, were calculated for 1:1 and 1:2 complexes as shown in equation 27-28. The associated Gibbs free energies were calculated from the measured association constants as given in equation 29.

$$\Delta E(1{:}1) = E(C_1) - E(IPU^a) - E(\text{trans-MAAH}) \quad \text{(eq. 27)}$$

$$\Delta E(1{:}2) = E(C_2) - E(IPU^a) - 2\times E(\text{trans-MAAH}) \quad \text{(eq. 28)}$$

$$\Delta G = -RT\ln(K) \quad \text{(eq. 29)}$$

Table 17 – Internal energies of complex formation reactions and the calculated Gibbs free energies from the measured association constant at 25 °C (the values are in kJ.mol^{-1}). Multiple values are given as without/with BSSE correction.

	Gas phase		DCM solution		Calculated ΔG from K	
	MAA^-	MAAH	MAA^-	MAAH	MAA^-	MAAH
1:1	-119.5 / -116.2	-59.0 / -55.8	-11.3 / -8.3	-11.3 / -8.2	-17.4	-15.6
1:2	-	-96.4 / -89.9	-	-11.2 / -4.9	-	-15.5

All the 1:1 complex formation reactions are exothermic, while the second step of the 1:2 complex formation for MAAH reactions are found to be slightly endothermic in DCM solution. As stated previously the calculations refute the formation of the 1:2 complexes of MAA^- both for solution and gas phase due to observed decomposition thereof. The calculated internal energies of the complex formation can be compared to the Gibbs free energies calculated from the association constants obtained from the NMR titrations. The implicit solvent calculations will decrease the reaction energies significantly as compared to the gas-phase interaction. This can be explained by the appearance of the solvent which will decrease the interaction strength between the parts of the complex[181]. The calculations were in good agreement with the Gibbs free energy values calculated from the measured association constants confirming the validity of computational investigation of such systems. The calculations showed that the formation of 1:2 complex from 1:1 complex in case of MAAH is slightly endothermic ($\Delta E(1{:}2) - \Delta E(1{:}1)$ = 0.1 kJ.mol^{-1}) whilst the formation of 1:1 complex

is exothermic ($\Delta E(1:1) = -11.3$ kJ.mol^{-1}), as it was found in the experiments $\Delta G(1:2) - \Delta G(1:1) = 0.1$ kJ.mol^{-1}, $\Delta G(1:1) = -15.6$ kJ.mol^{-1}. Interesting to note that the calculations do not reveal any energy differences between the IPU complexation with MAA^- and MAAH. This phenomenon confirms that the IPU complexation with MAA^- is strongly affected by the presence of PMP. Issues encountered in the presence of PMP were referred to above (NMR titrations studies), wherein the choice of the quantity of PMP used in the system is important.

4.4.3.4. MIP performance-modification indicators

The investigation of the impact of PMP was not only performed on the pre-polymerization solution (liquid state) but on the scavenger itself as well (liquid-solid surface interface). The adsorption isotherm of IPU on MIP2 was assessed both in the presence and in the absence of PMP following the polymer titration protocol described in chapter 3.7. Figure 45A demonstrates surface coverage (Θ) as a function of equilibrium concentration.

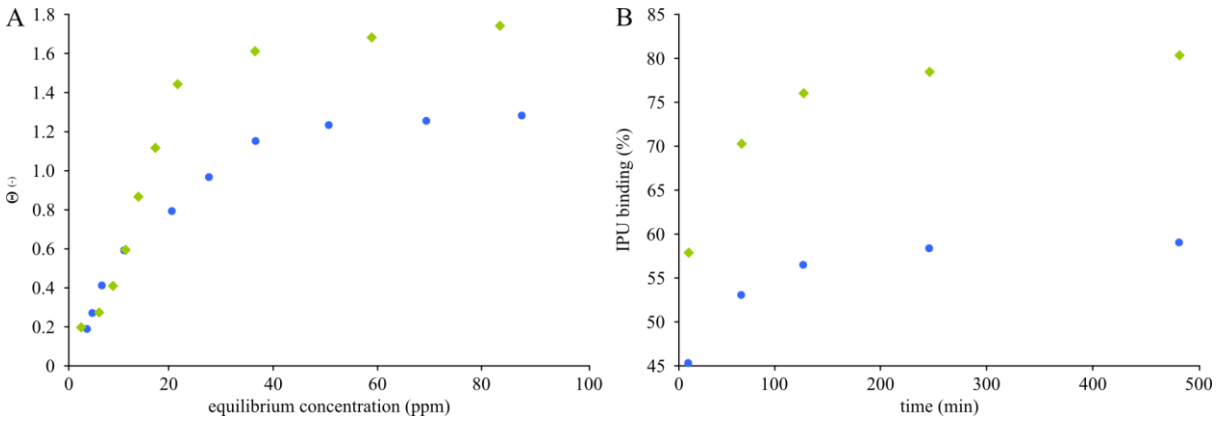

Figure 45 – Adsorption (A) and kinetic (B) isotherms of IPU uptake by MIP2 in the presence (♦) and in the absence (●) of PMP

In the absence of PMP the adsorption isotherm follows a normal saturation curve as expected and results in a maximum surface coverage of 1.283. On the contrary, the presence of PMP increases the maximum surface coverage being 1.743 which is in correspondence with the NMR and DFT findings, i.e. the imprinted polymer as well as the MAA monomer have higher affinity towards IPU in the presence of PMP. It should be noted that PMP gives rise to an anomalous isotherm at low equilibrium concentrations which can be explained by the participation of the PMP in the complex formation reaction as described in chapter 4.4.3.2. on NMR titrations. Figure 45B shows the progress of IPU binding as a function of time. It is difficult to directly draw conclusions from the kinetic isotherms since the maximum attainable

binding depends on the application of PMP. Hence, the present article introduces three new indicators to describe the effect of agents on MIP performance. As defined in equation 30, the *capacity modification index* (CMI) weights the improvement in MIP capacity achieved via target-scavenger-agent complexation system and relates it to the original MIP capacity not having applied the agent.

$$\mathrm{CMI} = \frac{\Theta_t^w}{\Theta_t^o} \qquad \text{(eq. 30)}$$

where Θ_t^w and Θ_t^o are the maximum surface coverage obtained in the presence and in the absence of the agent, respectively. In certain applications the time needed to reach binding equilibrium is of high importance and could have economic impacts on industrial applications. Accordingly, a time scale dependent formula is being introduced in equation 31 designated *accelerating index* (AI). Its definition is not as straightforward as the definition of CMI. To give an example, the increase in the costs will be not the same if the scavenging time will increase from 10 minutes to 20 minutes or from 10 h to 20 h. Therefore the following formula was suggested:

$$\mathrm{AI} = \frac{\frac{t^0}{t^w} + \frac{\lambda}{t^0}}{1 + \frac{\lambda}{t^0}} \qquad \text{(eq. 31)}$$

where λ is the *arbitrary time tolerance constant* and t^w and t^0 are the elapsed times corresponding to 90% equilibrium binding in the presence and in the absence of the agent, respectively. λ expresses the importance of equilibrium time for a given application and its restriction is $\lambda > t^0$. The complexity of AI definition justified by the fact that effect without the introduction of λ the increase from 10 min to 20 min would give the same AI value as the increase from 10 h to 20 h although the second case is much less favorable. This can be compensated by the right choice of λ, since above the time tolerance constant the AI increases significantly. Table 18 presents the effect of the equilibrium times on AI at a tolerance constant value of 1 h. If the equilibrium time is not crucial, a high time tolerance constant is chosen ($\lambda \rightarrow \infty$) quenching the effect observed equilibrium time on the accelerating index (AI $\rightarrow$ 1). On the contrary, when equilibrium time is a crucial application parameter, a low time tolerance constant is chosen ($\lambda \rightarrow 0$) intensifying the effect of observed equilibrium time on

the accelerating index (AI → t^0t^{-w}). Notice that in the latter case AI will depend just on the proportion of the corresponding elapsed times. When the time tolerance constant is set low compared to t^0 the same $t^wt^{-0} < 1$ proportion will account for higher acceleration index values, which means that the time saving is much more appreciated at larger time scales. On the contrary, $t^wt^{-0} > 1$ causes a rapid decrease of accelerating index. The overall *performance index* (PI) is defined in equation 32 as the multiplication of CMI and AI.

$$PI = CMI \cdot AI \qquad \text{(eq. 32)}$$

Table 18 – Dependence of the accelerating index on the t^0 and t^w values at λ = 1 h

t^w \ $t^0[h]$	1	2	5	10	50	100
0.1	5.50	7.00	8.50	9.18	9.82	9.91
0.5	1.50	1.67	1.83	1.91	1.98	1.99
1	1.00	1.00	1.00	1.00	1.00	1.00
2	0.75	0.67	0.58	0.55	0.51	0.50
3	0.67	0.56	0.44	0.39	0.35	0.34
5	0.60	0.47	0.33	0.27	0.22	0.21
10	0.55	0.40	0.25	0.18	0.12	0.11
15	0.53	0.38	0.22	0.15	0.08	0.08
20	0.53	0.37	0.21	0.14	0.07	0.06
24	0.52	0.36	0.20	0.13	0.06	0.05

Considering that in most of the cases in the literature (i) the rebinding studies are carried out overnight or 24 hours assuming that the equilibrium between the scavenger and the solution has been reached, and (ii) both the adsorption and kinetic isotherms are following a saturation curve, for practical reasons it is proposed to use the elapsed times until 90% of the total binding is reached to be compared. However, it cannot be foreseen whether a potential performance modification agent actually facilitates MIP performance, i.e. increases the MIP capacity and/or accelerates the adsorption process, or not. Furthermore, an agent may also cause adverse effects by competing with the analyte and promoting electronic and steric hindrance. Hence, a set of simulated adsorption and kinetic isotherms is shown in Figure 46 representing different case scenarios and Table 19 demonstrates all the possible outcomes of the analysis of the novel indexes.

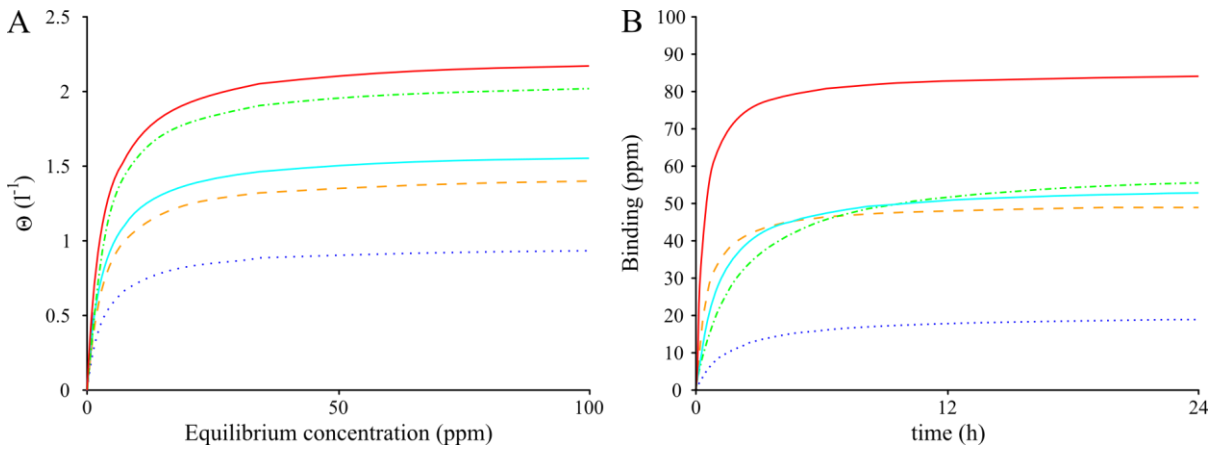

Figure 46 – Simulated adsorption (A) and kinetic (B) isotherm representing both elevated and hampered MIP performance where the lines represent Case 1 (-----), Case 2 (– – –), Case 3 (——), Case 4 (-·-·-) and Case 5 (——)

Table 19 – Comparison of the performance indexes based on the simulated isotherms

Case #	1	2	3	4	5
Agent	yes	yes	no	yes	yes
AI	0.67	2	1	0.5	3
CMI	0.6	0.9	1	1.3	1.4
PI	0.4	1.8	1	0.65	4.2

Adsorption isotherms of Case 1 and 2 featuring maximum surface coverage Θ_1-Θ_2 represent scenarios where the agent impede the analyte uptake resulting in lower Θ values than Θ_3 where the MIP was applied without the agent. On the other hand, adsorption isotherms of Case 4 and 5 indicate higher MIP capacity in the presence of the agent. Note, that although the shape of the adsorption isotherm might be anomalistic – as in the case of IPU – only the saturation point of the curve is incorporated in the CMI. On the other hand, AI incorporates the shape of the kinetic isotherm to a certain extent, given the fact that it is calculated based on reaching 90% of saturation which is strongly dependent on the shape of the curve. Since $t_5(\Theta_5) < t_3(\Theta_3)$ where no agent was applied, the AI is higher than 1 meaning that the agent has an accelerating effect on the analyte uptake by the scavenger. Furthermore, $\Theta_5 > \Theta_3$ indicting higher capacity when the agent is applied. Hence, both AI and CMI contribute to a higher PI value which means that the agent has an overall positive effect on the performance of the MIP. Following the same consideration, the case of t_1-Θ_1 results in AI, CMI and PI < 1 meaning that the agent has a negative, hampering effect both on the kinetics and adsorption behavior of the scavenger. On the other hand, t_2-Θ_2 and t_4-Θ_4 case scenarios represent opposite effects of the agent on the kinetics and adsorption. In case of t_2-Θ_2 the AI and CMI

values are higher and lower than in the absence of the agent, respectively. The t_4-Θ_4 case gives AI and CMI values lower and higher than in the absence of the agent, respectively. In these two cases the decision whether to use the agent during the MIP application depends on the objective of the work and one has to prioritize the importance of kinetics and adsorption. From an industrial application perspective – considering the example of IPU removal from APIs – both factors are crucial and especially in these cases the overall performance index can help to make a decision.

After the introduction of MIP performance-modification indicators, the particular case of PMP deprotonating agent is discussed. The impact of PMP on MIP2 performance can now be numerically expressed by CMI, AI and PI being 1.359, 0.796, 1.082, respectively. The CMI value higher than 1 indicates an increased performance related to higher capacity of the scavenger, while the AI value less then 1 demonstrates retarding effect of PMP on IPU recognition kinetics by MIP2 which implies that the particular case of PMP-MIP2 system falls into Case 4 (Table 19). The overall performance index value of 1.082 demonstrates that the effect of PMP is still positive on the MIP performance despite of the fact that it takes more time to reach the equilibrium of the adsorption process.

4.5. OSN-MIP hybrid process for API degenotoxification

Meta and IPU, molecular weights 521 $g.mol^{-1}$ and 144 $g.mol^{-1}$ respectively, were selected, as model API and potential GTI for the evaluation of the hybrid process. Combining the results of previous OSN membrane screening studies (chapter 4.3) with the use of the novel MIP2 developed specifically for IPU (chapter 4.4), a novel hybrid process for effective API degenotoxification was developed. The use of MIP2 resulted in efficient removal of IPU (~80%) in a single stage of about 80% IPU removal, even in the presence of high API concentrations. However, under such conditions, a significant fraction of the API, about 15%, binds non-specifically to the MIP. Thus the next step was to develop an improved MIP washing procedure that allows (i) quantitative recovery of the API which is non-specifically bound to the MIP in the first elution steps and (ii) removal of the IPU in the second elution steps, avoiding back contamination of the API and allowing recovery of the scavenger. A second aim is to evaluate strategies for high removals of IPU, achieving consistent low values of IPU contaminant, essentially through the combination of OSN and MIP in a hybrid process for purification of the API. Combination of OSN with other purification techniques can

already be found in the literature[110,209,210,211] but OSN-MIP hybrid processes have not been reported yet.

Furthermore, the initial equilibrium studies using MIP2 show that removal is limited to a maximum of about 80% of the total IPU at concentrations of 100 ppm. Therefore, high IPU removal, using MIP2 alone, requires a multistage procedure, in which the number of steps depends on the initial and target threshold IPU concentration. Notice also that the previous results giving 80% IPU removal were obtained with loads of MIP2 at 50 $g.L^{-1}$ in DCM at ratios of 2 mg-IPU/g-MIP2, in other words 100 ppm IPU contamination can be reduced only to 20 ppm. Note that the acceptable IPU limit depends on the daily dose of the API meaning that it is sufficient in certain cases to reduce the IPU limit to 20 ppm but more strict limits are expected for high-dose APIs. Furthermore, the initial IPU contamination of APIs can reach even 1,000 ppm which cannot be effectively lowered to the IPU threshold limit by MIP2. Therefore, a hybrid process consisting of OSN followed by a MIP stage was evaluated. The scheme of the hybrid process can be seen in Figure 47. In this approach, the larger fraction of IPU is removed in the OSN permeate using a low dilution ratio. Thereafter, MIP2 is used to remove the IPU at lower concentrations from the retentate solution thus minimizing the load required of the relatively expensive MIP2 and featuring only one MIP extraction step.

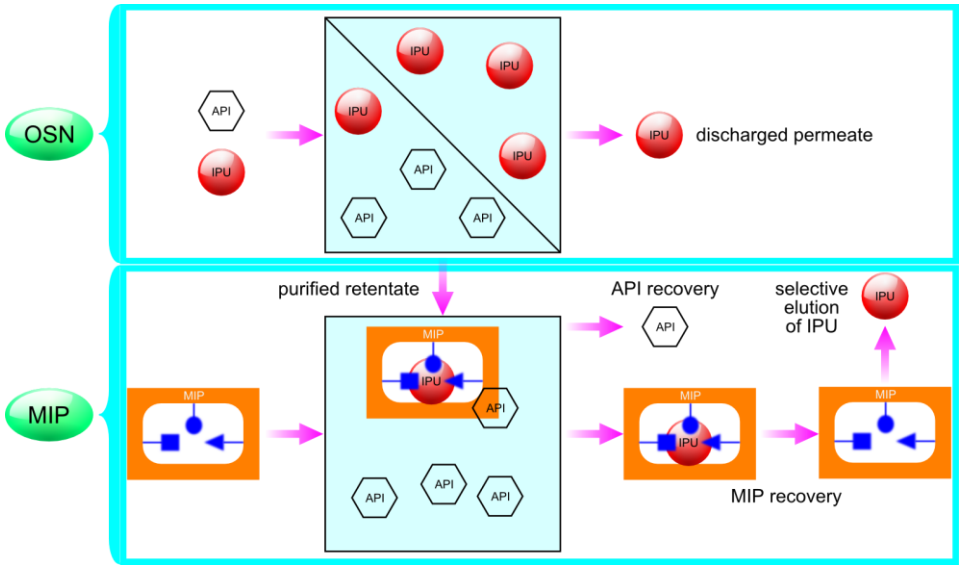

Figure 47 - Schematic principles of using OSN (stage 1) and MIP (stage 2) to remove IPU from API solutions

First, the use of OSN is discussed with regard to membrane selection and the effect of using different solvents and applied pressures, as well as diafiltration dilution ratios. The

development of an elution procedure is then described to recover the API bound to the MIP2 scavenger by non-specific interactions. The recovery of the MIP scavenger and the IPU washout efficiency was also evaluated. In the final chapter, the combination of OSN with MIP based purification is discussed.

4.5.1. Stage 1 evaluation: organic solvent nanofiltration

DCM is a solvent commonly used in industry and hence it was also used for developing and testing the novel MIP2 for IPU removal in previous studies. Therefore, DCM was used as the solvent in the preparation of model solutions for the evaluation of the MIP-OSN combinatory approach. Most OSN membranes are not compatible with DCM. The OSN membrane screening revealed that membrane rejection of IPU and Meta was dependent on both solvent and pressure. Therefore, Figure 48 compares the rejections obtained for IPU and Meta of the three thin film composite OSN membranes: SolSep NF010206, GMT-oNF-2 and MPF-44, tested in DCM at 10 bar and 20 bar in a cross-flow cell.

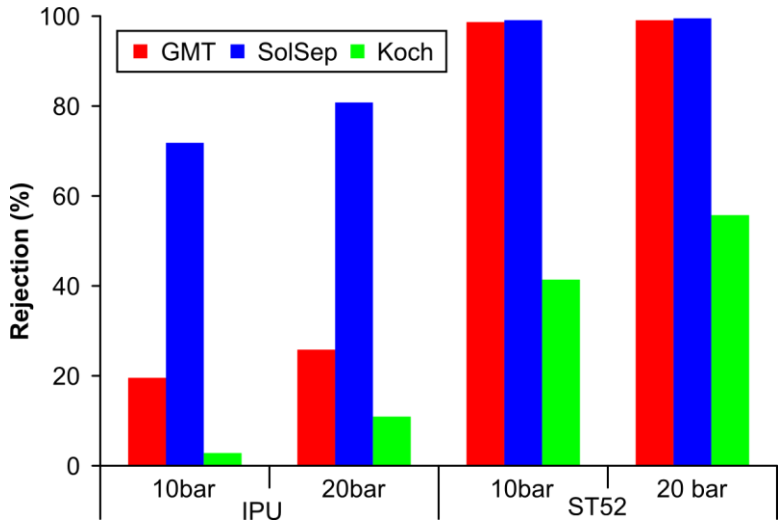

Figure 48 – Rejection of IPU and Meta at 10 bar and 20 bar in DCM on various OSN membranes

4.5.1.1. Membrane selection and solvent impact

The rejections obtained, show that when using DCM, not only the IPU (Mw 144 g.mol^{-1}), but also a significant fraction of Meta (Mw 521 g.mol^{-1}) crosses the Koch MPF-44 membrane, indicating that in DCM the MWCO should be significantly higher than the reported value of

250 Da[212] for this membrane or that the membrane is actually not entirely compatible with DCM. Thus, the use of Koch MPF-44 for the intended separation was ruled out. On the other hand, IPU rejection by SolSep is significantly higher than expected based on the OSN membrane screening or the reported MWCO of 300 Da[107] for this membrane. Hence, in order to push a higher fraction of IPU into the permeate, a higher dilution ratio is needed, which leads to higher API loss. The results indicate that the GMT membrane is the most suitable for separating Meta from IPU when dissolved in DCM, with a lower IPU rejection and a high Meta rejection. The use of a lower applied pressure, at a value of 10 bar can further be exploited to increase GTI permeation.

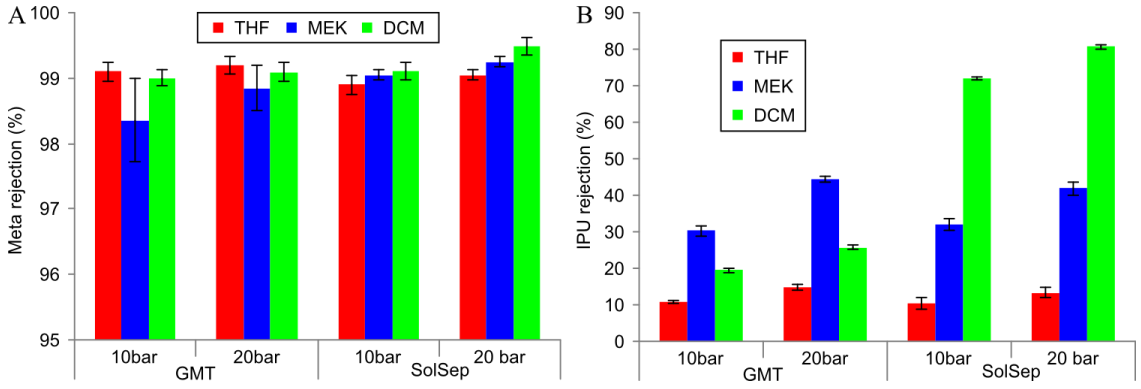

Figure 49 – Rejection of Meta (A) and IPU (B) on the GMT and SolSep membranes in THF, MEK and DCM solvents

The differences in rejections found for the same solute, but different solvents (Figure 49), is most probably due to the extent of membrane swelling. In order to further explore the effect of solvents on the rejections of the tested solutes, the rejections of SolSep and GMT membranes obtained for IPU and Meta in DCM, THF and MEK were compared. The rejection of Meta is around 99% for the two membranes and three solvents tested. However, IPU rejections are greatly altered by the solvent system used. The polarity index for MEK, THF and DCM are 4.7, 4.0 and 3.5, respectively. Both SolSep and GMT have lower rejections (10-15%) in THF than in MEK (30-45%), which could be explained by an increase of free volume as the more apolar solvent, THF, can cause slight swelling of the OSN membrane active layer. However, such correlation is not corroborated by the data for DCM (the most apolar solvent of the three), which drives rejections at intermediate values (20-25%) for GMT and significantly higher values (70-80%) for the SolSep membrane. It could be speculated that these results are due to DCM effects on transport mass transfer resistance in the active layers, the supporting layer of the membrane or interface between support and

active layer. Nevertheless, the data collected is important for process development confirming the use of GMT membrane for removal of IPU from Meta post reaction DCM stream by OSN diafiltration.

4.5.1.2. Organic solvent nano diafiltration

Continuous addition of fresh DCM allows the operation of OSN in diafiltration mode and washing out of IPU from the system through the permeate whilst the API is retained by the membrane. Therefore, an experimental evaluation of this approach was performed. The mass balances close well within a 3% error. Figure 50 shows experimental results against the values calculated on the basis of mass balances and previously estimated IPU and Meta rejection values of 19.8% and 99.0%, respectively. The detailed description of the calculations can be found in chapter 3.4. It is to be noted that the experimental results on IPU removal diverge from those calculated for lower IPU concentrations, which may indicate that rejection is concentration dependent and that IPU retention due to adsorption phenomena in the membrane becomes significant for lower IPU concentrations.

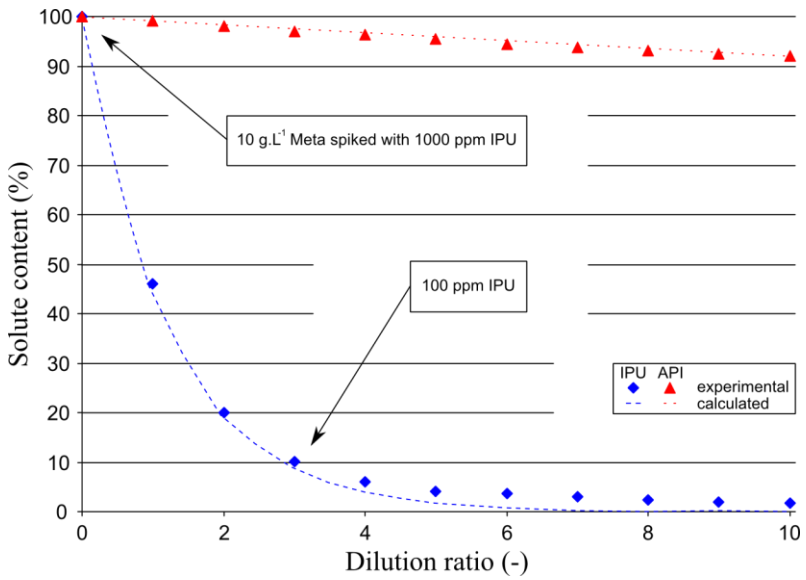

Figure 50 – Experimental results and calculated values of OSN diafiltration

Overall, the results show that significant amount of IPU can be removed using the OSN diafiltration approach. However, such removal is more significant for the initial concentrations at the beginning of the cycle. As the IPU content decreases the efficiency of its removal also decreases. The rate of the API loss is sustained throughout the diafiltration, and

achieves a value of 2.5% at a dilution ratio of 3. At this dilution ratio, a value of 100 ppm IPU content, corresponding to 90% removal, was achieved. Therefore, based on the diafiltration results, a dilution ratio 3 is judged to be a possible optimum end point for OSN diafiltration. Further treatment of the retentate by MIP2 for the additional removal of IPU is discussed in the next chapter.

4.5.2. Stage 2 evaluation: molecularly imprinted polymer phases

4.5.2.1. IPU removal from APIs by the novel scavengers

First of all, in search for the optimal phase ratio for removal of IPU from a solution at a fixed concentration (100 ppm) a polymer titration was carried out as described in chapter 3.7, in which the removal efficiency was investigated, using different amounts of MIP2. The percentages of IPU binding obtained, shown in Figure 51, led to the following conclusions: up to 50 mg polymer the uptake increases proportionally to the amount of polymer to reach 80% removal beyond which point the curve levels off to reach a maximum depletion level of 90% at 500 mg polymer. The level of depletion at the point of 50 mg polymer corresponds to an uptake of 13 μmol-IPU/g-MIP2 and remaining free concentration of 0.07 mM. Hence, adding more polymer to a solution where the free concentration is as low as 0.07 mM IPU will not increase significantly the degenotoxification of the solution. Hence, 50 mg scavenger was used for each rebinding assays discussed in this chapter.

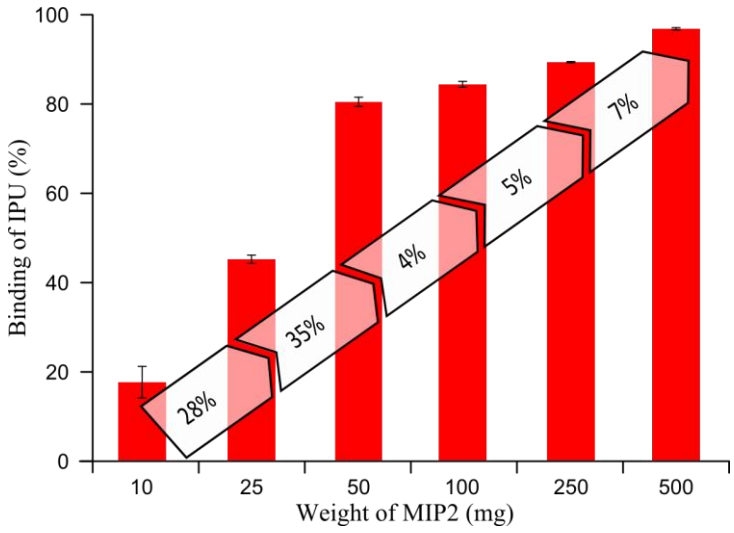

Figure 51 – Polymer titration: 100 ppm IPU solution in DCM was titrated with increasing amount of MIP2 scavenger

The solute binding percentage was investigated for binary model mixtures of IPU and APIs in the presence of the MIPs and the corresponding NIPs using DCM as solvent (Figure 52). It is interesting to note that the selectivity and capacity of IPU were higher for the polymers prepared in presence of the PMP base than for those where PMP was not used. This observation is valid for polymers prepared in the presence of a template (MIP2 vs. MIP1, 80% vs. 55%), but also for the corresponding reference polymers prepared in the absence of IPU (NIP2 vs. NIP1, 50% vs. 35%). The results are consistent with the measured and calculated association constants (Table 16 in chapter 4.4.3.3.).

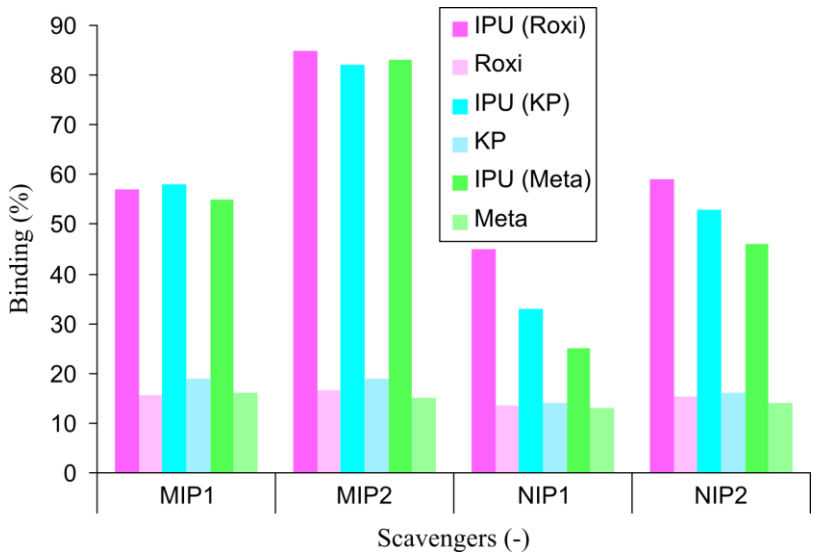

Figure 52 – Specific binding of IPU and non-specific binding of APIs in API post-reaction solutions (the brackets indicate the corresponding APIs). While the API binding is fairly constant at about 15% the IPU binding differs with the MIP scavengers. 1 mL DCM solution of 10,000 ppm API spiked with 100 ppm IPU was loaded on 50 mg scavengers.

The percentage of IPU binding is higher for both imprinted polymers when compared with the respective non imprinted polymer for both series 1 (MIP1 vs. NIP1, 55% vs. 25%-45%) and series 2 (MIP2 vs. NIP2, 80% vs. 45%-60%), showing that the introduction of the template molecule, IPU, during the preparation of the MIP samples have a significant impact not only on the selectivity but also on the capacity. Additionally, it should be noted that the percentage of IPU binding for the MIPs in the different tests was quite consistent with small standard deviation (2% for both MIP1 and MIP2), but the variation in IPU binding to the non-imprinted scavengers was larger (11 and 7% for NIP1 and NIP2, respectively).

The percentage of binding of the APIs, in spite of being present in a 100 fold excess over the GTI, were significantly lower with values around 15%, when compared with the values for IPU. The template and the base hence induce enhanced affinity for the GTI only, with no significant effect on the affinity for the APIs. The observed binding of APIs is low compared to the binding of IPU (~84%) where Roxi and Meta is bound at the same level (~15%) while KP has a slightly higher binding value (~19%). From the APIs tested, KP is the molecule most similar to the target IPU, both in terms of size and structure, since it includes an amide group able to interact with the carboxyl groups of the scavengers. Nevertheless, high specificity was achieved by the use of IPU as template during the preparation of the scavengers, proven by low KP binding. A larger fraction of the API remain free in solution, regardless of API size, chemical family and functional group; indicating that API binding to MIPs was non-specific.

It is interesting to note that the polymers are capable of efficient removal of the potentially genotoxic IPU from APIs of similar molecular sizes (e.g. KP, 170 $g.mol^{-1}$ versus IPU, 144 $g.mol^{-1}$). Such a level of discrimination is extremely challenging using other separation techniques, particularly those relying on molecular weight differences such as OSN. As mentioned, similarities between IPU and KP are not only size based, but KP also contains a quasi-urea substructure, thus the amide group can be considered a close analog of the template molecule, IPU (Figure 53). The selectivity displayed by the MIPs for IPU in this case illustrates the potential of the novel molecular imprinted polymers as specific scavengers for GTI removal. Given the superior performance of MIP2, further investigations were carried out using this polymer.

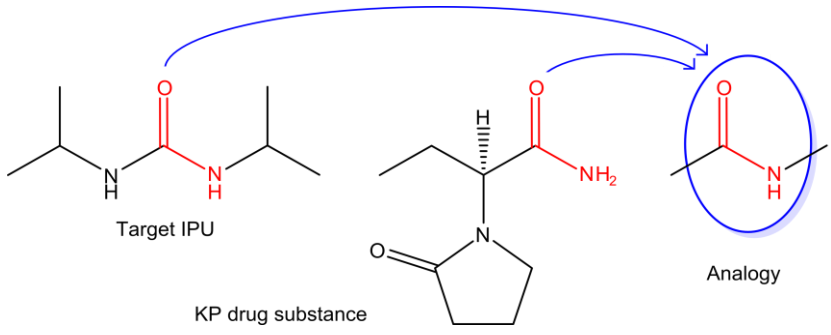

Figure 53 – Analogy between the target IPU and the KP drug substance

An additional binding experiment was performed in order to study the effect of API concentration on binding. Using an equimolar concentration of IPU (100 ppm, 0.7 mM) and

one of the APIs (Meta, 362 ppm, 0.7 mM) in DCM the percentage of IPU binding was 81.6 ± 0.6 % - in the same range as in the previous experiment - whereas the non-specific binding of API was now significantly lower (1.3 ± 0.4 %). Since the API concentration is now significantly lower (10,000 ppm → 362 ppm; about 30x), the results demonstrate that the binding of IPU to MIP2 is essentially independent of the API concentration.

From a trial planning and industrial point of view, it is important to have information on the dynamics of IPU and API binding to the polymer. Therefore, an experiment was performed in which samples of supernatant were collected over time to evaluate binding kinetics. The experiment was repeated twice with coefficients of variation lower than 1.2% and the average values are presented in Figure 54. It is noteworthy that the binding of the API (Meta) to MIP2 is virtually instantaneous and does not vary significantly over the 22 hours. However, IPU binding progresses overall more slowly – somewhat faster when it is the only solute dissolved (no API present) and more slowly in the presence of the API. This observation can be explained by the high amount of API, which covers part of the specific binding sites, slowing down the recognition of IPU. Experiments were stopped at 22 hours, when about 80% of the IPU was bound to MIP2. The data obtain do not fit zero or first order kinetics towards the IPU concentration, but do fit a second order reaction with a correlation factor of 0.99 and a kinetic constant of 9 x 10^{-6} $h^{-1}ppm^{-1}$. For a kinetic order of two, one can speculate that, for the recognition mechanism, the simultaneous binding of two molecules is required due to size or stabilization of MIP2-IPU bonds.

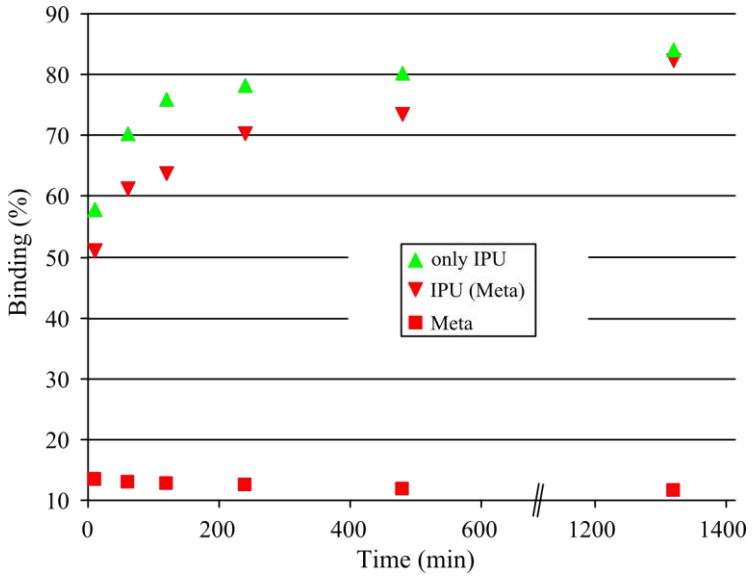

Figure 54 – Binding of IPU and Meta over time as a mixture and IPU-only

The imprinted polymers displayed superior recognition for IPU in comparison with different APIs. Regardless of the nature of the API in terms of size, chemical family and functional groups, the non-specific binding to API remains fairly constant. Even in typical industrial scenarios, where the IPU is present in low concentrations compared to high amounts of API, the experimental results indicate effective degenotoxification of about 80% at 2 mg-IPU/g-MIP2 with initial IPU concentration of 100 ppm. This resulted in a loss of about 15% API when present in a 100 fold excess to the potentially genotoxic impurity, due to non-specific binding.

For direct comparison of one single MIP2 step with OSN diafiltration, an additional experiment was performed with MIP2 and Meta loadings as above, but with a higher IPU concentration of 1,000 ppm. The results indicate that the percentage of IPU binding to the MIP2 was 49.9±0.4%, corresponding to about 495±4 ppm of IPU equilibrium concentration in solution. In other words, the results show that (i) MIP2 is capable of effectively removing IPU at lower concentrations and on the contrary (ii) the OSN diafiltration approach is superior to remove IPU at higher concentrations: IPU in solution is reduced from 1,000 pm to about 100 ppm (vs. about 500 ppm for MIP2 system) with only 2.5% loss of API (vs. 15% in the MIP2 system) at dilution ratio of 3.

MIP systems could be explored for further removal of IPU using a cascade type methodology where the supernatant of the first step is submitted to additional steps for sequential removal of further IPU. However, if this approach were to be applied other issues such as minimization of API loss and regeneration of MIP2 had to be addressed. Since a significant amount of API ends up bound to the MIP in the first step, a proper recovery step for such bound API – without back contamination of the IPU – would be crucial to improve the competitiveness of the MIP application. The recovery of used MIP2 is also an important consideration from a cost efficiency perspective. A single solvent or a mixed solvent system, able to wash off only the API in the first elution steps and then the specifically bound IPU in the following elution steps, would resolve this problem. The screening for such solvent systems is discussed in the following chapter.

4.5.2.2. Eluent selection: API recovery and MIP regeneration

As discussed before, the MIP selectively binds IPU but also binds about 15% of the API in each step through non-specific interactions, which represents inacceptable loss of product. Several solvents were screened for their ability to dissolve API (Meta), but not the potential GTI (IPU), by exploring the different strengths of interactions between polymer with GTI and API in these solvents. The objective was to be able to remove easily the API in an initial elution step and significant IPU removal in additional elution steps. Polymer swelling was also tested in the solvents used in binding tests or solid phase extractions. Figure 55 shows the specific swelling volumes estimated for MIP2 (the polymer selected for the development of the hybrid process) and MIP1, as well as the respective non-imprinted polymers NIP1 and NIP2. It is interesting to note that the lowest swellings were observed in DCM, the solvent used for preparation and IPU removal tests, than for any of the other solvents. In particular, MIP2 which has the highest affinity towards IPU has the lowest swelling. Swelling leads to significant changes in the properties of the polymers, affecting accessibility of the binding sites, and thus the adsorption-desorption process. Therefore, removal of IPU in a solvent with low swelling properties, such as DCM, and desorption in solvents, such as MIBK and MeOH that swell the polymer significantly can actually be beneficial, since it promotes easier removal from the enlarged polymer pores[213].

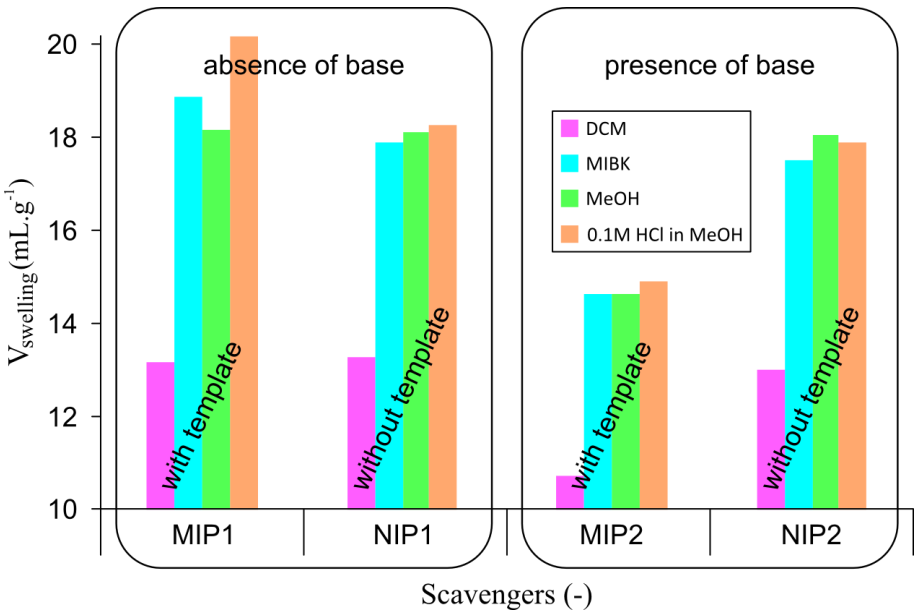

Figure 55 – Specific swelling volumes of the IPU selective scavengers

DCM is the solvent in which the initial binding step takes place. Therefore, the use of DCM for further API elution would be ideal, avoiding solvent swap and allowing recovery of the API fraction in the original solvent. However, the experimental data shown in Figure 56 indicates that the use of additional pure DCM results in back contaminating of the Meta, since DCM partly elutes IPU as well. This is an expected result, given the high solubility of IPU in this solvent.

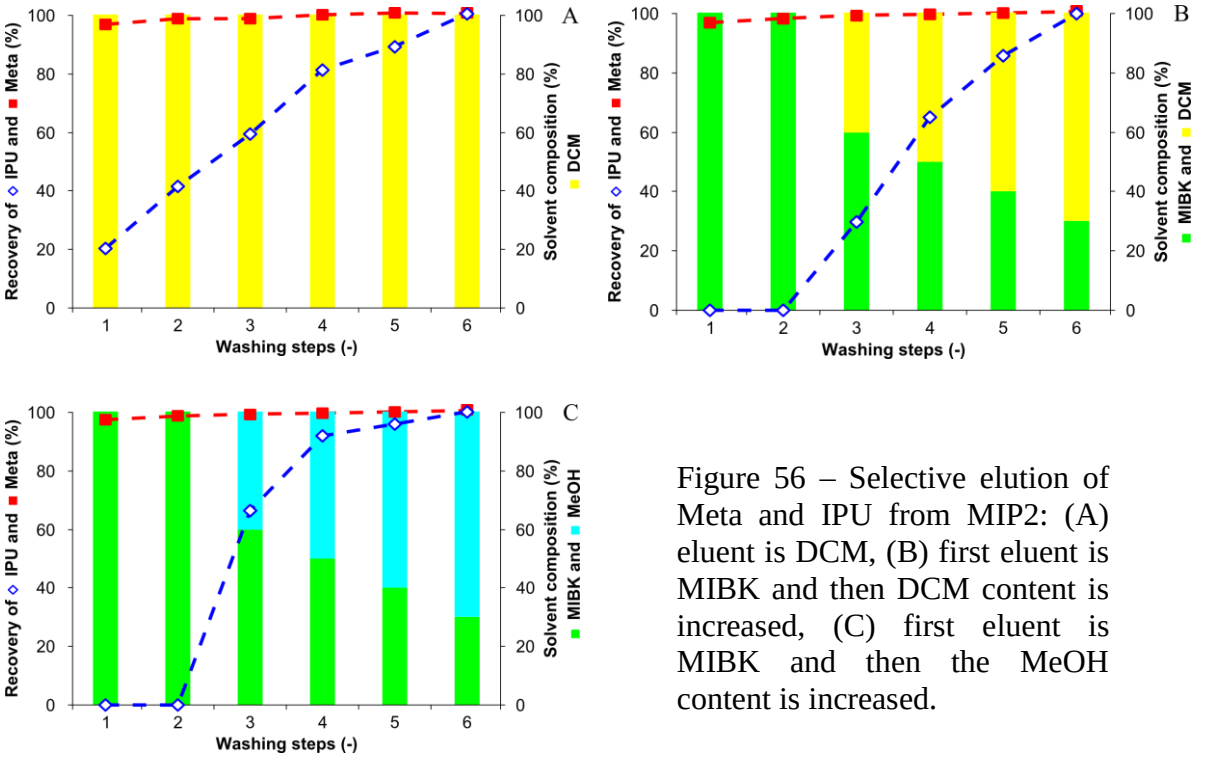

Figure 56 – Selective elution of Meta and IPU from MIP2: (A) eluent is DCM, (B) first eluent is MIBK and then DCM content is increased, (C) first eluent is MIBK and then the MeOH content is increased.

Therefore, in order to recover Meta from the MIP2 scavenger, a strategy of using two elution solvents was evaluated. Following preliminary results, MIBK was selected as the first solvent to be used. Meta is highly soluble, but IPU is insoluble in this solvent. Thus, the use of pure MIBK allows recovery of non-specifically bound Meta in the first or first two washes (Figure 56B) without significant cross contamination with IPU. This strategy has the drawback of recovering API in a solvent different from DCM, thus implying an undesirable solvent swap for the next processing step. Due to the high solubility of IPU in DCM and MeOH, these solvents were selected as secondary elution solvents to wash out the IPU, regenerating the MIP2. Methanol is a high polarity solvent, capable of disrupting the H-bonds in the host-guest interaction therefore, a faster IPU removal is possible with MeOH than with DCM (Figure 56C). 99% IPU removal was achieved in the washing performed with MIBK:MeOH (30:70). Therefore the MIBK/MeOH solvent system was selected to regenerate the MIP2 scavenger.

This demonstrates that an appropriate selection of solvents makes it possible to efficiently recover the fraction of 15% of API non-selectively bound to the MIP2 scavenger without contamination with IPU, addressing one of the main challenges identified in the use of MIPs.

4.5.2.3. Robustness of MIP recyclability

A second challenge is that, as IPU binding percentage decreases for higher IPU concentrations, removal of IPU down to the required low levels implies a sequence of several steps of IPU binding and MIP2 recycling, which is time consuming and cumbersome. As an example, a MIP cascade simulation based on a one-stage MIP application is demonstrated in Figure 57. Therefore, the multi-steps strategy often followed in OSN protocols[214,215] is not so often applied in MIP systems. Nevertheless, the novel MIP2 is particularly robust in terms of recyclability without loss of selectivity. Independently of operation mode, the option to recycle the MIP scavengers without any efficiency loss is crucial from an industrial point of view. Therefore, to illustrate the recyclability of the MIP2 scavenger, Figure 58 shows that the IPU binding values are between 80% and 85% for all the 18 assays performed sequentially using various polymer samples. These 18 assays were performed under identical conditions at 50 $g.L^{-1}$ of MIP2 in DCM featuring IPU concentration of about 100 ppm.

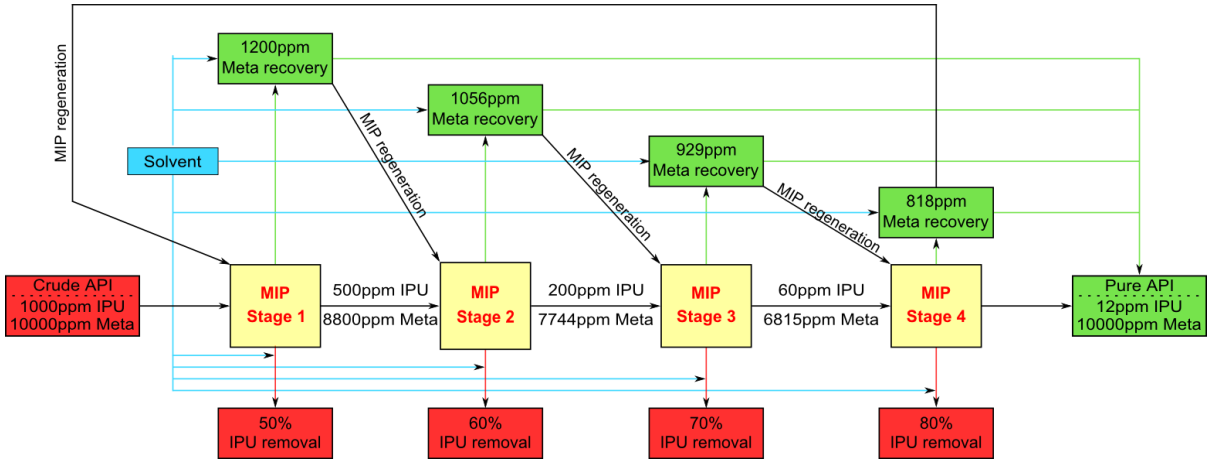

Figure 57 – Schematic representation of MIP cascade including Meta recovery and MIP regeneration (values presented are based on one-stage bulk rebinding experiments, thus they are only illustrative).

The results were assembled from several experiments reported throughout the project including the binding of IPU either alone or in the presence of different APIs, through kinetic and thermodynamic studies with a variety of elution solvents. In all these experiments the

final MIP2 regeneration employed was as follows: wash with 0.1 M HCl MeOH solution, dry in a vacuum oven and precondition with PMP base in DCM for further use.

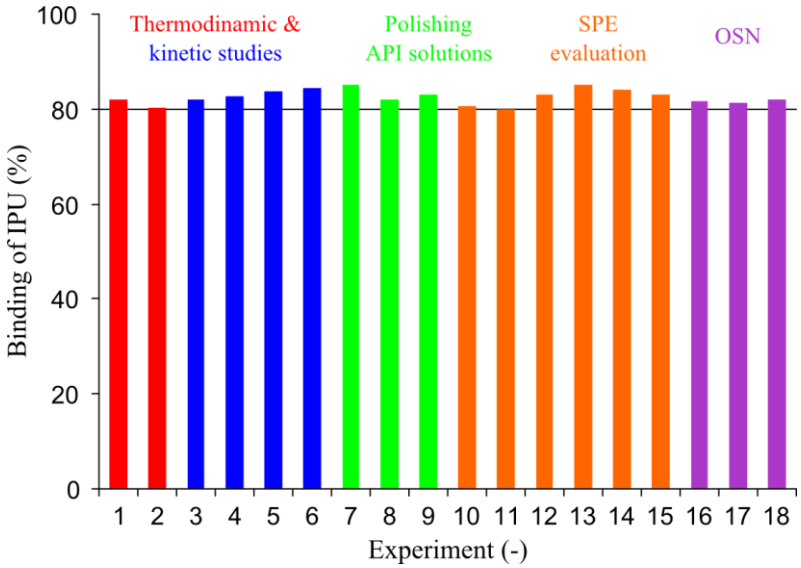

Figure 58 – IPU binding of MIP2 in the different experiments performed with MIP2 at 50 $g.L^{-1}$ in DCM and IPU concentration of about 100 ppm.

4.5.3. Exploring OSN diafiltration and MIP polishing of the retentate

Assessment of the OSN diafiltration and MIP2 systems independently was reported in the previous chapters, showing that the OSN diafiltration is more suitable for higher IPU concentrations being able to reduce IPU levels from 1,000 ppm to 100 ppm using a dilution ratio of 3 with only 2.5 %loss of Meta. However, IPU removal below 100 ppm by OSN was highly inefficient (see chapter 4.5.1). On the other hand, based on additional experiments of IPU binding to MIP2, the MIP approach suits the removal of IPU better from solutions where this solute is at low concentrations of about 100 ppm (see chapter 4.5.2.1). A suitable solvent system was selected to recover API, non-selectively bound to the MIP2 scavenger (see chapter 4.5.2.2). In this chapter a hybrid approach is suggested and evaluated experimentally. Diafiltration is first used to remove the greater part of the IPU and MIP2 is then used to polish the retentate stream resulting in ultra low levels of IPU content in the final Meta solution. The elution system developed in the previous section for the recovery of Meta and IPU was applied. A solution with 10,000 ppm Meta and 1,000 ppm IPU in DCM was submitted to diafiltration using the GMT-oNF-2 membrane and an applied pressure of 10 bar. The OSN diafiltration operation, run at an average solvent flux of 50 $L.m^{-2}.h^{-1}$ was stopped at a dilution

ratio of 3. The retentate was fed to MIP2 at a load of 50 $g.L^{-1}$ in the same solvent, DCM, corresponding to ratio of 2 mg-IPU/g-MIP2. After equilibration, the MIP2 was collected from the purified Meta solution and MIP2 retained for further recovery of the non-specifically bound Meta. Pure MIBK was used in the two first washing steps, followed by MIBK/MeOH solutions with increasing MeOH content in washing steps 3 to 6. The results obtained are illustrated in Figure 59 and follow expectations with virtually all of the Meta being recovered in the first two wash steps thus increasing the recovery of Meta to 99.7 %. The IPU was efficiently washed out of the MIP2 in the following steps.

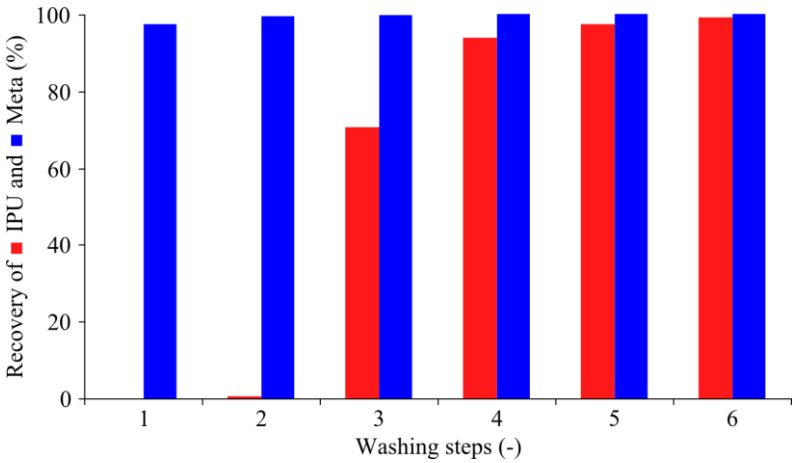

Figure 59 – Cumulative recovery of Meta and regeneration of the MIP2 scavenger after polishing the OSN retentate

Figure 60 provides a detailed schematic diagram of the hybrid process including the quantification of Meta and IPU at the different phases. The bulk of the Meta, 97%, is retained by the membrane and 90% of the IPU is discharged in the permeate. At this point, there is still 10% of IPU that remains in the retentate which corresponds to 10 mg-IPU/g-Meta (1 wt%). Therefore, the following MIP stage aims to decrease this level of contamination.

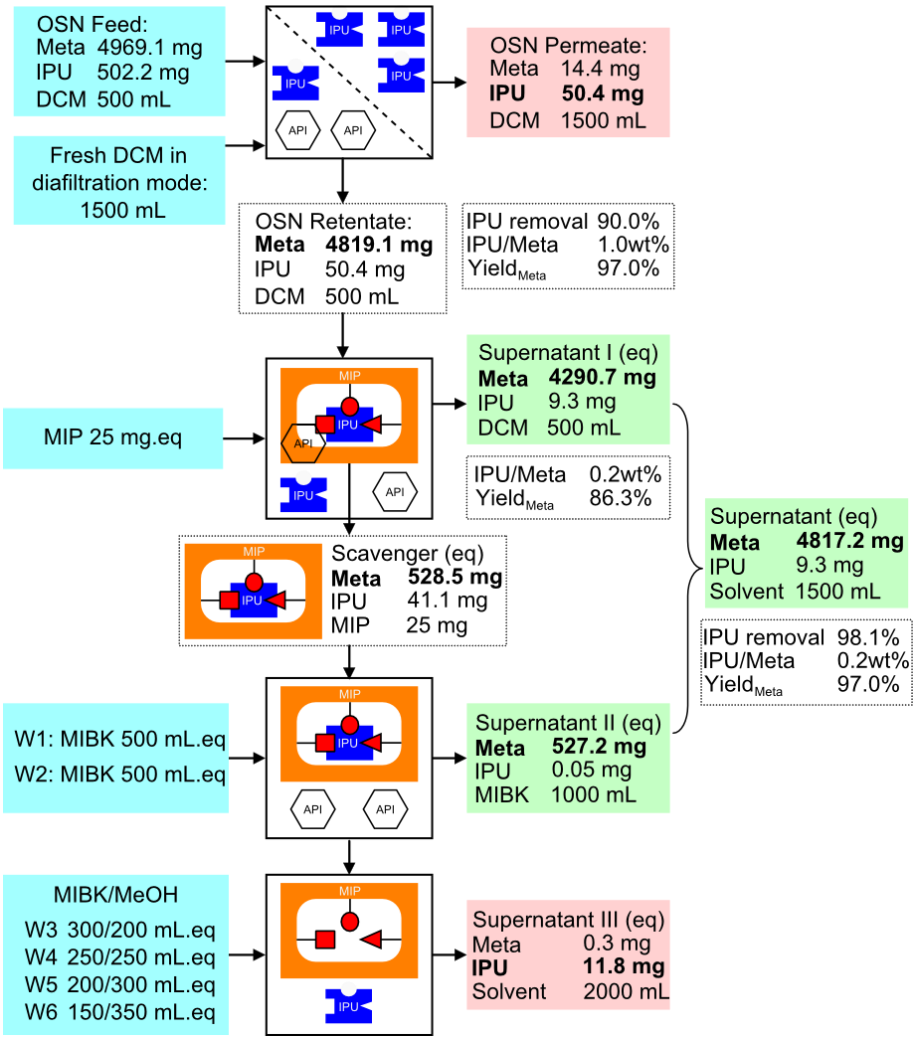

Figure 60 – Mass balance of the operation stages carried out during the hybrid process

The experimental data show that, using the appropriate system of eluting solvents, it is possible, without significant additional Meta loss (97 % yield of Meta), to bring down IPU levels to a value of 2 mg-IPU/g-Meta. Only one cycle using MIP was performed to obtain this level. Hence, assuming that in each cycle about 80% of the IPU is removed, by treatment of the supernatant I (Figure 60) it should be possible to reduced IPU content by about an order of magnitude per MIP cycle. However, this additional purification is achieved at the cost of the generation of a MIBK stream (supernatant II in Figure 60) in each cycle. The isolation of Meta therefore, involves a solvent swap back to the lower boiling point solvent, DCM. The removal of APIs from organic solvents by nanofiltration has been previously studied[216] and several groups have suggested the use of membranes for solvent exchanges[217,218,219] and for the recovery of solvents[220] in the pharmaceutical industry when heat sensitive compounds are involved or when the solvent has a high boiling point, making distillation unsuitable.

5. Conclusions and future outlook

In this chapter the conclusions of each projects of the thesis are presented, followed by a brief critical overview with the intention of both pointing out the limitations of the work and underlining where future work is recommended.

Trace analysis of genotoxic impurities calls for sensitive analytical detectors such as mass spectrometry. Instead of the conventional trial and error approach, design of experiments was applied in the LC-MS/MS method development. The novel strategy considering LC and MS instrumentation in one single DoE design – rather than applying DoE consecutively to LC and then MS – has been successfully tested and led to a robust method allowing the trace analysis of the model potentially genotoxic impurity, DMAP at 0.5 $ng.mL^{-1}$ absolute concentration which corresponds to 0.1 ppm limit of quantification in 5 $mg.mL^{-1}$ Mometasone furoate glucocorticoid. In addition the robustness of the method so obtained was assessed via the DoE approach, which not only quantified the highest deviation of peak area to be 23%, meeting the acceptance criteria, but also revealed the most important factor causing fluctuations in peak area as being the collision energy. The method developed is determined to be robust since minor changes in the factor levels have negligible effect on the response values. The proposed LC-MS/MS method also meets criteria such as ease of use, low cost per analysis, ultra low LOQ and high sample throughput. It has been demonstrated that DoE provides a reliable basis for LC-MS/MS optimization and provides a framework for changing all the important factors systematically, while requiring only a limited number of experiments. The method was validated and found to be repeatable, linear, precise and accurate in the range of 0.1 to 2 ppm enabling the method to quantify DMAP at its threshold concentration of 0.75 ppm in Meta. The results obtained on the application of DoE to quantify the potentially genotoxic impurity are promising. However, it should be noted that the selection of the ranges of the DoE factors is based on qualitative FIA and if too broad ranges are selected then DoE responses cannot be accrued for all cases. Hence, further work is needed to establish a more justified approach for range selection.

The comparative study of flash chromatography and recrystallization as conventional API purification technologies versus OSN proved the viability and sustainability of OSN as potential API purification technology. Degenotoxification of Mometasone furoate was successfully achieved for MeMS applying recrystallization, and for DMAP and MeMS by

flash chromatography and OSN. API losses during DMAP removal was 5% and 6.4% for OSN and flash chromatography, respectively. API losses during MeMS removal were 6.4%, 11.9% and 16.4% for OSN, flash chromatography and recrystallization, respectively. The cost analysis of the three processes concluded that recrystallization is the cheapest process, with intermediate energy intensity (due the need of solvent exchanges by distillation) and lower mass and carbon intensity, although it is more labor intensive and time consuming. However, the cost analyses of the purification processes are dominated by the loss of revenue due to API loss which makes recrystallization the least cost effective process in the present study. Recrystallization is the purification process approved in the manufacture of many APIs, therefore the use of recrystallization should not be discarded without careful analysis. Although flash chromatography is an efficient process for degenotoxification, particularly for DMAP, it is the most difficult to scale-up and involves high loads of solid waste disposal. Comparing the case of DMAP and MeMS removal from the API, in the case of DMAP the API ends up in a large volume of solvent and is then isolated by distillation, hence presenting higher energy intensity. OSN requires the use of 7 diavolumes, achieving adequate final GTI levels with acceptable API losses at the cost of high solvent consumption. Therefore, from an investment perspective, the option of solvent recycle becomes economically feasible only for OSN. On the contrary, from an environmental perspective, solvent recycle (i) has a high impact in each process by reduction of mass intensity by two orders of magnitude (from 400-1300 to 14-63 kg/kg-API depending on the process); and (ii) makes the three processes comparable with regard to their carbon intensity having reduced this to a range of 100-180 kg-CO_2/kg-API. The effect of solvent recycling also has a positive higher environment impact on OSN due to lower overall solvent consumption. OSN is a process easy to scale-up with low labor intensity and the processing time can be reduced by increasing the membrane area. However, in this case, when solvent recovery is included, the batch time increases significantly. Whilst considered green aspects it is worth mentioning that the post-reaction stream of Meta is in DCM, hence most of the work carried out during this PhD involves the use of DCM. Although after the approval of the API processing route, altering solvent is usually not an option for the manufacturers, it is highly recommended to replace DCM with a solvent featuring lower environmental, health and waste impacts. This solvent exchange requires large investment and tremendous work not only related to process chemistry but well-documented justification towards the authorities and new impurity profiling.

OSN was proven to be competitive in the process comparison assessment and hence various solvent resistant nanofiltration membranes were screened. The OSN diafiltration methodology proposed for API degenotoxification is based on commercial membranes, which are available in flat sheet or spiral wound modules enhancing the ease of scale-up. A large range of APIs and GTIs, covering different chemical families, were used as model compounds and rejections are provided, facilitating further process design and implementation. The applied membranes were examined with SEM, which suggests a thin film composite membrane configuration with an active layer of about 5 μm thickness. During the membrane screening process two solvents, THF and MEK, both being difficultly compatibile with polymeric membranes, were selected and membrane stability was successfully assessed. However, in subsequent studies, including process comparisons and a hybrid process, an even more challenging solvent, DCM, was used successfully. The effect of hydrogen peroxide in THF on membrane stability was also assessed and a limit of 5 ppm for OSN application was established. This value is well above the usual content in commercial THF, however due to long and/or inappropriate storage peroxide can accumulate in the solvent and the post reaction solution may contain residual peroxide reagent. The recommendation for OSN degenotoxification processes is to select a membrane with high rejection for the API (>95%) and to extend the number of diavolumes according with the requirements for GTI removals. The effect of pressure change on solute rejection was also explored to improve degenotoxification without provoking an increase in API loss. It should be mentioned that membrane stability problems – partial dissolution of the active layer – occurred depending on the batch of the membrane used. This observation indicates that the production of OSN membranes is not perfectly uniform and their performance may vary, calling for improvements in membrane preparation techniques.

Subsequently, IPU – representing an intermediate OSN case with higher GTI rejection – was chosen for investigation of molecular imprinting technology. ExploraSep® Plate A was screened and a hit scavenger was found, which interestingly is not a MIP but a NIP. Current industrial needs in Hovione called for a solvent exchange, which significantly decreased the IPU uptake. Hence, novel scavengers had to be designed featuring IPU as a template. The results show that a slightly modified conventional imprinting procedure based on methacrylic acid and ethylene glycol dimethacrylate can result in potent scavengers for IPU. The imprinted polymers displayed superior recognition for IPU, when compared with common APIs. Regardless of the nature of the API in terms of size, chemical family and functional

groups, the non-specific binding to API remains fairly constant. Even in typical industrial scenarios, where the IPU is present in low concentrations compared to high amounts of API, the experimental results indicate effective removal of about 80% of IPU at 2 mg-IPU/g-MIP2 with IPU concentration of 100 ppm in DCM. A notable improvement in MIP performance was achieved by addition of base in order to deprotonate the carboxylic moiety of the binding site. This promotes strong interactions between urea NH groups of the template and the negatively charged carboxylate groups of the scavenger. The quantum chemical investigation revealed a two-step complex formation mechanism in the absence of the deprotonating agent, whilst in its presence only the existence of 1:1 complexes were observed because the 1:2 complex decomposes due to the high negative charge density associated with the two methacrylate anions. The binding strength was derived through both quantum chemical calculations and NMR titrations both for 1:1 and 1:2 complexes featuring methacrylic acid and for 1:1 complexes featuring methacrylate anion. The resulting binding constants were in good agreement with a reasonably high degree of certainty. Adsorption isotherms demonstrated increased capacity of the imprinted scavenger in the presence of the deprotonating agent which is in agreement with the observed (NMR) and calculated (DFT) higher association constants in the presence of such an agent. These results justify and validate the simplification of using the pre-polymerization solution, instead of the complete imprinting system (i.e. disregarding the cross-linker), to study molecular recognition of MIPs. It has been demonstrated through the example of a deprotonating agent that the presence of an additional component can enhance the performance of imprinted polymers. Consequently, the introduction of performance-modification indicators such as capacity modification index, accelerating index and overall performance index has been proposed.

The methodology obtained based on OSN shows that OSN is an efficient process for removal of IPU from Meta at relatively high concentrations (~1,000 ppm) when using low diavolumes to avoid excessive loss of API. For diavolumes superior to 3, corresponding to IPU content in solution lower than 100 ppm, OSN becomes inefficient. On the contrary, the novel imprinted scavenger, MIP2, is more efficient when applied to IPU solutions in the lower concentrations ranges, with typical IPU removal efficiencies of 83%. Therefore, a hybrid process was developed which combines the advantages of molecular imprinting and organic solvent nanofiltration. An initial OSN stage is applied at a low dilution ratio, where the diafiltration process is efficient and then the retentate containing a low amount of IPU is submitted to the novel imprinted polymer for further IPU removal, The transition between OSN and MIP

stages takes place where the IPU concentration is approximately 100 ppm, a value particularly suitable for MIP2 operations. Meta with significantly lower contamination of by IPU was achieved using this hybrid approach. However, about 15% of Meta binds non-specifically to the scavenger. To address this challenge an elution system was developed using MIBK to recover Meta in the first two steps and mixtures of MIBK/MeOH in the 4 subsequent steps to recover the scavenger by eluting IPU. MIP2 was also efficiently recovered and reutilized over 18 operations without loss of selectivity towards IPU. This methodology can be used to explore other cases where ultra low concentrations of contaminants must be reached. A limitation of this hybrid process lies in the fact that an undesirable solvent exchange is necessary in order to recover the API non-specifically bound to the scavenger.

As a concluding remark, the close cooperation between Hovione as a pharmaceutical manufacturer and the Technical University of Dortmund as an academic institution provided a constant feedback between the research and market needs. In order to successfully complete the objectives of delivering nanofiltration and scavenging methodologies for API degenotoxification, commercially available solvent resistant nanofiltration membranes and specially developed imprinted scavengers were studied. Besides the contribution of the research presented on the implementation of both OSN and MIP technologies to pharmaceutical downstream processing, fundamental aspects of imprinting have also been investigated. Moreover, the findings during the PhD studies – funded by a Marie Curie ITN consortium – and carried out with a focus on the end user – laid the foundation for research by other colleagues within the consortium by identifying where further fundamental research is necessary to make the technologies more viable for the Pharmaceutical Industry. Based on the promising results, it is believed that the both nanofiltration and imprinting technologies have a significant role on the next generation of purification technologies for APIs.

6. Appendix

6.1. Tables

Table A1 – Model APIs of the OSN membrane screening

Class	Name, source	Abbrev., Mw ($g.mol^{-1}$)	Chemical structure	Description
Amides	Lacosamide UCB, Belgium	LA 250.2	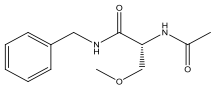	LA was developed by UCB for the adjunctive treatment of partial-onset seizuresand diabetic neuropathic pain marketed under the trade name Vimpat[221].
N-heterocycles	Levetiracetam UCB, Belgium	KP 170.2	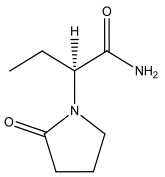	KP is an anticonvulsant drug used to treat epilepsy[222].
	Sumatriptan Hovione, Portugal	Suma 295.4	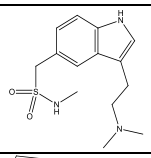	Suma is structurally similar to serotonin (5HT), and is also a 5-HT receptor agonist used in the treatment of migraine disorders[223].
	Irbesartan Jiacheng-Chem Enterprises Ltd., China	Irb 428.5	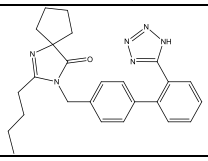	Irb is an Angiotensin Receptor Blocker (ARB) used mainly for the treatment of hypertension[223].
Steroids	Prednisolone Hovione, Portugal	Pred 361.2	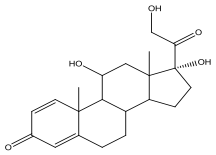	Pred is a corticosteroid drug with predominantly glucocorticoid and low mineralocorticoid activity, making it useful for the treatment of a wide range of inflammatory and auto-immune conditions such as asthma[224].
	Betamethasone Hovione, Portugal	Beta 392.4	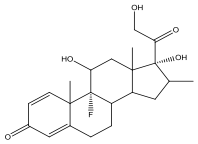	Beta is particularly suitable for treating cerebral edema and congenital adrenal hyperplasia, due to its lack of mineralocorticoid properties[225].
	Halobetasole propionate Hovione, Portugal	Halo 484.9	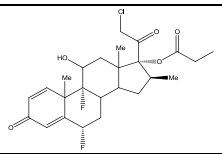	Halo has an action similar to Meta.
	Mometasone furoate, Hovione, Portugal	Meta 521.4	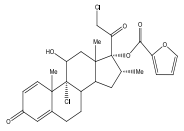	Meta is a glucocorticoids steroid used in the treatment of inflammatory skin disorders (such as eczema and psoriasis), allergic rhinitis (such as hay fever)[226].
Macrolides	Roxithromycin, Hovione, Portugal	Roxi 837.047	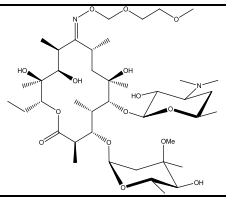	Roxi is a semi-synthetic macrolide antibiotic preventing bacteria from growing, by interfering with their protein synthesis[223].

Table A2 – Model GTIs of the OSN membrane screening

Class		Name	Abbrev, Mw ($g.mol^{-1}$)	Chemical Structure
Sulfonic esters	sulfate	dimethylsulfate	DMS 126.1	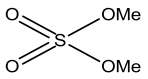
	mesylate	ethyl mesylate	EtMS 124.2	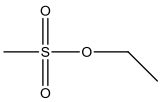
	tosylate	methyl tosylate	MeTS 186.2	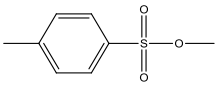
		ethyl tosylate	EtTS 200.3	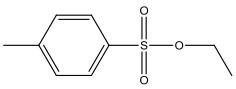
Amides		acetamide	AA 59.1	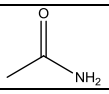
		thioacetamide	TA 75.1	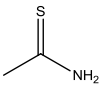
		N,N-dimethylcarbamoyl-chloride	DMCC 107.5	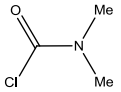
Ureas		1,3-diisopropylurea	IPU 144.2	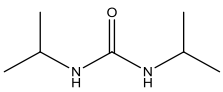
		1,3-dicyclohexylurea	CHU 224.3	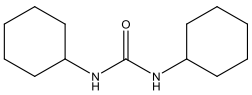
Others	aldehide	acrolein	ACR 56.1	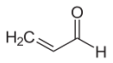
	haloalcohol	2-bromo-ethanol	BE 124.9	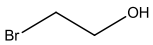

Table A3 – DoE runs based on the CCF design

#	E_{col}	E_{con}	V_{inj}	F	G
1	20	35	12.5	0.35	60
2	30	35	20	0.35	60
3	30	35	12.5	0.35	60
4	40	35	12.5	0.35	60
5	40	50	5	0.2	70
6	30	35	12.5	0.35	60
7	20	20	5	0.5	50
8	20	50	20	0.5	50
9	40	20	5	0.2	50
10	30	20	12.5	0.35	60
11	30	50	12.5	0.35	60
12	20	50	5	0.5	70
13	30	35	12.5	0.35	50
14	30	35	12.5	0.5	60
15	30	35	12.5	0.35	70
16	30	35	12.5	0.35	60
17	30	35	5	0.35	60
18	20	50	20	0.2	70
19	40	20	20	0.5	50
20	20	20	20	0.5	70
21	20	20	20	0.2	50
22	30	35	12.5	0.2	60
23	40	20	5	0.5	70
24	20	50	5	0.2	50
25	40	50	5	0.5	50
26	40	50	20	0.5	70
27	40	50	20	0.2	50
28	20	20	5	0.2	70
29	40	20	20	0.2	70

Table A4 – Descriptive statistics

	S/N	Sep	A_{peak}	Time
Min	11.09	3.39	926	4.02
Max	124.49	8.49	29046	10.00
Mean	48.30	5.42	10162	6.42
Q(25%)	19.60	4.48	3264	5.12
Q(75%)	72.81	6.61	16163	8.18
Median	46.19	4.87	7361	5.75
Std. Dev.	28.80	1.61	7634	1.97
Min/Max	0.08	0.40	0.03	0.40
N	29	29	29	29

Table A5 – Generated DoE runs for robustness testing

#	E_{col}	E_{con}	V_{inj}	F	G	T	Q_{res}
1	28	37	27	0.48	68	27	13
2	28	33	25	0.52	72	27	13
3	30	35	26	0.5	70	25	13.5
4	28	37	25	0.48	72	23	14
5	32	33	25	0.48	68	27	14
6	32	37	25	0.52	68	23	13
7	32	33	27	0.48	72	23	13
8	30	35	26	0.5	70	25	13.5
9	28	33	27	0.52	68	23	14
10	32	37	27	0.52	72	27	14
11	30	35	26	0.5	70	25	13.5

Table A6 – Scale-up assumptions and material inventory

		Lab Scale		Industrial Scale		Scale up factor
	API	**5**	g	10	kg	2000
	GTI	**1**	g	2	kg	2000
	DCM	**500**	cm^3	1	m^3	2000
Flash Chromatography						
Column specifications	Silica	**150.0**	g	330	kg	2200
	Silica	**300.0**	cm^3	0.6	m^3	2000
	Silica/API	**30**	-	**33**	-	1.1
	diameter	**5.0**	cm	0.63	m	
	section	19.6	cm^2	0.31	m^2	
	H	**15.3**	cm	1.9	m	
	H/diameter	**3.1**	-	3.1	-	1
(a) solution concentrations by distillation, (b) Elution conditions and (c) solvent volumes	(a) DCM distilled	**450.0**	cm^3	0.900	m^3	2000
	(b) Flow Rate	**50.0**	$cm^3.min^{-1}$	0.476	$m^3.h^{-1}$	
	(b) Linear velocity	2.55	$cm.min^{-1}$	1.53	$m.h^{-1}$	1.0
	DMAP removal					
	(c) Inlet DCM	**1425**	cm^3	3.135	m^3	2200
	(c) Inlet EtOAc	**75**	cm^3	0.165	m^3	2200
	(c) DMAP fraction	**300**	cm^3	0.76	m^3	
	(c) META fraction	**1200**	cm^3	2.64	m^3	
	(a) Distillate + filtered	**1195**	cm^3	2.63	m^3	
	MeMes removal					
	(c) Inlet DCM	**1063**	cm^3	2.3386	m^3	2200
	(c) Inlet EtOAc	**137**	cm^3	0.3014	m^3	2200
	(c) MeMs fraction	**750**	cm^3	1.75	m^3	
	(c) META fraction	**450**	cm^3	0.99	m^3	
	(a) Distillated+filtred	**400**	cm^3	0.98	m^3	

Table A6 continues on the next page

Continuation of Table A6 from the previous page

Crystallography						
Solvent exchange I	DCM distilled	**450**	cm^3	0.900	m^3	0
	Inlet MeOH	**100**	cm^3	0.200	m^3	2000
	Inlet MeOH	**100**	cm^3	0.200	m^3	2000
	Distillate	**200**	cm^3	0.400	m^3	
Crystallization I	Initial temp	**50**	ºC	50	ºC	
	Final Temp	**10**	ºC	10	ºC	
	Cooling rate	**30**	ºC/h	30	ºC/h	
	Initial time	**1**		1	h	
	Final time	**2**	h	2	h	
	MeOH washing	**40**	cm^3	0.080	m3	2000
	Filtrated	**85.0**	cm^3	0.170	m3	
Charcoal adsorption	Charcoal	**3**	g	6	kg	2000
	Inlet DCM	**100**	cm^3	0.200	m^3	2000
	Inlet MeOH	**100**	cm^3	0.200	m^3	2000
	Operation time	**2**	h	3	h	
	Recirculation flow rate	-		1.5	m^3/h	
	DCM Washing	**40**	cm^3	0.080	m^3	2000
Solvent exchange II	Distillate	**195**	cm^3	0.390	m^3	
	Inlet MeOH	**100**	cm^3	0.200	m^3	2000
	Distillate	**100**	cm^3	0.200	m^3	
Crystallization II	Initial temp	**50**	ºC	50	ºC	
	Final Temp	**10**	ºC	10	ºC	
	Cooling rate	**30**	ºC/h	30	ºC/h	
	Initial time	**1**		1	h	
	Final time	**2**	h	2	h	
	MeOH washing	**40**	cm^3	0.080	m^3	2000
	Filtrated	**85**	cm^3	**0.170**	m^3	
Organic Solvent Nanofiltration						
OSN diafiltration	Membrane	**105.6**	cm^2	20.0	m^2	1894
	Solvent flux	**5.5**	$cm^3.cm^{-2}.h^{-1}$	0.055	$m^3.m^{-2}.h^{-1}$	1
	Diafiltration flow rate	581	$cm^3.h^{-1}$	1.100	$m^3.h^{-1}$	1894
	DCM Preconditioning	**250**	cm^3	0.5	m^3	2000
	DCM diafiltration	**3500**	cm^3	7.0	m^3	2000
	Permeate (GTI fraction)	**3250**	cm^3	**7.5**	m^3	
	Retentate (Meta fraction)	**500**	cm^3	1	m^3	
	Distillate + filtrated	**450**	cm^3	0.990	m^3	

Table A7 – Measured IR spectrum of MAA in DCM and in $CHCl_3$

Wavenumber in DCM [cm^{-1}]	Wavenumber in $CHCl_3$ [207] [cm^{-1}]	Assignment
951(m)	946	$\delta_r CH_2$, νC-C
1009(w)	1010	$\delta_r CH_3$, $\delta_r CH_2$
1122(m)	-	wCH_3, wCCC
1204(m)	1205	νC-O, βOH, $\delta_r CH_3$
1221(w)	-	
1258(w)	-	From solvent: CH_2Cl_2
1300(m)	1300	βOH, $\delta_r CH_2$, νC-C
1319(sh)	1320	νC-C, βOH, νC-O, δ_{sci}OCO
1375(w)	1380	$\delta_{sy}CH_3$
-	1410	$\delta_{sci}CH_2$, $\delta_{as}CH_3$, $\delta_{sy}CH_3$
1431(w)	1435	$\delta_{as}CH_3$
1454(m)	1458	$\delta_{as}CH_3$, $\delta_{sci}CH_2$
1636(m)	1635	νC=C, $\delta_{sci}CH_2$
1697(vs)	1697	νC=O
1730(m)	-	overtone/combination
2930(br)	2932	$\nu_{sy}CH_3$
2963(br)	2964	$\nu_{as}CH_3$
2990(br)	2988	$\nu_{as}CH_3$
~3400	~3400	νOH

[a] The abbreviations s, as, ν, δ, β, sci, r, w mean symmetric, asymmetric, stretch, deformation, bend, scissoring, rock and wag respectively.

6.2. Figures

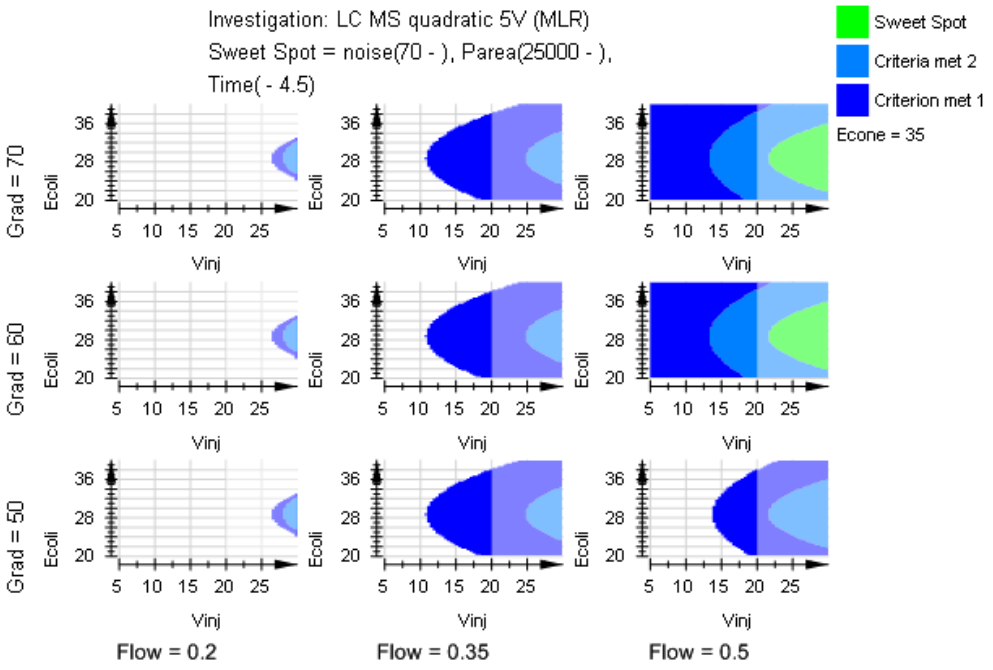

Figure A1 – Sweet spot plot of the CCF design

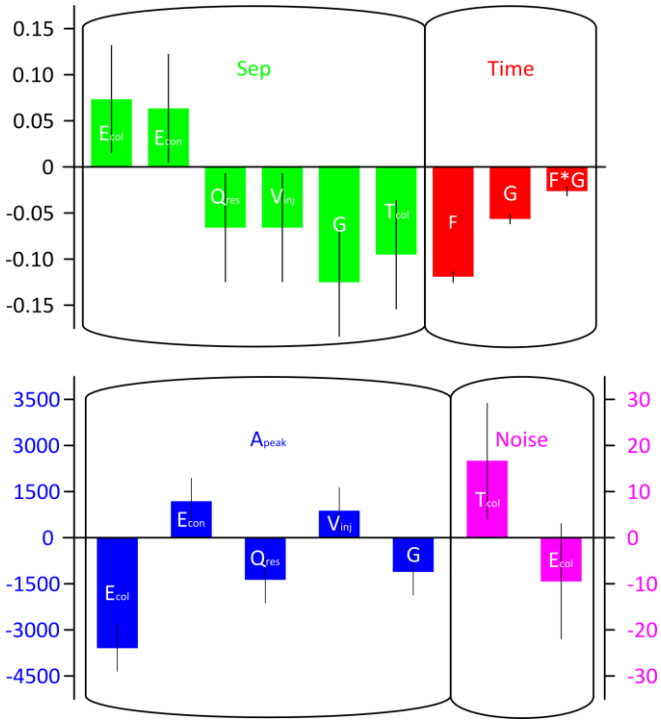

Figure A2 – Regression coefficient plot for the FF design of robustness

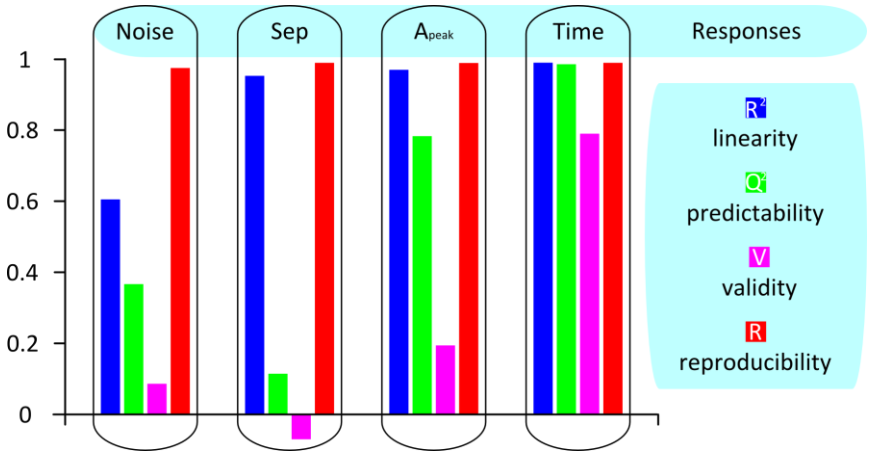

Figure A3 – Summary of fit for the FF design of robustness

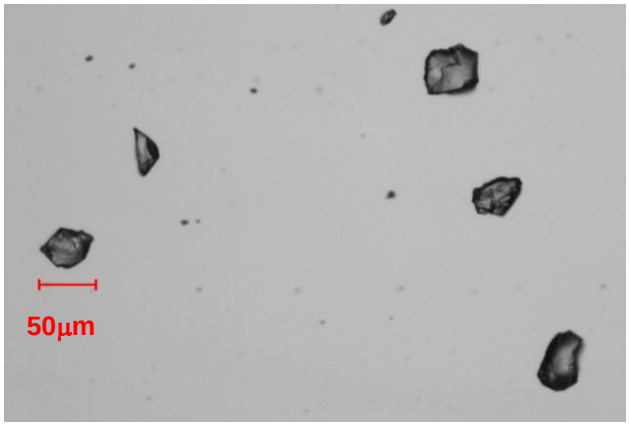

Figure A4 – Microscopy image of MIP2 polymer particles

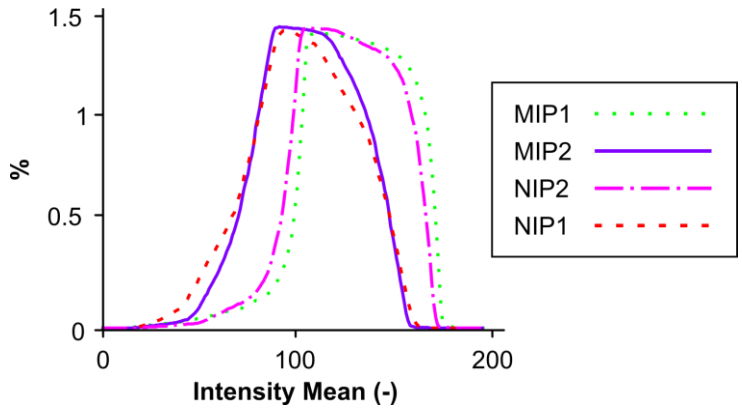

Figure A5 – Intensity shift between the polymer particles synthesized in the presence and absence of PMP base.

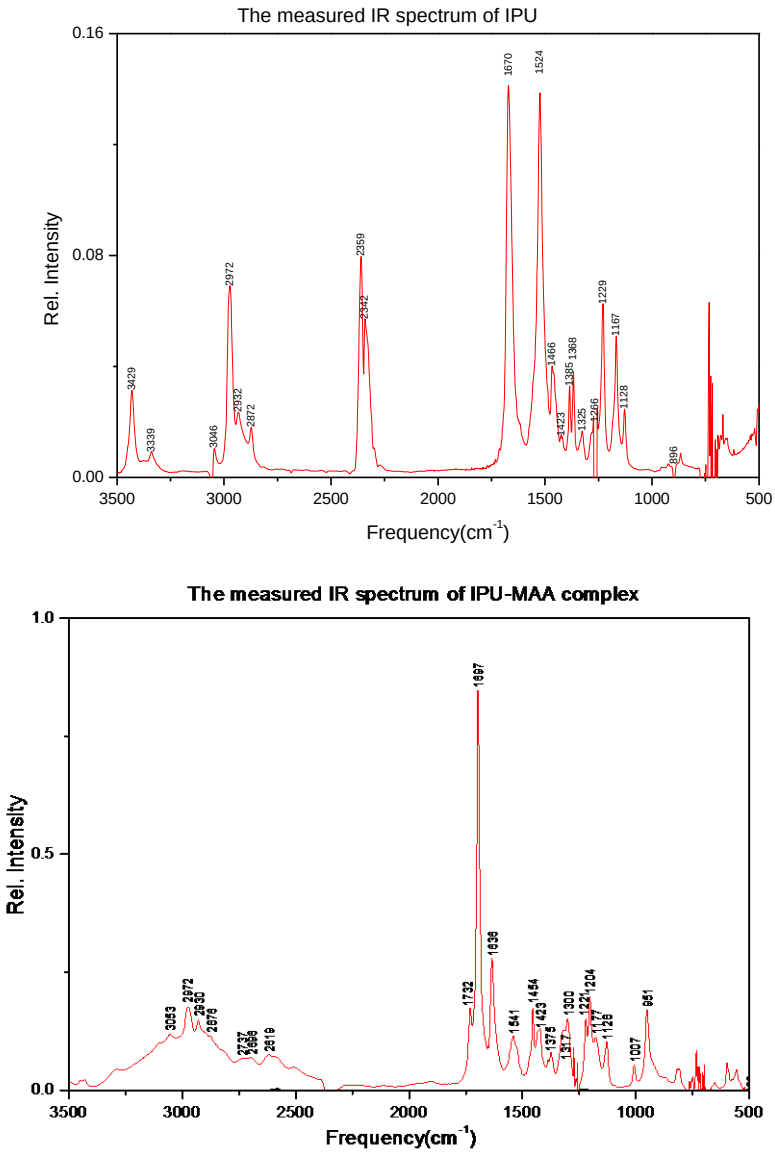

Figure A6 – IR spectra of IPU and the MAA-IPU complex

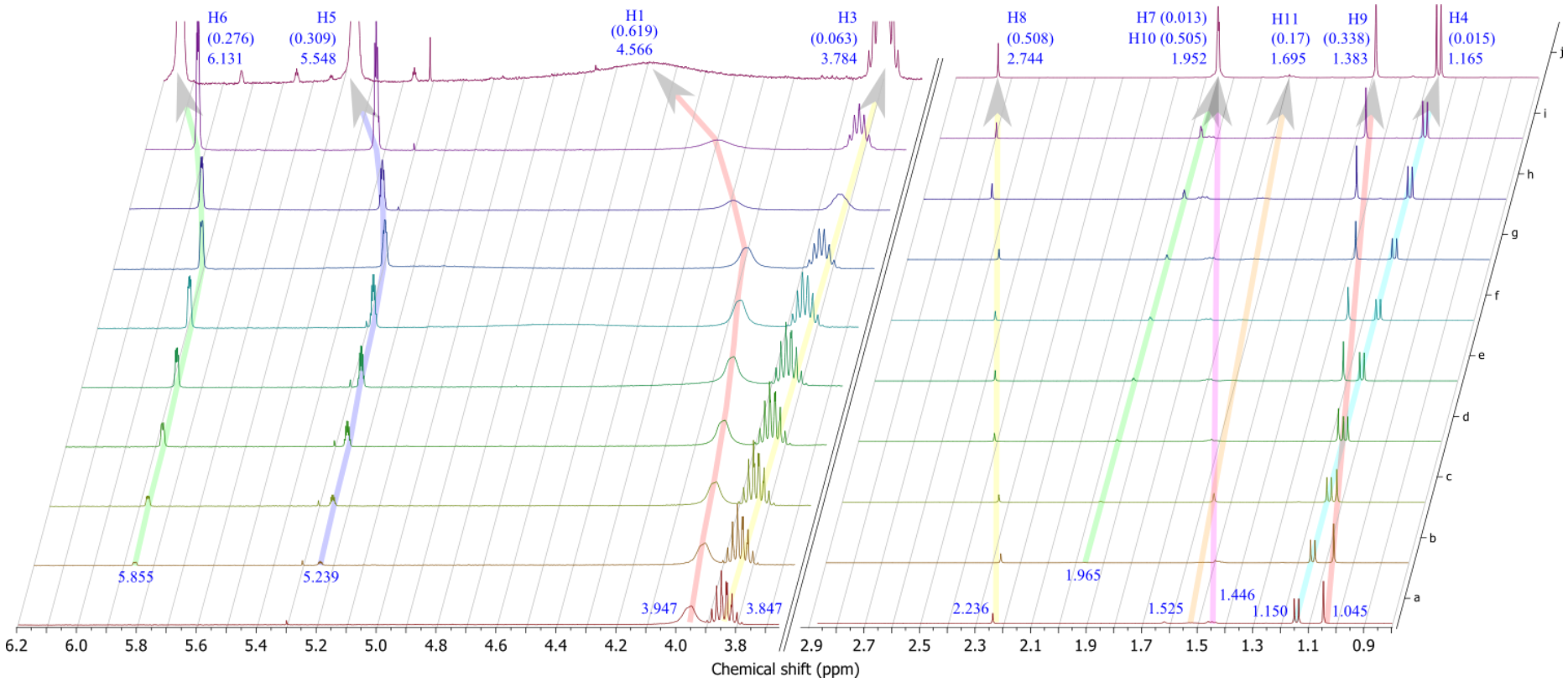

Figure A7 – Chemical shifts of all the protons during the titration of 10 mM IPU:PMP (1:1) with 0-5 equivalent MAA – the arrows indicate the increase of concentration

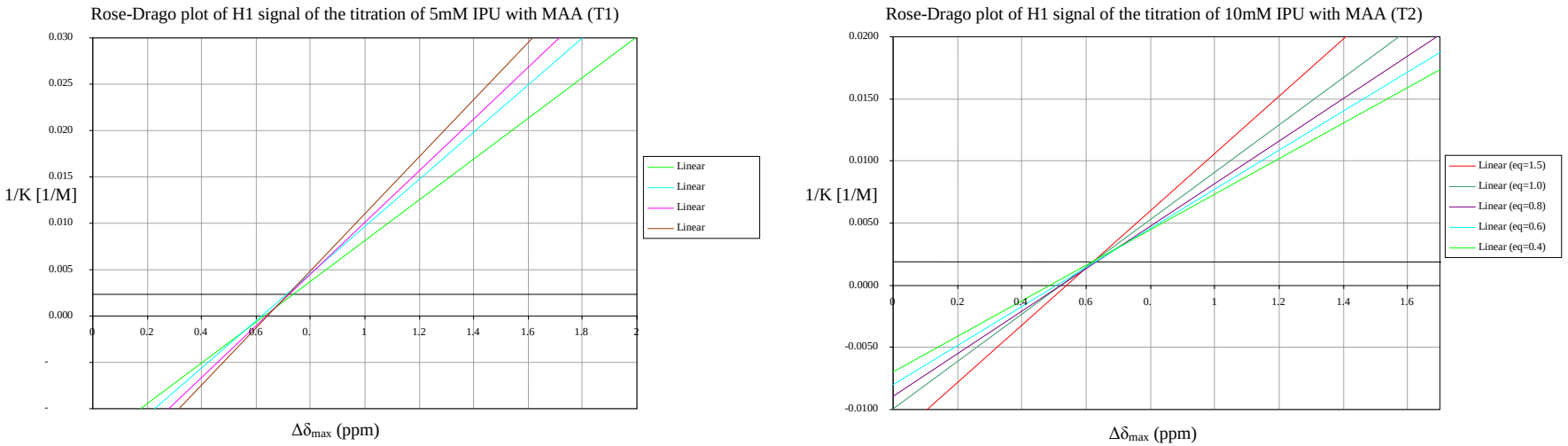

Figure A8 – Rose-Drago plots of T1 and T2. The black line points the average intersection of the lines. The chosen lines are in agreement with the Weber criteria (vide infra)[227,228].

7. Publications resulting from the work carried out in this thesis

7.1. Articles

"Unraveling the nature of recognition of genotoxin selective molecularly imprinted scavengers: binding characterization in the presence and absence of a deprotonating agent"
Gy. Székely, P. Pogány, M. Gil, W. Heggie, B. Sellergren
Chemistry - A European Journal (submitted)

"Green process engineering for sustainable API manufacturing: purification considerations"
Gy. Székely, M. Gil, B. Sellergren, W. Heggie, F.C. Ferreira
Green Chemistry (under review)

"Sources of genotoxic impurities in drug synthesis: a systematic review"
Gy. Székely, M. Sousa, F.C. Ferreira, M. Gil, W. Heggie
Chemical Reviews (under review)

"Design of experiments as a tool for LC-MS/MS method development for the trace analysis of the potentially genotoxic 4-dimethylaminopyridine impurity in glucocorticoids"
Gy. Székely, B. Henriques, M. Gil, A. Ramos, C. Alvarez
Journal of Pharmaceutical and Biomedical Analysis (dx.doi.org/10.1016/j.jpba.2012.07.006)

"Design, preparation and characterization of novel molecularly imprinted polymers for removal of potentially genotoxic 1,3-diisopropylurea from API solutions"
Gy. Székely, J. Bandarra, W. Heggie, F.C. Ferreira, B. Sellergren
Separation and Purification Technology 86 (2012) 190-198.

"A hybrid approach to reach stringent low genotoxic impurity contents in active pharmaceutical ingredients: combining molecularly imprinted polymers and organic solvent nanofiltration for removal of 1,3-diisopropylurea"
Gy. Székely, J. Bandarra, W. Heggie, B. Sellergren, F.C. Ferreira
Separation and Purification Technology 86 (2012) 79-87.

"Removal of potentially genotoxic acetamide and arylsulfonate impurities from crude drugs by molecular imprinting"
Gy. Székely, E. Fritz, J. Bandarra, W. Heggie, B. Sellergren
Journal of Chromatography A 1240 (2012) 52-58.

"Organic solvent nanofiltration: A platform for removal of genotoxins from active pharmaceutical ingredients"
Gy. Székely, J. Bandarra, W. Heggie, B. Sellergren, F.C. Ferreira
Journal of Membrane Science 381 (2011) 21-33.

"Genotoxic impurities in pharmaceutical manufacturing"
Gy. Székely, M. Gil, W. Heggie, B. Sellergren
Hungarian Chemical Journal LXVII (2012) 34-37.

Encyclopedia on Membranes (invited contributor by Springer-Verlag, Berlin, 2012)

7.2. Patents

"Polymers for drug purification"
B. Sellergren, E. Fritz, Gy. Székely (inventors) – SE1100473-6 PCT patent application

"Organic solvent nanofiltration for the removal of genotoxic impurities from active pharmaceutical ingredients"
Gy. Székely, J. Bandarra, W. Heggie (inventors) – PT105601 patent application

7.3. Posters

"Investigation of molecular recognition phenomena of genotoxin selective, methacrylate based molecularly imprinted polymers"
Gy. Székely, P. Pogány, M. Gil, W. Heggie, B. Sellergren
MIP2012 – Science and Technology, Paris, France, 27-30/8/2012

"Implementation of molecular imprinting technology in pharmaceutical downstream processing"
Gy. Székely, M. Gil, W. Heggie, B. Sellergren
MIP2012 – Science and Technology, Paris, France, 27-30/8/2012

"Molecularly imprinted polymers as polishing phases for degenotoxification of pharmaceuticals"
Gy. Székely, M. Gil, F.C. Ferreira, W. Heggie, B. Sellergren
HPLC2012 Conference, Anaheim, USA, 16-21/6/2012

"Trace analysis of potentially genotoxic aminopyridine impurities in steroids by LC-MS/MS technique via design of experiments"
Gy. Székely, B. Henriques, M. Gil, C. Alvarez, A. Ramos
HPLC2012 Conference, Anaheim, USA, 16-21/6/2012

„Molecularly Imprinted Polymers and Organic Solvent Nanofiltration – A hybrid process for removal of 1,3-diisopropylurea impurity from Active Pharmaceutical Ingredients"
Gy. Székely, J. Bandarra, W. Heggie, F.C. Ferreira, B. Sellergren
Affinity 2011, Tavira, Portugal, 16-19/6/2011

„Organic Solvent Nanofiltration for Removal of Genotoxins from Active Pharmaceutical Ingredients"
Gy. Székely, J. Bandarra, B. Sellergren, F.C. Ferreira
ICOM2011, Amsterdam, Netherland, 23-29/7/2011

„Integration of Organic Solvent Nanofiltration and Molecularly Imprinted Polymers for the removal of Genotoxic Impurities from Active Pharmaceutical Ingredients"
Gy. Székely, J. Bandarra, F.C. Ferreira, B. Sellergren
Marie Curie Conference 2010, Torino, Italy, 1-2/7/2010

„Molecularly imprinted polymers for purification of crude pharmaceutical products"
Gy. Székely, E. Fritz, J. Bandarra, B. Sellergren
6th International Conference on Molecular Imprinting, New Orleans, USA, 9-12/8/2010

„Molecularly imprinted polymers for purification of crude pharmaceutical products”
E. Fritz, Gy. Székely, B. Sellergren
3rd EuCheMS Chemistry Congress, Nurnberg, Germany, 29.8-2.9/2010

7.4. Lectures

“A hybrid approach to reach stringent low genotoxic impurity contents in APIs”
4th Graduate Student Symposium on Molecularly Imprinted Polymers
Imperial College, London, UK, 28-30/9/2011

“Molecular imprinting and organic solvent nanofiltration as new technologies for the purification of active pharmaceutical ingredients”
1st IRMED Summer School on Molecularly Imprinted Polymers
La Vieille Perrotine, Ile d'Oléron, France, 16-21/5/2011

Various research progress presentations at NEMOPUR Marie Curie ITN consortium organized project meetings:

Imperial College, London, UK, 12/7/2012
Imperial College, London, UK, 27/9/2011
Technical University of Dortmund, Dortmund, Germany, 8/2/2011
Imperial College, London, UK, 16-17/9/2010
Lonza, Visp, Switzerland, 16/4/2010
Technical University of Dortmund, Dortmund, Germany, 19/11/2009
GlaxoSmithKline, Stevenage, UK, 23/10/2009

8. References

[1] J. Li, F. Jiang, X. Wei, Anal. Chem. 82 (2010) 6074-6078.

[2] A. H. Kamel, W. H. Mahmoud, M. S. Mostafa, Anal. Methods 3 (2011) 957-964.

[3] E. Oral, N. A. Peppas, J. Biomed. Mat. Res. Part A 68 (2004) 439-447.

[4] K. Mosbach, Anal. Chim. Acta 435 (2001) 3-8.

[5] Z. Weng, S. Muratsugu, N. Ishiguro, S. Ohkoshi, M. Tada, Dalton Trans. 40 (2011) 2338-2347.

[6] G. Wulff, Chem. Rev. 102 (2002) 1-25.

[7] http://thomsonreuters.com/products_services/science/science_products/a-z/web_of_science/

[8] D.I. Robinson, Org. Process Res. Dev. 14 (2010) 946-959.

[9] D. Jacobson-Kram, T. McGovern, Adv. Drug Deliver. Rev. 59 (1) (2007) 38-42.

[10] R. Benigni, C. Bossa, Chem. Rev. 111 (2011) 2507-2536.

[11] A. Teasdale, Genotoxic impurities – strategies for identification and control, John Wiley and Sons Inc., 2010

[12] S.P. Raillard, J. Bercu, S.W. Baertschi, C.M. Riley, Org. Process. Res. Dev. 14 (2010) 1015-1020.

[13] D.J. Snodin, Org. Process Res. Dev. 15 (2011) 1243-1246.

[14] A. Pullman (Ed.) Carcinogenesis: fundamental mechanisms; Reidel Publishing, 1980

[15] C.D.N. Humfrey, Toxicol. Sci. 100 (2007) 24-28.

[16] E. J. Delaney, Regul. Toxicol. Pharmacol. 49 (2007) 107-124.

[17] E. Gocke, H. Bürgin, L. Müller, T. Pfister, Toxicol. Lett. 190 (2009) 254-265.

[18] D.P. Elder, D.J. Snodin, J. Pharm. Pharmacol. 61 (2009) 269-278.

[19] Press Release, European Medicines Agency, Doc.Ref.: EMA/CHMP/492059/2007

[20] C. Gerber, H. Toelle, Toxicol. Lett. 190 (2009) 248-253.

[21] M. Sartori, The war gases. Chemistry and Analysis, J&A Churchill Ltd, 1939

[22] G. Vavon, J. Conia, Compt. Rend. 223 (1946) 157-163.

[23] H.M. Bolt, B. Gansewendt, Crit. Rev. Toxicol. 23 (1993) 237-253.

[24] F.P. Guengerich, J. Biochem. Mol. Biol. 36 (2003) 20-27.

[25] S.R. Rajski, R.M. Williams, Chem. Rev. 98 (1998) 2723-2796.

[26] L.G. Hernandez, H. van Steeg, M. Luijten, J. van Benthem, Mutat. Res. 682 (2009) 94-109.

[27] G. Erhart, DE Patent 1111642, 1958

[28] The Carcinogenic Potency Database (http://potency.berkeley.edu)

[29] Garte S. J., Hood A. T., Hochwalt A. E., D'Eustachio P., Snyder C. A., Segal A., Albert R. E., Carcinogenesis 12 (1985) 1709-1712.

[30] U.S. Department of Health and Human Services. Hazardous Substances Data Bank, National Toxicology Information Program, National Library of Medicine, Bethesda, 1993

[31] W. Schindler, US Patent 2948718, 1960

[32] R.W. Draper, A.T. McPhail, M.S. Puar, E.J. Vater, L. Weber, Tetrahedron 55 (1999) 3355-3364.

[33] L. Müller, R.J. Mauthe, C.M. Riley, M.M. Andino, D. Antonis, C. Beels, J. DeGeorge, A.G.M. Knaep, D. Ellison, J.A. Fagerland, R. Frank, B. Fritschel, S. Galloway, E. Harpur, C.D.N. Humfrey, A.S. Jacks, N. Jagota, Regul. Toxicol. Pharm. 44 (2006) 198-211.

[34] EMA/CHMP/SWP/431994/2007 Rev. 3, 23 September 2010

[35] L. Huang, D. Yub, P. Hoa, K. Leeb, C. Chen, Synthesis and anti-HIV activity of bi-functional triterpene derivatives, Lett. Drug Des. Discov. 4 (2007) 471-478.

[36] B. Venkateswara, K. Ramanjaneyulu, T. Bhaskara, Synthesis and bioactivity evaluation of cinnamic acid esters from oxalis pescaprace, J. Chem. Pharm. Res. 3 (2011)589-594.

[37] A.R. Stamvik, S.K. Kristensson, K. Lundvall, US patent 4537722, 1985

[38] U. Zutter, H. Iding, P. Spurr, B. Wirz, J. Org. Chem. 73 (2008) 4895-4902.

[39] Y.Y. Yeung, S. Hong, E.J. Corey, J. Am. Chem. Soc. 128 (2006) 6310-6311.

[40] L. Gentric, I. Hanna, L. Ricard, Org. Lett. 5 (2003) 1139-1142.

[41] Final Report of the Safety Assessment of Urea, Int. J. Toxicol. 24 (2005) 1-56.

[42] J. Izdebski, J. Pelka, Peptide synthesis using disubstituted carbodiimides which form dichloromethane-soluble urea derivatives, in Peptides, Proceedings of the 18th European Peptide Symposium, 1984

[43] F. Kurzer, K. Douraghi-Zadeh, Chem. Rev. 67 (1967) 107-151.

[44] C. Deen, E. Claassen, K. Gerritse, N.D. Zegers, W.J. Boersma, J. Immunol. Methods 129 (1990) 119-125.

[45] J.C. Sheehan, G.P. Hess, J. Am. Chem. Soc. 77 (1955) 1067-1068.

[46] W.O. Foye, T. Lemke, D. Williams, Foye's principles of medicinal chemistry, Wolters Kluwer Press, 2008

[47] G.T. Hermanson, Bioconjugate techniques, Academic Press, 2008

[48] Pierson E., Tishier M., US Patent 2584496, 1952

[49] D.Q. Liu, M. Sun, A.S. Kord, J. Pharm. Biomed. Anal. 51 (2010) 999-1014.

[50] Gy. Székely, J. Bandarra, W. Heggie, B. Sellergren, F.C. Ferreira, J. Membr. Sci. 381 (2011) 21-33.

[51] M. Sun, D.Q. Liu, A.S. Kord, Org. Process Res. Dev. 14 (2010) 977-985.

[52] G. Vanhoenacker, E. Dumont, F. David, A. Baker, P. Sandra, J. Chromatogr. A 1216 (2009) 3563-3570.

[53] A.M. van Wijk, B. Beerman, H.A.G. Niederländer, A.H.G. Siebum, G.J. de Jong, Anal. Bioanal. Chem. 400 (2011) 1375-1385.

[54] S. Furlanetto, S. Orlandini, I. Giannini, G. Beretta, S. Pinzauti, Electrophoresis 30 (2009) 633-643.

[55] F.G. Vogt, A.S. Kord, J. Pharm. Sci. 100 (2011) 797-812.

[56] S. Fekete, J. Fekete, I. Molnár, K. Ganzler, J. Chromatogr. A 1216 (2009) 7816-7823.

[57] A. Giordani, W. Kobel, H.U. Gally, Eur. J. Pharm. Sci. 43 (2011) 1-15.

[58] N.V.V.S.S. Raman, A.V.S.S. Prasad, K.R. Ratnakar, J. Pharmaceut. Biomed. Anal. 55 (2011) 662-667.

[59] A. Schule, C. Ates, M. Palacio, J. Stofferis, J.-P. Delatinne, B. Martin, S. Lloyd, Org. Process Res. Dev. 14 (2010) 1008-1014.

[60] Z. Cimarosti, F. Bravo, P. Stonestreet, F. Tinazzi, O. Vecchi, G. Camurri, Org. Process Res. Dev. 14 (2010) 993-998.

[61] T. Laird, Org. Process Res. Dev. 7 (2003) 225-225.

[62] R. Kecili, D. Nivhede, J. Billing, M. Leeman, B. Sellergren, E. Yilmaz, Org. Process Res. Dev. 16 (2012) 1225-1229.

[63] Gy. Székely, E. Fritz, J. Bandarra, W. Heggie, B. Sellergren, J. Chromatogr. A 1240 (2012) 52-58.

[64] B.P. Chekal, A.M. Campeta, Y.A. Abramov, N. Feeder, P.P. Glynn, R.W. McLaughlin, P.A. Meenan, R.A. Singer, Org. Process Res. Dev. 13 (2009) 1327-1337.

[65] Kozma, D. Handbook of Optical Resolution via Diastereomeric Crystallisation, CRC Press, 2002

[66] F.C. Ferreira, N.F. Ghazali, U. Cocchini, A.G. Livingston, Tetrahedron Asymmetry 17 (2006) 1337-1348.

[67] S. Rohani, Control of Crystallization Processes in the Pharmaceutical Industry, ICheaP-9 conference, 10-13/05/2009, Rome, Italy

[68] B.Y. Shekunov, P. York, J. Cryst. Growth 211 (2000) 122-136.

[69] S. Kim, C. Wei, S. Kiang, Org. Process Res. Dev. 7 (2003) 997-1001.

[70] F.C. Ferreira, H. Macedo, U. Cocchini, A.G. Livingston, Org. Process Res. Dev. 10 (2006) 784-793.

[71] Y. Yang, R. Tjia, Comput Chem Eng 34 (2010) 1030-1035.

[72] S. Puranik, P Pai, G. Rao, Indian J. Pharm. Sci. 69 (2007) 352-359.

[73] S.L. Prabu, T.N.K. Suriyaprakash. Int. J.l of Pharmaceut. Sci. Rev. Res. 3 (2002) 1-8.

[74] R.H.C. Lee, C. Strulson, J. Plewa, E. Kolodziej, V. Antonucci, B. Mao, C.J. Welch, Z. Ge M.A. Al-Sayah, Org. Process Res. Dev. 14 (2010) 1021-1026.

[75] N. Iverlund, A. Parsons, F. Muller, Chem. Eng. Res. Des. 87 (2009) 852-858.

[76] C.J. Welch, J. Albaneze-Walker, W.R. Leonard, M. Biba, J. DaSilva, D. Henderson, B. Laing, D.J. Mathre, S. Spencer,X. Bu, T. Wang, Org. Process Res. Dev 9 (2005) 198-205.

[77] C.J. Welch, M. Shaimi, M. Biba, J.R. Chilenski, R.H. Szumigala Jr., U. Dolling, D.J. Mathre, P.J. Reider, J. Sep. Sci 25 (2002) 847-850.

[78] S. Tanada, N. Kawasaki, M. Araki, M. Isomura, J. Colloid Interf. Sci. 214 (1999) 106-108.

[79] C.J. Welch, M. Biba, A. Drahus, D. Conlon, H. Tung, P. Collins, J. Liq. Chromatogr. 26 (2003) 1959-1968.

[80] D.W. Guest, J. Chromatogr. A 760 (1997) 159-162.

[81] T. Arai, J. Chromatogr. B Biomed. Sci. Appl. 717 (1998) 295-311.

[82] S.R. Maddula, M. Kharkar, K. Manudhane, S. Kale, A. Bhori, A. Lali, P.K. Dubey, K.R. J. Sarma, A. Bhattacharya, R. Bandichhor, Org. Process Res. Dev. 13 (2009) 683-689.

[83] W.C. Still, M. Kahn, A. Mitra, A. J. Org. Chem. 43 (1978) 2923-2925.

[84] K. Cziner, T. Virkki-Hatakka, M. Hurme, I. Turunen, Chem. Eng. Technol. 28 (2005) 1490-1499.

[85] M. Degerman, N. Jakobsson, B. Nilsson, Chem. Eng. Technol. 31 (2008) 875-882.

[86] T. Winkelnkemper, G. Schembecker, Sep. Purif. Technol. 71 (2010) 356-366.

[87] C. Jimenez-Gonzalez, D.J.C. Constable, C.S. Ponder, Chem. Soc. Rev. 41 (2012) 1485-1498.

[88] C. Jimenez-Gonzalez, C.S. Ponder, Q.B. Broxterman, J. Manley, Org. Process Res. Dev. 15 (2011) 912-917.

[89] D.J.C. Constable, A.D. Curzons, V.L. Cunningham, Green Chem. 4 (2002) 521-527.

[90] A.D. Curzons, D.J.C. Constable, D.N. Mortimer, V.L. Cunningham, Green Chem. 3 (2001) 1-6.

[91] C. Jimenez-Gonzalez, P. Poechlauer, Q.B. Broxterman, B.S. Yang, D. am Ende, J. Baird, C, Bertsch, R.E. Hannah, P. Dell'Orco, H. Noorman, S. Yee, R. Reintjens, A. Wells, V. Massonneau, J. Manley, Org. Process Res. Dev. 15 (2011) 900-911.

[92] Kwok D., Tsai D. J., Tann C., Fu X., WO Patent 9800437, 1997

[93] E.L. Shapiro, US Patent 4472393, 1984

[94] W. Heggie, J. Bandarra, US Patent 6177560, 2001

[95] Hwang, C. K.; Li, W. S.; Nicolaou, K.C., Tetrahedron Lett. 25 (1984) 2295-2296.

[96] Y. Yoshida, Y. Sakakura, N. Aso, S. Okada, Y. Tanabe, Tetrahedron 55 (1999) 2183-2192.

[97] A.D. Curzons, D.C. Constable, V.L. Cunningham, Clean Products and Processes 1 (1999) 82-90.

[98] R.K. Henderson, C. Jiménez-González, D.J.C. Constable, S.R. Alston, G.G.A. Inglis, G. Fisher, J. Sherwood, S.P. Binks, A.D. Curzons, Green Chem. 13 (2011) 854-862.

[99] K. Alfonsi , J. Colberg, P.J. Dunn , T. Fevig , S. Jennings , T.A. Johnson , H.P. Kleine, C. Knight , M.A. Nagy, D.A. Perry, M. Stefaniak, Green Chem. 10 (2008) 31-33.

[100] D.J.C. Constable, C. Jimenez-Gonzalez, R.K. Henderson, Org. Process Res. Dev. 11 (2007) 133-137.

[101] A.D. Curzons, D.J.C. Constable, D.N. Mortimer, V.L. Cunningham, Green Chem. 3 (2001) 1-6.

[102] M. Berrios, R.L. Skelton, Chem. Eng. J. 144 (2008) 459-465.

[103] T. Winkelnkemper, G. Schembecker, Sep. Purif. Technol. 72 (2010) 34-39.

[104] J. García-Serna, J.L. Martínez, M..J Cocero, Green Chem. 9 (2007) 111-124.

[105] Y. H. T. See, F. W. Lim, A. G. Livingston, J. Mem. Sci. 301 (2007) 3-10.

[106] http://duramem.evonik.com/sites/dc/Downloadcenter/Evonik/Product/DuraMem-PuraMem/brochures

[107] P. Cuperus, Chemie Ingenieur Technik 77 (2005) 1000-1001.

[108] Solsep membrane modules for organic membrane filtration separation at http://www.solsep.com

[109] Inopor at http://www.inopor.com/en/membranes_e.html

[110] C.J. Pink, H. Wong, F.C. Ferreira, A.G. Livingston, Org. Process Res. Dev. 12 (2008) 589-595.

[111] Y. Zhang, B. Bruggen, G.X. Chena, L. Braeken, C. Vandecasteele, Sep. Purif. Technol. 38 (2004) 163-172.

[112] L. S. White, J. Mem. Sci. 286 (2006) 26-35.

[113] K. Vanherck, P. Vandezande, S. Aldea, I. Vankelecom, J. Mem. Sci. 320 (2008) 468-476.

[114] P. Vandezande, L. Gevers, I. Vankelecom, Chem. Soc. Rev. 37 (2008) 365-405.

[115] J. Geens, B. D. Witte, B. van der Bruggen, Sep. Sci. Technol. 42 (2007) 2435.

[116] N.F. Ghazali, F.C. Ferreira, A. J. White, A.G. Livingston, Tetrahedron: Asymmetry 17 (2006) 1846-1852.

[117] F.C. Ferreira, L.C. Branco, K.K. Verma, J.G. Crespo, C.A.M. Afonso, Tetrahedron: Asymmetry 18 (2007) 1637-1641.

[118] S. Aerts, H. Weyten, A. Buekenhoudt, L. Gevers, I. Vankelecom, P. Jacobs, Chem. Comm. 6 (2004) 710-711.

[119] P. Gryp, A. Barnard, J.P. Cronje, D. Vlieger, S. Marx, H.C.M. Vosloo, J. Membr. Sci. 353 (2010) 70-77.

[120] H.T. Wong, C.J. Pink, F.C. Ferreira, A.G. Livingston, Green Chem. 8 (2006) 373-379.

[121] H.T. Wong, Y.H.T. See, F.C. Ferreira, R. Crook, A. G. Livingston, Chem. Comm. 19 (2006) 2063-2065.

[122] K. Haerens, S. Deuren, E. Matthijs, B. Bruggen, Green Chem. 12 (2010) 2182-2188.

[123] A.C. Odena, P. Vandezande, D. Fournier, W. Camp, F.D. Prez, I. Vankelecom, Chem. Eur. J. 16 (2010) 1061-1067.

[124] J.C. Lin, A.G. Livingston, Chem. Eng. Sci. 62 (2007) 2728-2736.

[125] J.P. Sheth, Y. Qin, K.K. Sirkar, B.C. Baltzis, J. Membr. Sci. 211 (2003) 251-261.

[126] R.V. Blanco, F.C. Ferreira, R.F. Jorge, A.G. Livingston, J. Membr. Sci. 317 (2008) 50-64.

[127] J.L.C. Santos, A.H. Montesinos, A. Karpinsky, S. Velizarov, J. Crespo, Desalination, 199 (2006) 448-450.

[128] J.L. Santos, P. Beukelaar, I. Vankelecom, S. Velizarov, J. Crespo, Sep. Purif. Technol. 50 (2006) 122-131.

[129] J.L. Santos, A. Hidalgo, R. Oliveira, J.G. Crespo, J. Membr. Sci. 300 (2007) 191-204.

[130] A. Dobraka, B. Verrechta, H. Dungena, A. Buekenhoudtc, I. Vankelecom, B. Bruggen, J. Membr. Sci. 346 (2010) 344-352.

[131] J. Geens, A. Hillen, B. Bettens, B. Bruggen, C. Vandecasteele, J. Chem. Technol. Biotechnol. 80 (2005) 1371-1377.

[132] S. Darvishmanesh, A. Buekenhoudt, J. Degreve, B. Bruggen, Sep. Purif. Technol. 70 (2009) 46-52.

[133] S. Darvishmanesh, J. Degreve, B. Bruggen, Phys. Chem. Chem. Phys. 12 (2010) 13333-13342.

[134] P.K. Owens, L. Karlsson, E.S.M Lutz, L.I Andersson, TrAC Trends Anal. Chem. 18 (1999) 146-154.

[135] S. Piletsky, S. Alcock, A. Turner, Trends Biothecnol. 19 (2001) 3-12.

[136] L. Fischer, R. Mueller, B. Ekberg, K. Mosbach, J. Am. Chem. Soc. 113 (2011) 9358-9360.

[137] M. Kempe, K. Mosbach, L. Fischer, J. Mol. Recognit. 6 (1993) 25-29.

[138] O. Ramström, C. Yu, K. Mosbach, J. Mol. Recognit. 9 (1996) 691-696.

[139] http://www.biotage.co.jp/pages/446/Japan_NovDec2010_ExploraSepSeminar.pdf

[140] E. Yilmaz, R. Kecili, Fast Identification of Selective Resins for Genotoxic Impurity Removal Via Screening of Molecularly Imprinted Resins Libraries, HPLC2012, 16-21/06/2012, Anaheim, CA, USA

[141] Gy. Székely, J. Bandarra, W. Heggie, F.C. Ferreira, B. Sellergren, Sep. Purif. Technol. 86 (2012) 190-198.

[142] B. Sellergren (Ed.), Molecularly Imprinted Polymers: Man-Made Mimics of Antibodies and Their Applications in Analytical Chemistry, Elsevier, 2001

[143] A. Nematollahzadeh, W. Sun, C.S. Aureliano, D. Lütkemeyer, J. Stute, M.J. Abdekhodaie, A. Shojaei, B. Sellergren, Angew. Chem. Int. Ed. 50 (2011) 495-498.

[144] J.L. Urraca, C.S. Aureliano, E. Schillinger, H. Esselmann, J. Wiltfang, B. Sellergren, J. Am. Chem. Soc. 133 (2011) 9220-9223.

[145] L. Ye, O. Ramström, R.J. Ansell, M.O. Mansson, K. Mosbach, Biotechnol. Bioeng. 64 (1999) 650-655.

[146] Gy. Székely, J. Bandarra, W. Heggie, B. Sellergren, F.C. Ferreira, Sep. Purif. Technol. 86 (2012) 79-87.

[147] E.V. Piletska, A.R. Guerreiro, M.J. Whitcombe, S.A. Piletsky, Macromolecules 42 (2009) 4921-4928.

[148] Z. Jie, H. Xiwen, Anal. Chim. Acta 381 (1999) 85-91.

[149] J. O´Mahony, B.C.G. Karlsson, B. Mizaikoff, I.A. Nicholls, Analyst 132 (2007) 1161-1168.

[150] K. Hirose, J. Inclus. Phenom. Macrocycl. Chem. 39 (2001) 193-209.

[151] L. Caron, C. Christine, S. Tilloy, E. Monflier, D. Landy, S. Fourmentin, Supramol. Chem. 14 (2002) 11-20.

[152] C. Dethlefs, J. Eckelmann, H. Kobarg, T. Weyrich, S. Brammer, Eur. J. Org. Chem. 11 (2011) 2066-2074.

[153] Z. Sun, L. Li, X.M. Qiu, F. Liu, B. Yin, Int. J. Pharm. 316 (2006) 7-13.

[154] M. Johnston, B. Shapiro, T. Proulx, A. Godwin, H. Pearce, J. Am. Chem. Soc. 97 (1975) 542-555.

[155] J. Reuben, J. Am. Chem. Soc. 95 (1973) 3534-3540.

[156] D. Kneeland, K. Ariga, V.M. Lynch, C. Huang, E.V. Anslyn, J. Am. Chem. Soc. 115 (1993) 10042-10055.

[157] N.K. Wilson, J. Am. Chem. Soc. 94 (1972) 2431-2436.

[158] Y. Zhang, D. Song, L.M. Lanni, K.D. Shimizu, Macromolecules 43 (2010) 6284-6294.

[159] J. Saloni, P. Lipkowski, S.S.R. Dasary, Y. Anjaneyulu, H. Yu, G. Hill, Polymer 52 (2011) 1206-1216.

[160] P. Job, Ann. Chim. 9 (1928) 113-203.

[161] C.Y. Huang, Meth. Enz. 87 (1982) 509-525.

[162] L. Fielding, Tetrahedron 56 (2000) 6151-6170.

[163] H.A. Benesi, J.A. Hildebrand, J. Am. Chem. Soc. 71 (1949) 2703-2707.

[164] M.W. Hanna, A.L. Ashbaugh, J. Phys. Chem. 68 (1964) 811-816.

[165] G. Scatchard, Ann. N. Y. Acad. Sci. 51 (1949) 660-672.

[166] R.L. Scott, Rec. Trav. Chim. Pays-Bas 75 (1956) 787-789.

[167] N.J. Rose, R.S. Drago, J. Am. Chem. Soc. 81 (1959) 6138-6141.

[168] H.N. Wachter, V. Fried, J. Chem. Educ. 51 (1974) 798-799.

[169] A. P. Bisson, C.A. Hunter, J.C. Morales, K. Young, Chem. Eur. J. 4 (1998) 845-851.

[170] R.E. Lenkinski, G.A. Elgavish, J. Reuben, J. Magn. Res. 32 (1978) 367-376.

[171] M.M. Kopecni, R.J. Laub, D.M. Petkovic, J. Phys. Chem. 85 (1981) 1595-1599.

[172] A. Veselkov, A. Lantushenko, O. Rogova, D. Veselkov, D.B. Davies, Rus. J. Org. Chem. 39 (2003) 87-91.

[173] P. Groote, P.G. Rouxhet, J. Devaux, P. Godard, Ap. Spec. 55 (2001) 877-887.

[174] A. Idrissi, P. Damay, K. Yukichi, P. Jedlovszky, J. Chem. Phys. 129 (2008) 164512.

[175] L. Levi, S. Srebnik, J. Phys. Chem. B 114 (2010) 16744-16751.

[176] X. Wu, W.R. Carroll, K.D. Shimizu, Chem. Mater. 20 (2008) 4335-4346.

[177] T. Takeuchi, A. Dobashi, K. Kimura, Anal. Chem. 72 (2000) 2418-2422.

[178] T. Sagawa, K. Togo, C. Miyahara, H. Ihara, K. Ohkubo, Anal. Chim. Acta 504 (2004) 37-41.

[179] A. Bhaskarapillai, S. Chandra, N.V. Sevilimedu, B. Sellergren, Biosens. Bioelectr. 25 (2009) 558-562.

[180] F. Ahmadia, J. Ahmadi, M. Rahimi-Nasrabadi, J. Chromatogr. A 1218 (2011) 7739-7747.

[181] M.B. Gholivand, M. Khodadadian, Talanta 85 (2011) 1680-1688.

[182] M. Tabandeh, S. Ghasamipour, M. Tabatabaei, M. Hasheminejad, J. Chromatogr. B 898 (2012) 24-31.

[183] I. Yungerman, S. Srebnik, Chem. Mater. 18 (2006) 657-663.

[184] B.C.G. Karlsson, J. O'Mahony, J.G. Karlsson, H. Bengtsson, L.A. Eriksson, I.A. Nicholls, J. Am. Chem. Soc. 131 (2009) 13297-13304.

[185] D.T. Burns, K. Danzer, A. Townshend, Pure Appl. Chem. 74 (2002) 2201-2205.

[186] H.E. Gottlieb, V. Kotlyar, A. Nudelman, J. Org. Chem. 62 (1997) 7512-7515.

[187] E.P. Barrett, L.G. Joyner, P.P. Halenda, J. Am. Chem. Soc. 73 (1951) 373-380.

[188] M. Mulder, Basic principles of membrane technology, Kluwer Academic Publishers, 1996

[189] W.M. Nelson, Green Solvents for Chemistry: Perspectives and Practice, Oxford University Press, 2003

[190] EMA guidelines “Limits for Genotoxic Impurities” EMA/CHMP/QWP/251334/2006

[191] C.E.C.A. Hop, M. Dakubu, J.L. Holmes, Org. Mass Spectrom. 23 (1988) 609-612.

[192] L. Eriksson, E. Johansson, N. Kettaneh-Wold, C. Wikström, S. Wold, Design of Experiments – principles and applications, Umetrics Academy Publisher, 2008

[193] R. K. Sinnott, Chemical Engineering Design, Volume 6, Butterworth-Heinemann; 4th edition , 2005

[194] Impact assessment of potential restrictions on the marketing and use of dichloromethane in paint strippers, final report by Risk & Policy Analysts Limited, Norfolk, UK, 2007

[195] S. Lee, G. Robinson, Process Development Fine Chemicals from Grams, Oxford university press 1995

[196] A. Kleemann, J. Engel, B. Kutscher, D. Reichert, Pharmaceutical substances: syntheses, patents, applications; Thieme, 1999

[197] Dermatologic Disease Database, http://www.aocd.org/skin/dermatologic_diseases/steroids.html

[198] J. Billing, B. Boyd, E. Yilmaz, Cross-reactivity of imprinted polymers - the ExploraSep concept, MIP2006 conference, 10-14/09/2006, Cardiff, UK

[199] A.R. Rees, E. Yilmaz, O. Karlsson, Revolutionary product for the identification of new separation materials, R&D magazine, Press release by MIP Technologies, 2009

[200] http://www.biotage.com/DynPage.aspx?id=111255

[201] A.J. Hall, P. Manesiotis, M. Emgenbroich, M. Quaglia, E. Lorenzi, B. Sellergren, J. Org. Chem. 70 (2005) 1732-1736.

[202] S. Brunauer, P.H. Emmett, E. Teller, J. Am. Chem. Soc. 60 (1938) 309-319.

[203] K. Kaneko, J. Membr. Sci. 96 (1994) 59-89.

[204] K.S.W. Sing, D.H. Everett, R.A.W. Haul, L. Moscou, R.A. Pierotti, J. Rouquerol, T. Siemienieswska, Pure Appl. Chem. 57 (1985) 603-619.

[205] F. Svec, J.M.J. Fréchet, Chem. Mater. 7 (1995) 707-715.

[206] J. Saloni, S.S.R. Dasary, Y. Anjaneyulu, H. Yu, G. Hill, Struct. Chem. 21 (2010) 1171-1184.

[207] H.M. Badawi, M.A. Khaldi, S.S.A. Abbad, Z.H.A. Sunaidi, Spectrochim. Acta A 68 (2007) 432-442.

[208] Drugfuture Database (http://www.drugfuture.com/chemdata/pempidine.html)

[209] J.H. Kim, P.K. Park, C.H. Lee, H.H. Kwon, S. Lee, J. Membr. Sci. 312 (2008) 66-75.

[210] S. Sarkar, A.K. SenGupta, J. Membr. Sci. 324 (2008) 76-84.

[211] J. Meier, T. Melin, L.H. Eilers, Desalination 146 (2002) 361-366.

[212] http://www.kochmembrane.com/pdf/flat_sheet_test_products/FlatSheetProducts.pdf (March 19, 2008)

[213] B. Sellergren, Macromol. Chem. 190 (1989) 2703-2711.

[214] J.C.T. Lin, L.G. Peeva, A.G. Livingston, Separation of pharmaceutical process-related impurities via an organic solvent nanofiltration membrane cascade, AIChE Meeting, 12-17/11/2006, San Francisco, CA, USA

[215] A. Caus, S. Vanderhaegen, L. Braeken, B. Bruggen, Desalination 241 (2009) 111-117.

[216] J. Green, B. De Witte, B. Bruggen, Sep. Sci. Technol. 42 (2007) 2435-2449.

[217] J.C.T. Lin, A.G. Livingston, Chem. Eng. Sci. 62 (2007) 2728-2736.

[218] J.P. Sheth, Y. Qin, K.K. Sirkar, B.C. Baltzis, J. Membr. Sci. 211 (2003) 251-261.

[219] A.G. Livingston, L.G. Peeva, S. Han, D. Nair, S.S. Luthra, L.S. White, L.M.F. Dos Santos, Ann. N. Y. Acad. Sci., 984 (2003) 123-141.

[220] B. De Witte, Membrane technology for solvent recovery in pharmaceutical industry, International Workshop on Membranes in Solvent Filtration, 23-24/03/2006, Leuven, Belgium

[221] M.A. Rogawski, Epilepsy Res. 69 (2006) 273-294.

[222] www.drugbank.ca

[223] www.pubchem.com

[224] D. Czock, F. Keller, F.M. Rasche, U. Häussler, Clin. Pharmacokinet. 44 (2005) 61-98.

[225] J.E.F. Reynolds (Ed.), The Extra Pharmacopoeia, 30th edition, 1993

[226] C. Crim, L.N. Pierre, P.D. Daley-Yates, Clin. Therapeut. 23 (2001) 1339-1354.

[227] G. Weber: Molecular Biophysics; B. Pullman, M. Weissbluth, Eds.; Academic: New York, 1965; 369-397.

[228] G. Weber, S.R. Anderson, Biochem. 4 (1965) 1942-1947.